Molecular characterization of Hsp90-kinase interactions

by

Kliment Andreyvich Verba

DISSERTATION

Submitted in partial satisfaction of the requirements for the degree of

DOCTOR OF PHILOSOPHY

in

Biochemistry and Molecular Biology

in the

GRADUATE DIVISION

of the

UNIVERSITY OF CALIFORNIA, SAN FRANCISCO

[redacted]

Acknowledgements

First of all, I would like to thank David for being a tremendous mentor. There are many reasons for this, but I have space to list only some of them. First is his unwavering scientific rigor. Whenever exploring ideas, or making presentations, or just discussing random things in the common area David would always offer valuable scientific criticism of my ideas and I found it to be extremely valuable. It certainly made me a better scientist and a better thinker. Importantly, no matter how critical he can be of ideas, he has always been extremely supportive. Second is his general enthusiasm and commitment to ideal science, where one follows worthy ideas purely for scientific reasons without regard for bureaucratic system of funding, publishing, etc. It is amazing for a person who has been doing science for this long to remain this idealistic about science, and such idealism and enthusiasm is contagious. Finally, David managed to foster such an atmosphere and attract a group of such amazing people to his lab that I cannot imagine doing a PhD in any other place. It's a lab full of not colleagues but truly friends. The Agard lab is a diverse but closely knit pack, unrivaled in the level of stimulating discussions, support and alcohol consumption, and there are many specific people I need to thank.

When I joined, Laura Lavery, Rebeca Choy, Liz Montabana and Elaine Kirschke set the tone and the atmosphere of the lab, and it was an amazing place to be. They were incredibly smart, skilled and always willing to offer help, and I learned a great deal from all of them inside and outside of lab. My PhD would in no way be the same on both, scientific and personal level without them. I also now know how to smoke a brisket, Texas style. Thanks Laura! And how to make Ponche Crema. Thanks Rebeca!

I would also like to thank James Kraemer for his scientific feedback, encyclopedic

knowledge and willingness to drive to In and Out.

I would also like to thank the post docs in the lab. I rotated with Timothy Street and had an amazing time, he was a great mentor. You could always talk to Timo about deep fundamentals of protein folding, bench top SAXS machines, chevron plots, etc. Also, I have never been told I am wrong in a nicer way than by Timo. Dan Southworth and Justin Kollman always had a perfect dose of scientific skepticism and great advice like what exact infinitesimally small amount of cross linker to use. Ulrike Boetcher taught me everything I know about yeast and western blots, and protocols from Ulrike are the clearest, most detailed and most robust protocols I have ever seen. I certainly need to thank James Partridge for introducing me to Corpse Reviver #2 and the Aviation. I would like to thanks Sam Li for his countless advice on CTF, fancy image filters and other aspects of microscopy. Garrett Greenan taught me about levels of sassiness that I didn't even imagine existed. Finally, I would like to thank Ray Wang for being so pumped up about Hsp90 and all his help with Rosetta.

I would like to thank the current grad students in the lab, especially the "Rose and bros" group, ie Daniel Elnatan, Andrew Lyon, Rose Citron and Miguel Betegon. Anyone who has interacted with Daniel for at least a minute knows how enthusiastic, positive and helpful he can be. Also, I have spent countless hours with Daniel tinkering with random electronic projects, discussing new ways of 3D printing stuff, on different image processing algorithms, and other things. I have spent probably the same amount of hours discussing all sorts of things with Miguel, from conversion of matter into information, to what may possibly exist in world of infinite universes. Its been awesome! I would like to thank Rose for her always unique yet well thought out point of view on things and also

for encouraging me to go to the symphony and the ballet. Also, thanks for letting me ride your scooter, that thing probably saved me from dozens of hours of being stuck in traffic! I would like to thank Andrew for being so fancy, I feel just being around him I would become a little bit classier. Also, he has all kinds of knowledge on Bayesian statistics and it probably helped me out during my PhD.

Mariano Tabios and Joyce Ramponi deserve a special thanks, and not just because without them lab would seize functioning. Joyce has been incredibly helpful at isolating me from all kinds of administrative things, where due to her hard work things just happen. Also, the crabbing trips are amazing, thanks for organizing them! Mariano not just makes sure that the lab runs like a well-oiled machine, but also sets a very positive atmosphere in the lab, where you can always talk to him about your experiments and somehow feel better afterwards. Also, Mariano pushed my skiing limits, without him snowboarding would be neither as fun nor would I have improved this much. Finally he is also my neighbor and I couldn't ask for a better neighbor!

There are many people at UCSF outside of the lab I need to thank. First of all, I need to thank my thesis committee, Carol Gross and Natalia Jura. They have been incredibly supportive and helpful during my thesis work. I also would like to thank many other faculty at UCSF with whom I would randomly talk in lunch lines or at social hour, and they would remember what I actually worked on, ask me questions and actually care about the project. These sort of interactions are what makes UCSF so special.

I would like to thank TeamCCB, ie Noel Jee, Justin Rettenmaier, Daniel Kaemmerer and Aaron Mendez. Without them first two years wouldn't so much fun, from card counting in rural casinos to doing business plan competitions, it has been awesome. I

got to thank Adam Larson for being my banya and junk-yard buddy. Justin Farlow always supplied me with fresh venison, good big ideas and working with him has always been a pleasure, be it TAing pharmacy students or building a rally car together. Finally, Natalie Petek from my class has been awesome, super helpful and supportive. Without our beer and coffee sessions grad school would be that much more stressful.

Countless people outside UCSF either made me going to grad school possible at all and/or been incredibly helpful during my PhD. First, I would like to thank my undergraduate research advisers, Miriam Segura-Totten and Carla Mattos. They really gave me tons of freedom and advice, I learned a ton, and most importantly got super excited about science and biophysics in particular. Without them I in no way would be where I am now. I would like to thank my close high school friends, Kabir and Ankit. Even though we all are in different parts of the country, they would always find time and ways to come and visit and have always been supportive.

I would of course like to thank my family. My dad from very early age would encourage experimentation and physical based way of thinking. My sister and mom are responsible for me coming to US, getting me through college and supporting me through grad school, and I am forever indebted to them. I had countless scientific and other conversations with my brother in law, which certainly had a big impact on me.

Finally I would like to thank my spouse, Maria. She has been such an irreplaceable part of my life in the past ten years that it is hard to imagine what it would be like without her. Really, thank you for everything, for all the support, understanding, and love.

Abstract

The Hsp90 molecular chaperone and its Cdc37 co-chaperone help stabilize and activate over half of the human kinome. However, neither the mechanism by which these chaperones assist their client kinases nor why some kinases are addicted to Hsp90 while closely related family members are independent is known. Missing has been any structural understanding of these interactions, with no full-length structures of human Hsp90, Cdc37 or either of these proteins with a kinase. My thesis work focused on characterizing these interactions on a molecular level. I started with *in vitro* investigation of interactions between Hsp90/Cdc37 and Her2 kinase domain, only to find that under most conditions these proteins didn't form a complex, although there was a subtle difference in kinase activity in response to Hsp90. I also was able to form *in vitro* complex between Hsp90/Cdc37 and bRaf kinase and followed this up by some preliminary biochemical characterization and EM. However, the main focus of my work was cryoEM work on Hsp90/Cdc37/Cdk4 kinase complex, where I was able to attain a 3.9Å reconstruction of this complex. In this structure, Cdk4 is in a novel conformation, with its two lobes completely separated. Cdc37 mimics part of the kinase N-lobe, stabilizing an open kinase conformation by wedging itself between the two lobes. Finally, Hsp90 clamps around the unfolded kinase β5 strand and interacts with exposed N- and C-lobe interfaces, safely trapping the kinase in an unfolded state. Based on this novel structure, extensive previous data, and also recent advancements from other groups I propose a new model of kinase activity and regulation.

Table of Contents

List of Tables:

Chapter 1:

List of Figures:

Chapter 1:

Chapter 2:

Chapter 3:

Introduction

Hsp90 (Heat Shock Protein 90 kDa) is an essential chaperone in all eukaryotes(*1, 2*). It is highly conserved from bacteria to humans, and is abundantly expressed, at levels up to 2 percent of the total cell protein during stress conditions. Although Hsp90 promotes folding of nascent polypeptide chains like canonical chaperones, Hsp90 is unique in that it directly facilitates function by activating proteins for protein-protein and protein ligand interactions and blocking degradation by the proteasome.

Many Hsp90 substrate "clients" are key players in cell signaling pathways. Clients include steroid hormone receptors, like the glucocorticoid and estrogen receptors, key signaling kinases, like Cdk4, Raf, Src and Her2 receptor kinase, polymerases and E3 ubiquitin ligases and telomerase. By interacting with many different signal transduction systems, Hsp90 regulates multiple aspects of cellular activity including cell proliferation, DNA maintenance, mitochondrial import and protein degradation. Remarkably, about 10 percent of yeast proteome has been estimated to be dependent on Hsp90. The heterogeneity of this group is vast, with protein sizes ranging from 20 kDa immunophilins to huge complexes such as telomerase. How Hsp90 can retain specificity while interacting with so many different substrates is a major question in the field.

Recently, much has been learned about Hsp90 mechanistically. Crystal structures of bacterial Hsp90 without nucleotide and with ADP were solved by the Agard group(*3*) and an ATP bound yeast homologue was solved by the Pearl group(*4*). Hsp90 exists as an obligate dimer. Each monomer consists of three domains, N-terminal, middle and C-terminal domain, with C-terminal domains constituting the dimerization interface. The N-terminal domain binds and hydrolyzes ATP. Hsp90 undergoes large conformational

changes upon ATP binding and hydrolysis. It has been shown by Small Angle X-Ray Scattering (SAXS) and Electron Microscopy (EM) that the conformations of Hsp90 represented in the crystal structures are only snapshots of a much larger range of domain movement that is likely important for recognition of such a diverse substrate repertoire(*5*). The cycle of ATP hydrolysis is indispensable for Hsp90's activity on its substrates, where inhibition of hydrolysis with drugs such as Geldanamycin(GA) leads to client instability(*6*). Latest biochemical evidence and crystal structure from our lab indicates that hydrolysis of ATP by Hsp90 is sequential and goes through an asymmetric state(*7*)(*8*). Hsp90 also interacts with many co-chaperones, like Hop, Cdc37, p23 and chaperones, like Hsp40 and Hsp70, which potentially may leverage some of this asymmetry. Some co-chaperones regulate the Hsp90 ATPase cycle (*e.g.* p23, Aha1), others are involved in general substrate loading (Hop, Hsp40/70) and maturation (immunophilins), while others act to recruit specific classes of substrates such as kinases by Cdc37, however the exact functional roles of these chaperones are unknown.

Despite its obvious importance and extensive effort, answers to fundamental questions of how Hsp90 recognizes its clients and how Hsp90 uses the energy of ATP binding and hydrolysis to fold/activate its clients remained unanswered. This is likely due to the experimental challenges associated with Hsp90's conformational flexibility, instability of its substrates, and overall complexity of the Hsp90 pathways. However, due to the importance of Hsp90's clients, elucidating these questions promises great rewards, in terms of basic understanding of the molecular and cellular biology and advancement of clinical sciences.

To address these questions, I chose to investigate interactions between Hsp90 and

kinases during my thesis work. During first 2-3 years I was focused on interactions between Hsp90 and Her2 kinase domain, trying to build the system bottom up, from purified components, as is described in more detail in Chapter 2. However, after much effort, although progress was made, I was not able to establish interactions that were amenable to immediate structural or biochemical investigations. I also investigated another system, with solubilized bRaf V600E kinase domain. I did some preliminary experiments with it by negative stain EM and NMR, which are also described in Chapter 2.

Our collaborator, Akhiko Arakawa from Yokoyama lab at RIKEN was working on the same problem but with a Cdk4 kinase. His approach however was different, where based on the previous work(*9*) he was trying to co-purify Hsp90/Cdc37/Cdk4 kinase from insect cells for crystallography, via overexpression of these proteins. Crystallization was not going well so we started a collaboration where he provided the sample and I studied it by cryoEM. We were able to obtain a high-resolution structure of the complex, which led to a paper in Science(*10*) that is reproduced in Chapter 1 of this thesis. In Chapter 3 I will draw conclusions on the work I have done, mainly the cryoEM structure and how it incorporates together with the latest progress in the field. This chapter is based on review article currently in preparation. In chapter 4 I will briefly discuss future directions.

1. L. M. Gierasch, A. Horwich, C. Slingsby, S. Wickner, D. Agard, in *Series in structural biology Vol. 6*. (World Scientific, New Jersey, 2016), pp. 1 online resource (vii, 319 pages).
2. M. Taipale, D. F. Jarosz, S. Lindquist, HSP90 at the hub of protein homeostasis:

emerging mechanistic insights. *Nat Rev Mol Cell Biol* **11**, 515-528 (2010).

3. A. K. Shiau, S. F. Harris, D. R. Southworth, D. A. Agard, Structural Analysis of E. coli hsp90 reveals dramatic nucleotide-dependent conformational rearrangements. *Cell* **127**, 329-340 (2006).
4. M. M. Ali *et al.*, Crystal structure of an Hsp90-nucleotide-p23/Sba1 closed chaperone complex. *Nature* **440**, 1013-1017 (2006).
5. K. A. Krukenberg, D. R. Southworth, T. O. Street, D. A. Agard, pH-dependent conformational changes in bacterial Hsp90 reveal a Grp94-like conformation at pH 6 that is highly active in suppression of citrate synthase aggregation. *J Mol Biol* **390**, 278-291 (2009).
6. M. Sakagami, P. Morrison, W. J. Welch, Benzoquinoid ansamycins (herbimycin A and geldanamycin) interfere with the maturation of growth factor receptor tyrosine kinases. *Cell Stress Chaperones* **4**, 19-28 (1999).
7. L. A. Lavery *et al.*, Structural asymmetry in the closed state of mitochondrial Hsp90 (TRAP1) supports a two-step ATP hydrolysis mechanism. *Mol Cell* **53**, 330-343 (2014).
8. Daniel Elnatan, Miguel Betegon, Yanxin Liu, Theresa Ramelot, Michael A Kennedy, David Agard. Symmetry broken and rebroken during the ATP hydrolysis cycle of the mitochondrial Hsp90 TRAP1. bioRxiv doi:10.1101/107094
9. C. K. Vaughan *et al.*, Structure of an Hsp90-Cdc37-Cdk4 complex. *Mol Cell* **23**, 697-707 (2006).
10. K. A. Verba *et al.*, Atomic structure of Hsp90-Cdc37-Cdk4 reveals that Hsp90

traps and stabilizes an unfolded kinase. *Science* **352**, 1542-1547 (2016).

Chapter 1.

Atomic structure of Hsp90:Cdc37:Cdk4 reveals Hsp90 regulates kinase via dramatic unfolding.

Kliment A. Verba[1], Ray Yu-Ruei Wang[1], Akihiko Arakawa[2], Yanxin Liu[1], Mikako Shirouzu[2], Shigeyuki Yokoyama[2], David A. Agard[1].

Affiliations:

[1]Howard Hughes Medical Institute and the Department of Biochemistry & Biophysics, University of California San Francisco, San Francisco, CA 94158, USA.

[2]RIKEN Systems and Structural Biology Center, 1-7-22 Suehiro-cho, Tsurumi-ku, Yokohama 230-0045, Japan.

Abstract: The Hsp90 molecular chaperone and its Cdc37 co-chaperone help stabilize and activate over half of the human kinome. However, neither the mechanism by which these chaperones assist their client kinases nor why some kinases are addicted to Hsp90 while closely related family members are independent is known. Missing has been any structural understanding of these interactions, with no full-length structures of human Hsp90, Cdc37 or either of these proteins with a kinase. Here we report a 3.9Å cryoEM structure of the Hsp90:Cdc37:Cdk4 kinase complex. Cdk4 is in a novel conformation, with its two lobes completely separated. Cdc37 mimics part of the kinase N-lobe, stabilizing an open kinase conformation by wedging itself between the two lobes. Finally, Hsp90 clamps around the unfolded kinase β5 strand and interacts with exposed N- and C-lobe interfaces, safely trapping the kinase in an unfolded state. Based on this novel structure and extensive previous data, we propose unifying conceptual and mechanistic models of chaperone-kinase interactions.

The human kinome is responsible for regulating about a third of all proteins through phosphorylation(*1*). Proper regulation of this process is important, as misregulated kinase activity can lead to cell death and disease(*2*). To achieve fine regulation, kinase activity can be sensitively modulated by multiple allosteric inputs. Thus, kinase domains are organized so that dispersed small structural changes caused by binding of regulatory domains/proteins or phosphorylation, can significantly alter kinase activity. Examples of such regulator interactions abound, via SH2/SH3 domains for Src family kinases, dimerization for EGFR or Raf family kinases, and cyclin regulation for Cdks being well characterized examples(*3*).

Beyond these specific regulators, the Hsp90 molecular chaperone, a member of the general cellular protein folding machinery, also plays a fundamental role in the regulation of many kinases(*4*). While usually chaperones facilitate the early steps of protein folding, Hsp90 also functions late in the folding process to help both fold and activate a set of protein "clients" (~10% of the proteome)(*5*). Notably ~60% of the human kinome interacts with Hsp90 with the assistance of its kinase specific cochaperone Cdc37(*6*). Pharmocologic inhibition of Hsp90 leads to rapid ubiquitinylation and degradation of client kinases. As many Hsp90/Cdc37-dependent kinases are key oncoproteins, (vSrc, bRafV600E, Her2, etc.) several Hsp90 inhibitors are undergoing clinical trials as cancer therapeutics(*7*).

Hsp90 is a well conserved, but highly dynamic molecular machine. Each monomer within the Hsp90 dimer has three structural domains: a C-terminal domain (CTD) responsible for dimerization; a middle domain (MD) implicated in client binding; and the N-terminal domain (NTD) that binds ATP. Without bound nucleotide, Hsp90

mostly populates a variety of "open" states, whereas nucleotide binding promotes formation of a closed state in which the NTDs also dimerize, followed by hydrolysis(*8, 9*). The rates of closure and hydrolysis are homologue specific, with human cytosolic Hsp90s almost always open, while yeast Hsp90 preferentially adopts a fully closed state (*10*). Towards the end of the NTD is a highly charged region ("charged linker") that shows wide variation in length and composition between species. The function and the structure of the charged linker are unclear, but deletion can impact Hsp90 function(*11*).

Cdc37 is less well studied. The monomeric protein can also be divided into three domains: an N-terminal domain of unknown structure that interacts with kinases, a globular middle domain which interacts with Hsp90 and an extended C terminal domain, of unknown function(*12*). Although there is a cocrystal structure of the Cdc37 middle/C domains (Cdc37 M/C) bound to the Hsp90-NTD(*13*), there is evidence that Cdc37 may also interact with the MD of Hsp90(*14*). Phosphorylation of Cdc37 serine 13 plays an important role, providing stabilizing interactions *in vitro(15)* and being functionally necessary *in vivo(16)*.

Although there is a wealth of *in vivo* data, a physical understanding of how Hsp90 and Cdc37 facilitate kinase function is lacking. Equally unclear is why some kinases are strongly Hsp90-dependent whereas closely related kinases are Hsp90-independent. Despite numerous attempts to identify a consistent motif responsible for Hsp90 interaction, the only general trend that has emerged is that client kinases appear to be less thermally stable than non-clients(*6*). In support of this, binding of kinase inhibitors or allosteric regulators reduce Hsp90 interactions(*17, 18*). While reasonable that less stable kinases might depend on Hsp90, it remains unclear why this happens or what Hsp90

recognizes. Despite its obvious value, obtaining a crystal structure of an Hsp90:Cdc37:kinase complex has been unsuccessful due to the dynamic nature of Hsp90-client interactions, and challenges in reconstituting the complex. Encouraged by previous negative stain EM studies(*19*) and the recent advances in cryoEM detectors and processing methodologies that together make analysis of such a small, asymmetric complex feasible(*20*), we undertook cryoEM studies of the human 240KDa Hsp90:Cdc37:Cdk4 kinase complex.

Complex formation and cryoEM structural analysis

Human homologues of all three proteins were co-expressed in Sf9 insect cells. A stable ternary complex that survived rigorous dual-tag purification formed in the presence of molybdate (Fig S1). Although the mode of molybdate action is unknown, it affects Hsp90's hydrolysis rate and helps stabilize Hsp90-client interactions(*21*). Simply mixing components individually purified from insect cells did not yield any detectable complex; therefore either post translational modifications specific to the complex or other components (like Hsp40/Hsp70) are required. Despite significant effort to optimize conditions and image processing, preferential particle orientation and conformational heterogeneity limited initial reconstructions from data collected in house to about 6-8Å resolution. To move forward a much larger data set was collected at National Resource for Automated Molecular Microscopy (NRAMM)(*22*). Data quality was verified as 2D classification of ~800,000 initially picked particles yielded classes with visible high-resolution features (Fig S2). 3D classification and refinement resulted in a 4Å map (Fig S3, S4 and Table S1), with most of Hsp90 being better resolved (3.5Å), while the lowest

resolution regions were around 6Å (Fig 1A).

Hsp90 is in a closed conformation in the complex

Refining the 4Å map with a tighter mask around Hsp90 generated a higher resolution, 3.9Å density for Hsp90 and neighboring regions (Fig. 1B inserts)(*22*). This map was of sufficient quality to accurately build and refine an atomic model of human Hsp90 based on a homology model derived from yeast Hsp90 (Fig 1B and S5). Surprisingly, reconstructions of complex prepared with Hsp90 with deleted charged linker never yielded good results, likely due to increased heterogeneity. Hsp90 adopts a symmetrical (RMSD between monomers=0.82Å), closed conformation, closely resembling the yHsp90 closed state(*23*). This was unexpected, as without crosslinker, closed hHsp90 had not previously been observed. While the molybdate added during purification may contribute, the closed state is likely a consequence of the ternary complex. In our map, which was refined without symmetry, the strongest density is symmetric at the γ-phosphate location for nucleotide binding sites at both NTDs of Hsp90 (Fig S6). This suggests that either the complex traps Hsp90 in an ATP state, or, more likely, ADP-molybdate acts as a post hydrolysis transition state inhibitor, thereby helping stabilize the closed conformation. The hHsp90 model determined here is similar to the yeast Hsp90 (RMSD=1.59Å), with a small rotation in the CTD and correlated movements throughout (Movie S1). Additionally, a number of loops disordered in the crystal structure were ordered in our model, as they were interacting with the kinase. (Fig 2B) The charged linker is visible in 2D classes, but absent from the 3D reconstruction, suggesting a highly flexible structure (Fig S2).

The N-lobe of Cdk4 is significantly unfolded and threads through Hsp90

Two regions of the 4Å map cannot be accounted for by Hsp90: a long coiled-coil like protrusion and a globular density on one side of Hsp90 (arrows, Fig 1B). While we initially suspected that these corresponded to the Cdc37M/C (globular domain with long helix), as our map improved the globular domain fit became worse. To obtain an unbiased fit, an exhaustive search was performed against all protein folds in the CATH database (~16000 PDBs) (*22*). Disregarding algorithmic errors, the top scoring hits were all variations on the kinase C-lobe, with Cdc37M/C scoring considerably worse (Fig S7). Based on this, the Cdk4 C-lobe was placed into the density(*24*), resulting in a high quality fit (Fig 2A). By contrast, not only no suitable density exists for the folded kinase N-lobe but it would sterically clash with Hsp90. Remarkably, tracing the kinase density from the C-lobe towards the N-terminus, there was a clear tubular region going through the lumen of Hsp90 (Fig 2A, 2B). Thus, a drastically altered conformation of the kinase N-lobe is being stabilized by Hsp90. (Movie S2) Threading the Cdk4 sequence into this density, reveals that β4 and β5 strands have been ripped apart and instead □5 interacts with a previously mapped general Hsp90 client binding site via extensive hydrophobic interactions(*25*) and two salt bridges (Fig 2C). Potentially due to these interactions, there is a rotation of Hsp90 CTD towards the kinase (as compared to yHsp90 structure) at the MD:CTD interface, which was identified as asymmetric in previous work(*26*) (Movie S1). Altogether this suggests that the MD:CTD interface may be used to communicate Hsp90's hydrolysis state to the client. Unfortunately, in the highest resolution map no density was visible for kinase residues N-terminal of the β5 strand.

Cdc37 is split into two domains and wraps around Hsp90

While there is no available 3D structural information for the Cdc37 N-terminal domain, sequence analysis (MARCOIL) predicts significant coiled coil structure. Supported by our observations of high helical content by CD and NMR (Fig S8), this provides a good candidate for the non-globular map density (Fig 1B). That density, transitions from helical to strand like, wrapping around the Hsp90MD and adding an additional β-strand to the 1AC β-sheet (2CG9 nomenclature). Unfortunately, as with the kinase, this □□strand does not connect to any density on the other side, thwarting a complete fit of Cdc37. Showing the power of single particle cryoEM, local rounds of 3D classification yielded a 7Å map (Fig S3, S9) showing clear globular density that connected through the β−strand to the coiled-coil region (Fig 3A). This new density was unambiguously fit by the crystallized Cdc37M/C fragment. Using a combination of the two maps, we were able to fit Cdc37M/C residues 148-260 and de-novo build residues 1-147 of human Cdc37 (Fig 3A) (*22*). Although further classification revealed some density beyond residue 260, it was too weak to model with confidence.

Locating the remainder of the kinase N-lobe and verification

The local 3D classification also revealed the remainder of the kinase N-lobe (Fig 3B and Movie S3). In two of the classes, distinct globular densities were visible that connected to the tubular density derived from the unfolded Cdk4 N-lobe. At the same time, the density for the middle domain of Cdc37 was either very weak or absent, suggesting an anti-correlation between Cdc37M/C:Hsp90 interactions and kinase N-

lobe:Hsp90 interactions. We were able to roughly fit the rest of the Cdk4N lobe into these densities, allowing us to build a complete model of Hsp90:Cdc37:Cdk4 complex (Fig 4 and Movie S4). Given the unusual split domain conformation for both the kinase and cochaperone, it was important to verify our structural assignments. Towards that end, we covalently tagged Cdc37 at its N terminus and Cdk4 at its C terminus with T4 lysozyme. The two different complexes were expressed and purified from yeast, followed by cryoEM reconstruction of each. These two structures clearly show lysozyme density consistent with our map interpretation (Fig S10).

Cdc37 precisely mimics a conserved feature of kinase N-lobe-C-lobe interactions and makes novel interactions with Hsp90

There are a number of striking features from the resulting model (Fig 4) that explain a wealth of accumulated, seemingly contradictory observations. The Cdc37NTD forms a long coiled-coil with a leucine zipper like motif. The N-terminus of this coiled-coil interacts with Cdk4 through extensive hydrophobic and hydrogen bonding interactions, burying 725 $Å^2$ (Table S2) in surface area, and mimicking interactions that the kinase αC-β4 loop normally makes with the C-lobe (Fig 5A). More strikingly, the following loop in Cdc37, overlays perfectly with the αC-β4 loop of multiple kinases, packing tightly against the kinase C lobe (Fig 5A, bottom insert), explaining why this Cdc37 region is so conserved (Fig. S11). Thus Cdc37 binds to the kinase C-lobe by mimicking interactions the N-lobe would normally have made, stabilizing separation of the two kinase lobes.

The interactions between Cdc37 and Hsp90 are significantly different from those

seen in the previous crystal structure of fragments of each protein. Instead of binding to an Hsp90NTD surface that would only be accessible in the open state, in the Hsp90 closed state, Cdc37M/C interacts with Hsp90MD, although these interactions are fairly limited (only about 340Å^2 out of 2650Å^2 total buried surface area) (Fig 4). More extensive are interactions from Cdc37 residues 120-129, which pack a β-strand against Hsp90 MD (Fig 5B). Additionally part of the Cdc37NTD binds to a new site on the closed Hsp90NTD, somewhat mimicking interactions seen between p23 and Hsp90 (Fig 5B, top insert). There is also a network of ionic interactions between Cdc37NTD and Hsp90MD, which explains previously identified salt sensitivity of Cdc37/Hsp90 binding (Fig 5B, bottom insert). Our structure thus helps explain recent data that *C. elegans* Cdc37 interacts with the middle domain of Hsp90(*27*), rather than the NTD as observed in previous human domain binding studies. Instead of assuming that *C. elegans* is different or that the interactions observed with isolated domains were incorrect, we propose that Cdc37/kinase first binds Hsp90 in its open conformation as seen in the crystal structure, and then rearranges to the site on the middle domain upon Hsp90 closure, as seen in our structure.

Phosphorylation of Cdc37 stabilizes kinase bound conformation

Phosphorylation at the completely conserved Cdc37:S13 is important for kinases to function, and was thought to be directly involved in kinase binding (*15,16*). In our structure there is density for the phosphorylated-serine13, which forms a salt bridge with Cdc37:R36 and Cdc37:H33, stabilizing the very N-terminus of the coiled coil (Fig 5B middle insert). This provides a molecular rationale for previous observations of a Cdc37

conformational change upon phosphorylation(*28*). Of note, this phosphate also contributes to the overall electrostatic nature of Hsp90-Cdc37 interactions, forming a salt bridge with Hsp90:K406.

The residues comprising Cdc37/Hsp90NTD and Cdc37/kinase interaction surfaces are extremely well conserved (Fig S11), further validating the significance of the interactions observed here.

Hsp90/Cdc37 capture and stabilize structural transitions within the kinase

In ternary complex, Cdk4 assumes a conformation drastically different than previously seen for any kinase structure. The kinase hinge region and β4-β5 sheets are completely unfolded, with the N lobe and C lobe being pried apart and stabilized by new interactions with Hsp90 and Cdc37. Based on this, we propose a model where it is not a specific binding sequence, but the propensity for the kinase to unfold to a N-lobe/C-lobe separated open state, that determines whether a particular kinase will be a client. Furthermore, the fact that many non-client kinases depend on Hsp90 during initial folding would suggest that the open kinase state we observe is an on pathway folding intermediate.

In agreement with the model, the β3-αC loop of Cdk4 (strong client) has seven glycines versus one/two glycines in the same loop of Cdk2 and Cdk6 (non client and weak client respectively). Mutating this loop in Cdk4 to the Cdk6 sequence stabilizes the protein(*29*). In a similar manner, a single point mutation derived from EGFR (non-client) in the αC-β4 loop was able to abrogate the interactions of HER2 (strong client) with, and dependence on, Hsp90/Cdc37(*30*). This point mutation would potentially introduce a salt

bridge stabilizing the kinase loop (Fig S12), and hence the association between the kinase lobes.

Our model explains why a sequence motif responsible for Hsp90 interactions has yet to be found. The remarkable allostery of kinases allows distant and seemingly un-related mutations to destabilize the N-lobe/C-lobe interface explaining often confusing mutagenesis results between individual kinases. The same allostery is used by Hsp90 non-client kinases to exit Hsp90 dependence after initial folding, by making stabilizing interactions with regulatory partners/extra domains (cyclin, dimerization partners, SH2/SH3 domains, etc.)

Linking kinase unfolding to assembly and activity

Given such a model, why might it be beneficial for a large percentage of human kinases to significantly populate a folding intermediate even when mature? Rather than being a vestige of the kinase evolutionary past, with Hsp90 buffering gain of function destabilizing mutations (*31*), we argue that being able to safely populate such an open folding intermediate has a direct functional/regulatory benefit. Recent computational efforts have suggested a connection between folding and kinase activity(*32, 33*). The concept is that the most favorable way to transition between the inactive and active states is to transition through a more open, unfolded state rather than through a more classical rigid-body transition. Although the opening transition seen in simulations is far more subtle than that observed here, we suggest that the concept still applies (Fig 6A). The generally lower stability of client kinases would lead to enhanced sampling of the open state, thereby encouraging chaperone binding (Fig 6B). Chaperone stabilization of a

kinase open state could increase the overall rates of interconversion and/or protect a potentially vulnerable state from either aggregation or recognition by the ubiquitinylation machinery. Moreover, the open state could be the preferred substrate for adding/removing post-translational modifications as well as for facilitating a dynamic equilibrium with critical stabilizing interactions.

Life cycle of kinase:Hsp90:Cdc37 interactions

Our structure also provides a basis for speculation on how the observed state might arise and mature (Fig 6C). Hsp90 would first interact with Cdc37/kinase via previously published crystal structure contacts (Fig 6C, state II). Whether assistance from Hsp70/Hsp40 as with the glucocorticoid receptor would be required at this step is yet unclear(*34*), but the inability to directly form the complex from components and Chk1 reconstitution experiments(*35*) are suggestive. During the cycle, Cdc37 would act as a quality control checkpoint, where only upon proper folding of the N-lobe would it dissociate from the kinase. Long coiled-coil would allow Cdc37/kinase to stay attached to Hsp90 during multiple ATP hydrolysis events. If the kinase would fail to dissociate after many hydrolysis events, one can imagine degradation machinery being recruited to the complex. While Fig 6C captures the essence of the available data, other models are possible.

Beyond revealing the kinase open state, our cryo EM reconstruction allowed us to build first atomic models for the human cytosolic Hsp90 and the kinase interacting N terminus of Cdc37. The ability to collect a large number of particles coupled with the capabilities of single electron counting detectors and 3D classification software, allowed

us to visualize multiple conformations, providing a qualitative assessment for the dynamic nature of the complex. Overall, our structure has explained a number of often contradictory, biochemical observations and provided both mechanistic and conceptual models of Hsp90:kinase interactions, that can be tested in future experiments. It also indicates the potential of single particle cryoEM for exploring other challenging dynamic, asymmetric complexes at near atomic resolution.

References

1. S. S. Taylor, M. M. Keshwani, J. M. Steichen, A. P. Kornev, Evolution of the eukaryotic protein kinases as dynamic molecular switches. *Philos Trans R Soc Lond B Biol Sci* **367**, 2517-2528 (2012).
2. J. Zhang, P. L. Yang, N. S. Gray, Targeting cancer with small molecule kinase inhibitors. *Nat Rev Cancer* **9**, 28-39 (2009).
3. J. A. Endicott, M. E. Noble, L. N. Johnson, The structural basis for control of eukaryotic protein kinases. *Annu Rev Biochem* **81**, 587-613 (2012).
4. J. Brugge, W. Yonemoto, D. Darrow, Interaction between the Rous sarcoma virus transforming protein and two cellular phosphoproteins: analysis of the turnover and distribution of this complex. *Mol Cell Biol* **3**, 9-19 (1983).
5. M. Taipale, D. F. Jarosz, S. Lindquist, HSP90 at the hub of protein homeostasis: emerging mechanistic insights. *Nat Rev Mol Cell Biol* **11**, 515-528 (2010).
6. M. Taipale *et al.*, Quantitative analysis of HSP90-client interactions reveals principles of substrate recognition. *Cell* **150**, 987-1001 (2012).

7. Y. Miyata, H. Nakamoto, L. Neckers, The therapeutic target Hsp90 and cancer hallmarks. *Curr Pharm Des* **19**, 347-365 (2013).

8. K. A. Krukenberg, T. O. Street, L. A. Lavery, D. A. Agard, Conformational dynamics of the molecular chaperone Hsp90. *Q Rev Biophys* **44**, 229-255 (2011).

9. M. P. Mayer, L. Le Breton, Hsp90: breaking the symmetry. *Mol Cell* **58**, 8-20 (2015).

10. D. R. Southworth, D. A. Agard, Species-dependent ensembles of conserved conformational states define the Hsp90 chaperone ATPase cycle. *Mol Cell* **32**, 631-640 (2008).

11. S. Tsutsumi *et al.*, Charged linker sequence modulates eukaryotic heat shock protein 90 (Hsp90) chaperone activity. *Proc Natl Acad Sci U S A* **109**, 2937-2942 (2012).

12. J. Shao, A. Irwin, S. D. Hartson, R. L. Matts, Functional dissection of cdc37: characterization of domain structure and amino acid residues critical for protein kinase binding. *Biochemistry* **42**, 12577-12588 (2003).

13. S. M. Roe *et al.*, The Mechanism of Hsp90 regulation by the protein kinase-specific cochaperone p50(cdc37). *Cell* **116**, 87-98 (2004).

14. J. M. Eckl *et al.*, Cdc37 (cell division cycle 37) restricts Hsp90 (heat shock protein 90) motility by interaction with N-terminal and middle domain binding sites. *J Biol Chem* **288**, 16032-16042 (2013).

15. S. Polier *et al.*, ATP-competitive inhibitors block protein kinase recruitment to the Hsp90-Cdc37 system. *Nat Chem Biol* **9**, 307-312 (2013).

16. C. K. Vaughan *et al.*, Hsp90-dependent activation of protein kinases is regulated

by chaperone-targeted dephosphorylation of Cdc37. *Mol Cell* **31**, 886-895 (2008).

17. M. Taipale *et al.*, Chaperones as thermodynamic sensors of drug-target interactions reveal kinase inhibitor specificities in living cells. *Nat Biotechnol* **31**, 630-637 (2013).

18. E. E. Boczek *et al.*, Conformational processing of oncogenic v-Src kinase by the molecular chaperone Hsp90. *Proc Natl Acad Sci U S A* **112**, E3189-3198 (2015).

19. C. K. Vaughan *et al.*, Structure of an Hsp90-Cdc37-Cdk4 complex. *Mol Cell* **23**, 697-707 (2006).

20. Y. Cheng, Single-Particle Cryo-EM at Crystallographic Resolution. *Cell* **161**, 450-457 (2015).

21. S. D. Hartson, V. Thulasiraman, W. Huang, L. Whitesell, R. L. Matts, Molybdate inhibits hsp90, induces structural changes in its C-terminal domain, and alters its interactions with substrates. *Biochemistry* **38**, 3837-3849 (1999).

22. See methods and materials.

23. M. M. Ali *et al.*, Crystal structure of an Hsp90-nucleotide-p23/Sba1 closed chaperone complex. *Nature* **440**, 1013-1017 (2006).

24. T. Takaki *et al.*, The structure of CDK4/cyclin D3 has implications for models of CDK activation. *Proc Natl Acad Sci U S A* **106**, 4171-4176 (2009).

25. O. Genest *et al.*, Uncovering a region of heat shock protein 90 important for client binding in E. coli and chaperone function in yeast. *Mol Cell* **49**, 464-473 (2013).

26. L. A. Lavery *et al.*, Structural asymmetry in the closed state of mitochondrial Hsp90 (TRAP1) supports a two-step ATP hydrolysis mechanism. *Mol Cell* **53**, 330-343 (2014).

27. J. M. Eckl *et al.*, Hsp90.Cdc37 Complexes with Protein Kinases Form Cooperatively with Multiple Distinct Interaction Sites. *J Biol Chem* **290**, 30843-30854 (2015).

28. W. Liu, R. Landgraf, Phosphorylated and unphosphorylated serine 13 of CDC37 stabilize distinct interactions between its client and HSP90 binding domains. *Biochemistry* **54**, 1493-1504 (2015).

29. P. J. Day *et al.*, Crystal structure of human CDK4 in complex with a D-type cyclin. *Proc Natl Acad Sci U S A* **106**, 4166-4170 (2009).

30. W. Xu *et al.*, Surface charge and hydrophobicity determine ErbB2 binding to the Hsp90 chaperone complex. *Nat Struct Mol Biol* **12**, 120-126 (2005).

31. J. Lachowiec, T. Lemus, E. Borenstein, C. Queitsch, Hsp90 promotes kinase evolution. *Mol Biol Evol* **32**, 91-99 (2015).

32. O. Miyashita, J. N. Onuchic, P. G. Wolynes, Nonlinear elasticity, proteinquakes, and the energy landscapes of functional transitions in proteins. *Proc Natl Acad Sci U S A* **100**, 12570-12575 (2003).

33. Y. Shan, A. Arkhipov, E. T. Kim, A. C. Pan, D. E. Shaw, Transitions to catalytically inactive conformations in EGFR kinase. *Proc Natl Acad Sci U S A* **110**, 7270-7275 (2013).

34. E. Kirschke, D. Goswami, D. Southworth, P. R. Griffin, D. A. Agard, Glucocorticoid receptor function regulated by coordinated action of the Hsp90 and Hsp70 chaperone cycles. *Cell* **157**, 1685-1697 (2014).

35. S. J. Arlander *et al.*, Chaperoning checkpoint kinase 1 (Chk1), an Hsp90 client, with purified chaperones. *J Biol Chem* **281**, 2989-2998 (2006).

Acknowledgments

We thank members of NRAMM-Scripps for help collecting data, Yao Fan for the yeast expression vector, Naomi Ohbayashi and Mutsuko Niino (RIKEN Center for Life Science Technologies) for help with Sf9 protein expression, Dr. Neil F Rebbe (The University of North Carolina at Chapel Hill) and Dr. Ernest Laue (The University of Cambridge) for the plasmids encoding human HSP90b and Cdc37, respectively, D.A.A. lab members for helpful discussions and Natalia Jura for reading the manuscript. Support for this work was provided by PSI-Biology grant U01 GM098254 (to D.A.A.), AACR-BCRF Grant 218084 for Translational Breast Cancer Research (to D.A.A.), The Cabala Family gift (to D.A.A.), HHMI Helen Hay Whitney Foundation Fellowship (to Y.L.), HHMI International Student Research Fellowship (to K.V.) and the Howard Hughes Medical Institute (to D.A.A.). Some of the work presented here was conducted at NRAMM, which is supported by a grant from the National Institute of General Medical Sciences (9 P41 GM103310) from the National Institutes of Health. Some of the work used the Extreme Science and Engineering Discovery Environment (XSEDE), which is supported by National Science Foundation grant number ACI-1053575.

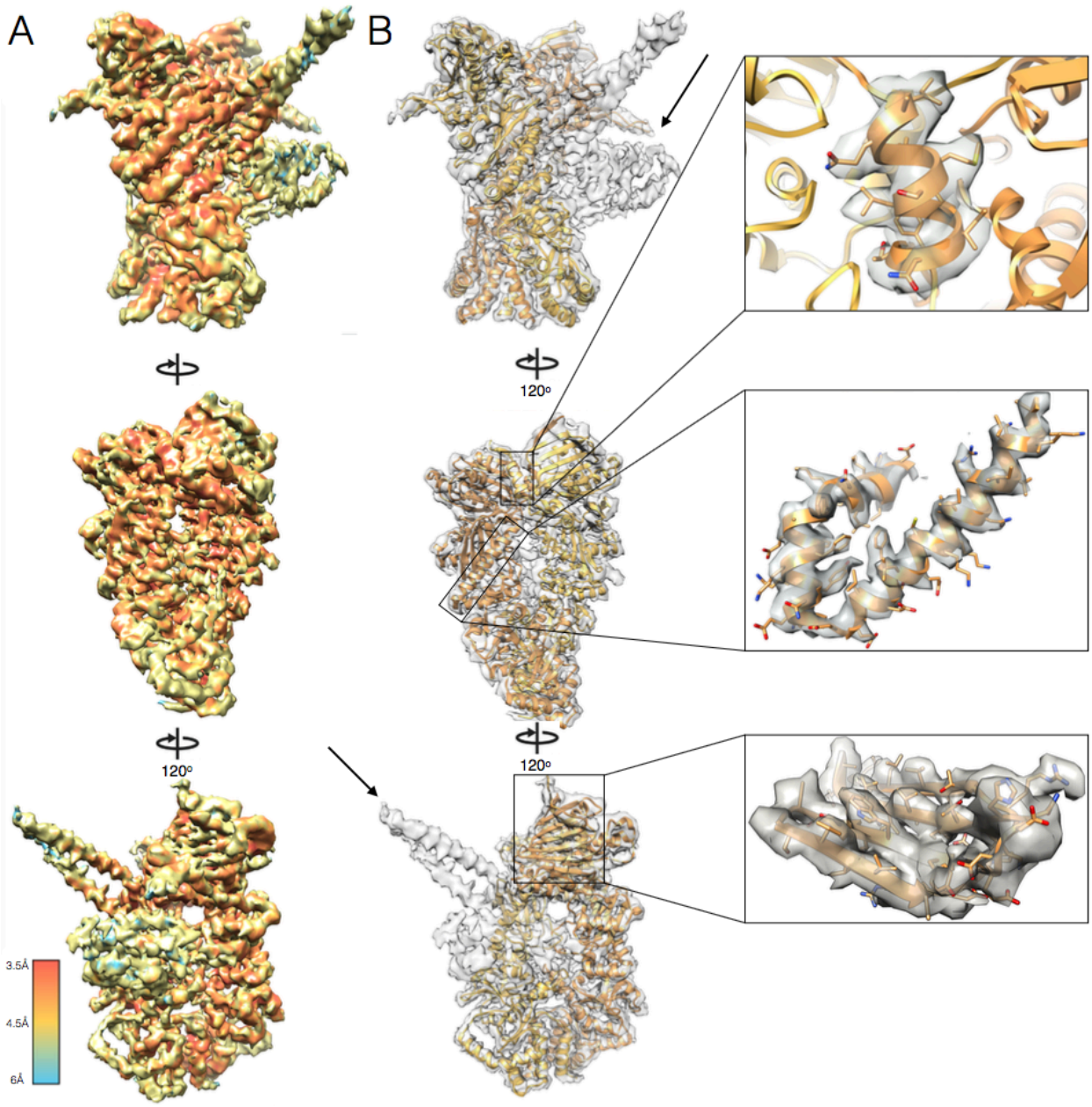

Fig. 1. The 4Å map of Hsp90/Cdc37/Cdk4.

(A) Density map colored by resolution. (B) hHsp90β model built into the density map, with different monomers colored shades of orange. Inserts show high resolution features. Arrows show density un-accounted for by Hsp90.

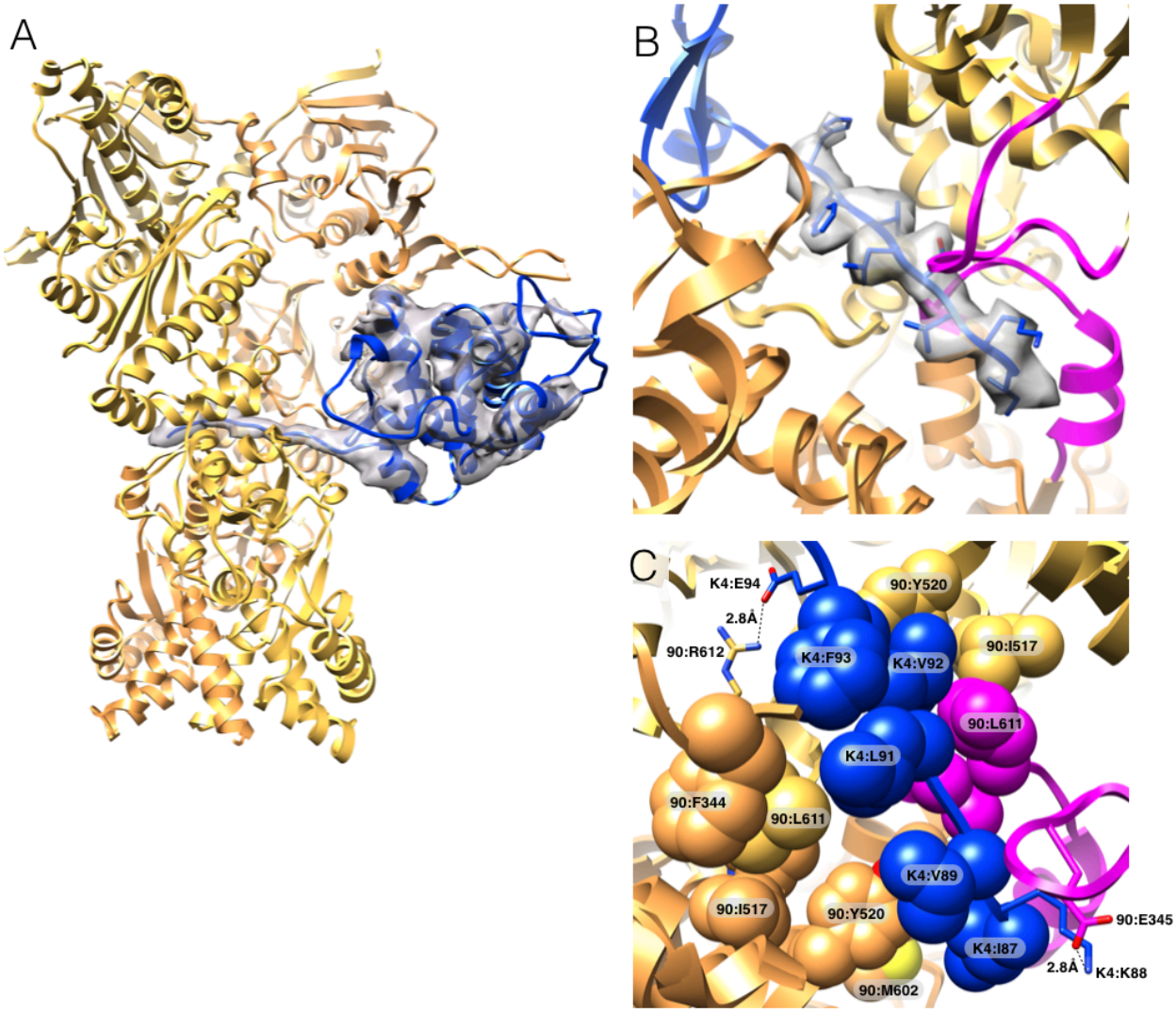

Fig. 2. Cdk4 is unfolded when complexed with Hsp90 and Cdc37

(A) Cdk4 (K4) C-lobe (blue) fit into the map (B) The tubular density from high-resolution map through the lumen of Hsp90 is perfectly fit by an unfolded β5 sheet (in sticks) of Cdk4. In magenta are previously disordered client interacting loops on Hsp90. (C) Cdk4/Hsp90 interface with hydrophobic residues in spheres, salt bridges in sticks.

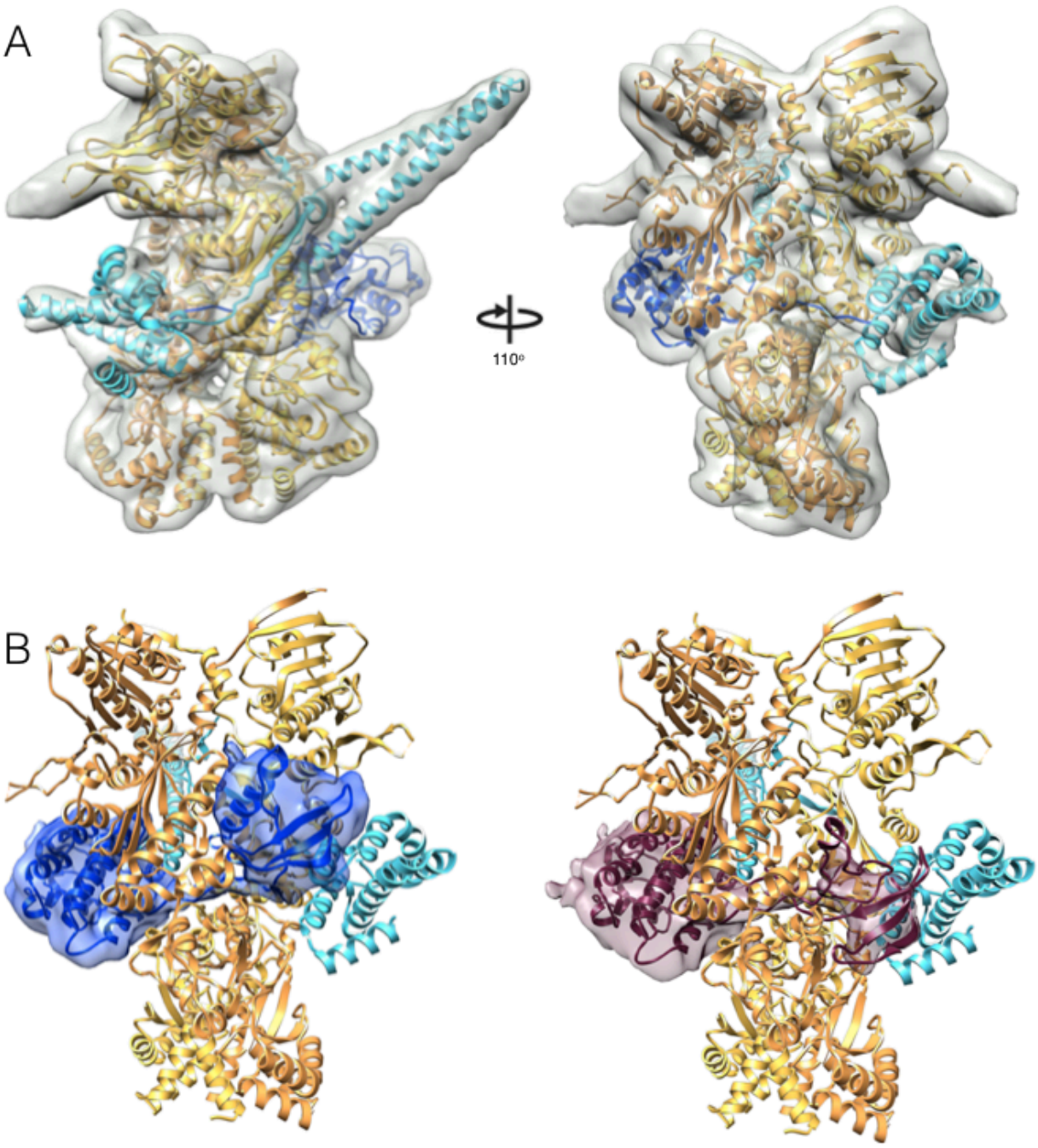

Fig. 3. Rounds of focused 3D classification yield distinct densities for Cdc37 and the Cdk4 N-lobe.

(A) One of the new classes has clear density for the Cdc37 (37) M/C fragment crystal structure. In teal is our complete Cdc37 model (residues 1-260). Note the □-strand wrapping around the outside of Hsp90 connecting the two major Cdc37 domains. (B)

Two additional classes show new density for the missing Cdk4 N-lobe. The classes minus the Hsp90/Cdc37 density, in blue and maroon, highlight the two new Cdk4 N lobe conformations. Fitted kinase models are in ribbons.

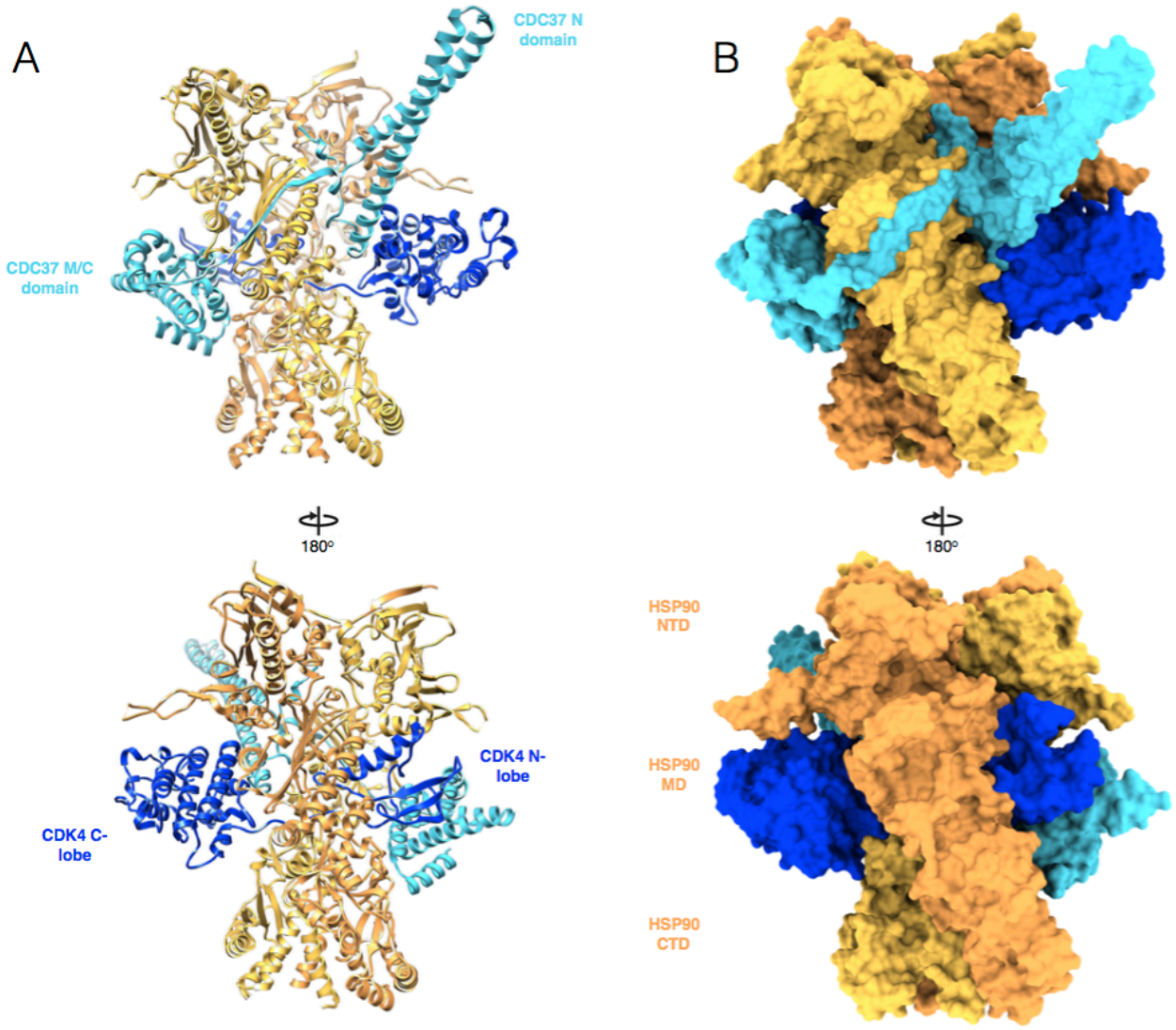

Fig. 4. Hsp90, Cdc37, and Cdk4 are intricately interwoven in the complex.

Two views of the complete model, showing ribbon in (A) and surface in (B)

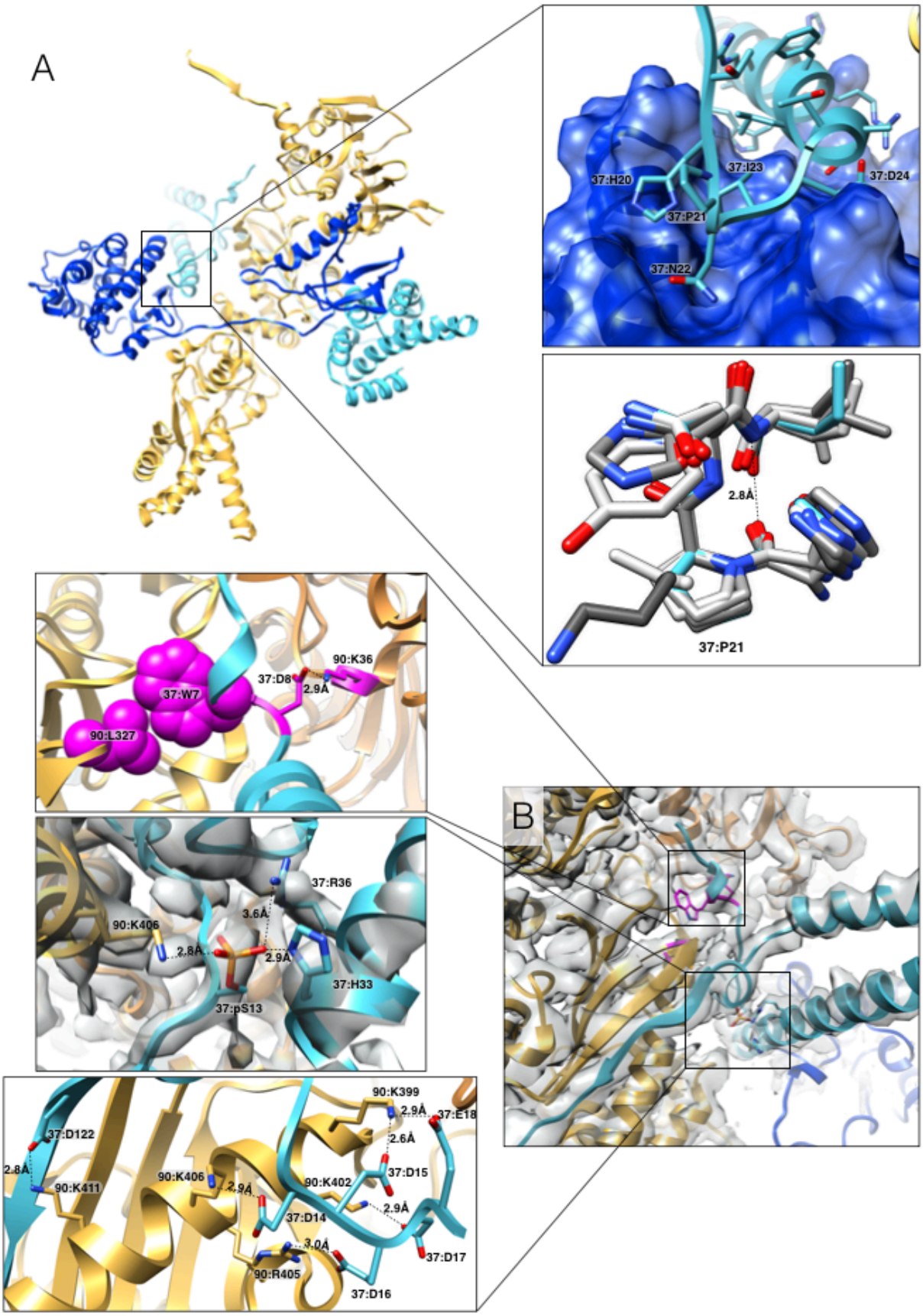
A
37:H20
37:I23
37:D24
37:P21
37:N22
2.8Å
37:P21
90:K36
37:D8
2.9Å
37:W7
90:L327
37:R36
3.6Å
90:K406
2.8Å
2.9Å
37:H33
37:pS13
B
90:K399
2.9Å
37:E18
2.6Å
37:D122
2.8Å
90:K411
90:K406
2.9Å
90:K402
37:D15
2.9Å
37:D14
3.0Å
37:D17
90:R405
37:D16

Fig. 5. High-resolution details of Cdc37 interactions with Hsp90 and Cdk4.

(A) Overall arrangement of Hsp90/Cdc37/Cdk4 (one Hsp90 monomer removed for clarity). The insets highlight Cdc37/Cdk4 interaction features: top – Cdc37/Cdk4 interact via hydrophobic interactions and backbone hydrogen bonds, with perfect shape complementarity, bottom - overlay of Cdc37's conserved HPN motif (teal) perfectly mimicking type I β-turn of αC-β4 loop of 6 different kinases (shades of gray). (PDB codes: 3g33, 2itp, 1qmz, 3pp0, 1jnk, 4fk3) (B) Zooming in on Hsp90/Cdc37 interactions. Top insert: Cdc37/Hsp90 interactions mimic p23/Hsp90 interactions identified previously (magenta). Middle insert: phospho-Ser13 stabilizes local Cdc37 structure through interactions with conserved R36 and H33 and also interacts with Hsp90 at K406. Bottom insert: six salt bridges stabilizing Hsp90/Cdc37 interactions.

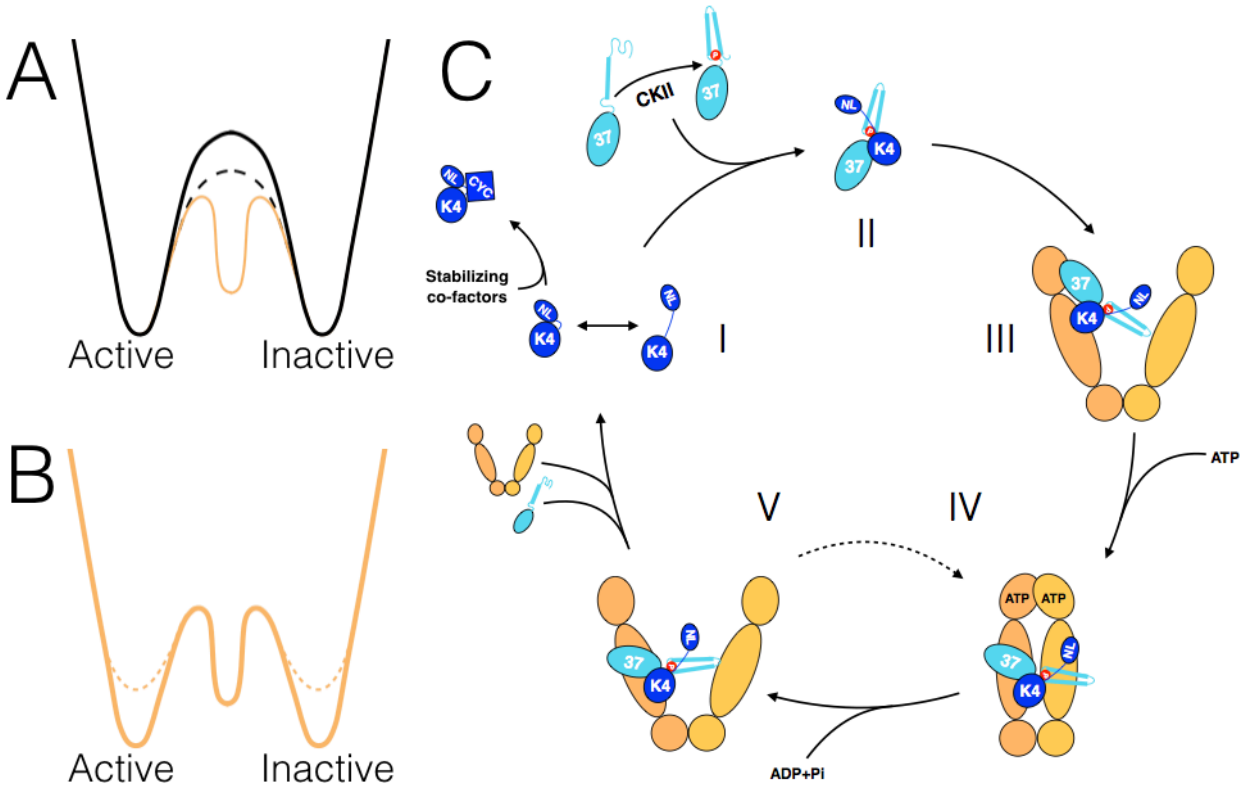

Fig. 6. Conceptual model for linkage between kinase folding and activation and proposed model for the Hsp90:Cdc37:kinase cycle.

(A) Transitioning between states through an unfolded intermediate (dashed line) has a lower energy barrier than through rigid body motion (solid line). The Hsp90:Cdc37 stabilizes such an unfolded intermediate (orange solid line) (B). By comparison with non-clients (solid line), the active and inactive states of client kinases (dashed line) are de-stabilized. (C) Speculative model for an Hsp90:Cdc37:Kinase cycle. (I) The kinase domain transiently samples an open state. Interactions with co-factors (like cyclins, SH2/SH3 domains, etc.) stabilizes the kinase native state, disfavoring the open state. (NL-N-lobe, CYC-Cyclin) CKII phosphorylated Cdc37 captures the open state by binding the kinase C-lobe (II). Cdc37/kinase then binds to open Hsp90 (III). Hsp90 binds

to ATP and closes upon the unfolded part of the kinase. Cdc37 migrates down, resulting in the structure described here (IV). Upon hydrolysis of ATP, Hsp90 opens with Cdc37/Cdk4 still bound, giving a chance for the kinase to fold (V). If it folds, it displaces Cdc37 and leaves the complex. If however it fails to displace Cdc37, then Hsp90 is able to re-bind ATP and go back to state IV, repeating the process. At some point during this cycle, PP5 phosphatase is recruited to the complex to de-phosphorylate Cdc37.

Materials and Methods

Expression and purification of Hsp90/Cdc37/Cdk4 complex

Expression of the complex in Sf9 cells.

Such prepared sample was used for all the reconstructions except T4 Lysozyme labeled complexes. The plasmids encoding the full-length human HSP90b and Cdc37 were kindly provided by Dr. Neil F Rebbe (The University of North Carolina at Chapel Hill) and Dr. Ernest Laue (The University of Cambridge), respectively. The cDNA clone for Cdk4 was purchased from Origine.

The DNA fragment of the full-length Hsp90β (residues 1-724) or the linker-deleted Hsp90β (residues 1-220-GGGG-274-724), in which the linker region (residues 221-273) were replaced by GGGG, was independently amplified by PCR and subcloned into the baculovirus transfer vector pFastBacHT (Thermo Fisher Scientific, USA) as a fusion with an N-terminal Flag tag and a TEV cleavage site. The DNA fragment of the Cdk4 (residues 1-303) for a fusion with an N-His tag and a TEV cleavage site and Cdc37 (residues 1-378) without tag were subcloned as the above-mention methods. The Flag-tagged Hsp90, the His_6-tagged Cdk4 and Cdc37 was co-expressed in Sf9 cells using BAC-to-BAC Baculovirus Expression System (Thermo Fisher Scientific, USA).

Protein purification from Sf9 cells.

The infected Sf9 cells were lysed and sonicated in 20 mM Tris-HCl (pH 7.5), 150 mM NaCl, 20 mM imidazole, 10 mM $MgCl_2$, 10 mM KCl, 20 mM Na_2MoO_4. The protein solution was applied to a HisTap column (GE Healthcare, UK) and then eluted with a buffer containing 500 mM imidazole. Elution solution was applied to Anti-FLAG

M2 agarose (SIGMA) and eluted a buffer (20 mM Tris-HCl (pH 7.5), 150 mM NaCl, 10 mM $MgCl_2$, 10 mM KCl) with a 100 □g/ml FLAG peptide (SIGMA) to remove Cdc37 and Cdk4 unbound Hsp90. The Flag and His_6 tag of the eluted sample was cleaved by TEV protease at 4°C for overnight. In turn, the solution was flowed through a HisTap column again to remove a cleaved Flag and His_6 tag. The flow-through fraction was separated by an ion exchange column (MonoQ, GE Healthcare) and a size exclusion chromatography column (Superdex200, GE Healthcare) in a final buffer containing 20mM Tris-HCl (pH 7.5), 150 mM NaCl, 10 mM KCl, 10 mM MgCl2, 20 mM Na_2MoO_4, 2mM DTT. The sample was concentrated to final concentration of about 10 mg/ml and stored at -80°C until use.

Expression of the complex in *Saccharomyces cerevisiae*.

To co-express human Hsp90β, human Cdc37 and human Cdk4 we utilized viral 2A peptides. This way we were able to construct a single plasmid, which had all three proteins in it. The exact 2A sequence we used (P2A) was sourced from Porcine Teschovirus-1 and was GSGATNFSLLKQAGDVEENPGP(*37*). The resulting construct was of this arrangement:
hCdc37-TEVsite-P2A-hHsp90β-TEVsite-FLAG-P2A-hCdk4-TEVsite-HisTag.
This construct was generated and cloned into 83nu yeast expression vector (GAL1 promoter, His marker) using Gibson Assembly(NEB). For T4 Lysozyme tagging T4Lys was added at either N terminus of Cdc37 or C terminus of Cdk4, separated from proteins by Gly-Ser (cloning was done at 96Proteins, South San Francisco). The resulting

plasmids were sequence verified, transformed into JEL1 (MAT-alpha, leu2 trp1 ura3-52 prb1-1122 pep4-3 deltahis3::PGAL10-GAL4) yeast strain using Zymo Research EZ Transformation protocol and plated on SD-HIS plates. After 3 days a colony was picked and 250mL O/N culture (SD –His) was inoculated. Next day 1L of YPGL media was inoculated with 10mLs of the O/N culture. After about 24h (OD of 1), galactose was added to a final concentration of 2% w/v to induce protein expression. The culture was pelleted after 6h of growth.

Purification of the complex from *Saccharomyces cerevisiae*.

The cells were lysed in 20mM Tris pH7.5, 150mM NaCl, 20mM Imidazole, 10mM $MgCl_2$, 10mM KCl, 20mM $NaMoO_4$ (Lysis Buffer) with Roche protease inhibitors by Emusiflex (Avestin). Lysate was cleared by centrifuging at 30000g for 30 minutes and bound to pre-equilibrated Ni-NTA beads (ThermoFisher) for 1h at 4°C. The beads were washed with 20 bed volumes of Lysis buffer, and then were eluted into Lysis buffer + 500mM Imidazole. The resulting eluate was then incubated with pre-equilibrated M2 Anti FLAG magnetic beads (Sigma Aldrich) for 1h at 4°C. Beads were washed with 10 bed volumes of Lysis buffer, and the sample was eluted with 3 bed volumes of Lysis buffer with 75ug/mL of FLAG peptide, twice. TEV was added to the eluent and it was dialized against 20mM Tris pH7.5, 100mM NaCl, 10mM $MgCl_2$, 10mM KCl, 20mM $NaMoO_4$ (Dialysis Buffer) O/N. The sample was then diluted 1:1 with the Dialysis buffer without NaCl and was loaded onto pre-equilibrated 10/300 MonoQ column (GE Healthcare). After washing out the unbound sample, a gradient was run up to 1M NaCl with fractionation to elute the bound complex (came off at about 25% conductivity). The

fractions were pooled, concentrated and then loaded on 16/60 S200 Superdex (GE Healthcare) column pre-equilibrated in 20mM Tris pH7.5, 150mM NaCl, 10mM KCl, 20mM $NaMoO_4$, 1mM DTT. The peak fractions (at about 0.5CV) were pooled, concentrated, flash frozen in liquid nitrogen and stored at -80°C.

Work on Cdc37-NTD expressed in *E.coli*

Expression and purification of Cdc37-NTD from *E.coli*.

DNA corresponding to residues 1-126 of human Cdc37 was codon optimized for bacterial expression and ordered from ThermoFisher. Subsequently this construct was cloned into pet28a vector via Gibson assembly. Bl21Star (DE3) cells were transformed and plated. Colony was picked and an overnight culture in LB with antibiotic was grown. 6L of LB media with antibiotic were spiked with the O/N culture and induced at OD ~0.6 with 400uM of IPTG. After 3h of growth with shaking at 37C cells were pelleted by centrifugation. Cell pellets were solubilized in Lysis buffer (50mM Tris pH7.5, 500mM NaCl, 20mM Imidazole, 5mM BMe) and lysed on Emulciflex. The lysate was clarified by centrifuging at 30000g for 30 minutes, and the supernatant was collected. The supernatant was incubated with pre-equilibrated in Lysis buffer Ni-NTA beads (ThermoFisher) for 1h at 4C, rotating. The sample was eluted of the beads with Lysis buffer with 500mM Imidazole. TEV was added and the eluent was dialyzed against Dialysis Buffer (20mM Tris pH8, 10mM NaCl, 1mM DTT) at 4C O/N. The sample was diluted 1:1 with Dialysis buffer without salt and loaded on 10/300 MonoQ column. Protein was eluted by running a gradient to 1M NaCl over 20 column volumes. Appropriate peaks were collected and subsequently loaded on 16/60 Superdex 200

column. Appropriate peaks were collected, concentrated and flash frozen. For N^{15} growth the protocol was the same, except M9 minimal media with 1g/L N^{15} ammonium sulfate was used instead of LB during growth and expression.

NMR measurement on Cdc37-NTD.

HSQC measurements were performed on a Bruker Avance 800 on fully N^{15} labeled Cdc37-NTD. Chemical shifts were visualized in ccpNMR.

CD measurement on Cdc37-NTD

Cdc37-NTD was buffer exchanged into 10mM Potassium Phosphate pH7.4, 50mM sodium sulfate buffer. Protein was diluted to 0.4 mg/ml and 1mm CD cuvette was used. CD spectra were collected on Jasco J710 from 185nm to 260nm.

Cryo-EM data acquisition

Main data collection

Initially all the samples were screened using negative stain via standard protocols (~100nM protein concentration)(*38*). Cryo-EM grids were prepared with Vitrobot Mark III (FEI Company), using 20°C and 90% humidity. 3uL aliquots of sample at concentration of 1.1uM were applied to glow discharged C-flat 400 mesh 1.2/1.3 thick carbon grids (Protochips), single blotted for 4 to 6 sec and plunge frozen in liquid ethane cooled by liquid nitrogen. DDM was added to the protein to a final concentration of 0.085mM before applying sample to the grids. The grids with T4 Lysozyme labeled complex were prepared the same as above. Images were taken at NRAMM Scripps on

FEI Titan Krios electron microscope operating at 300kV with a nominal magnification of 22500x. Images were recorded by Gatan K2 Summit detector (Gatan Company) with super resolution mode(0.66Å/pix). Defocus varied from 1.4um to 3.8um. Each image was fractionated to 38 frames (0.2sec each, total exposure of 7.6 seconds) with dose rate of 5.8e/Å/sec for a total dose of 44e/Å^2. Leginon software was used for all the data collection. 3718 total images were collected. For more details see Table S1.

T4 Lysozyme labeled complex data collection.

FEI Polara microscope operating at 300kV, at nominal magnification of 31000x, was used for data collection. Images were recorded with Gatan K2 Summit detector in Super Resolution mode (0.61Å/pix). Each image was fractionated into 30 frames (0.2 seconds each, 6 seconds total) at 6.7/Å^2/sec for a total dose of 40e/Å^2. Leginon software was used for all the data collection. For more details see Table S1.

Image processing

Generating an initial reconstruction

Using EMAN2(*39*) for all aspects of processing, including initial model generation (e2initialmodel), a 3D reconstruction was generated from about 10000 negative stain particles. As mentioned in the main text, over multiple cryoEM data collections on F30 Polara, a 7Å reconstruction was obtained, using negative stain map as an initial model. The collection parameters were the same as T4 Lysozyme collections, but using UCSFImage4. This reconstruction, low pass filtered to 30Å, was used for particle picking and as an initial model for the NRAMM reconstruction.

General processing and obtaining the 3.9Å and 4Å reconstructions.

Image stacks were corrected for motion and summed as described previously(*40*), resulting in binned sums (1.315Å/pix). For particle picking the images were binned to 5.2Å/pix and Gaussian bandpass filtered between 15Å and 500Å using EMAN2. SamViewer template based picking was then used to pick particles from all the micrographs, followed by manual review of all the picks(*41*). After such procedure 802877 particles were picked in total and extracted from images binned to 2.6Å/pix. CTFFIND4 was used to estimate defocus parameters for all the images(*42*). Relion 1.4 was used for all the following steps unless noted otherwise(*43*). Reference free 2D classification into 300 classes for 75 iterations was performed followed by manual examination of the resulting class averages. Low resolution/signal to noise/feature class averages and contributing particles were discarded, resulting in 670000 particles left. The resulting particles were 3D classified into 4 classes resulting in two classes having high-resolution features (390000 particles). At this stage particles were extracted from 1.315Å/pix micrographs and all the following processing was done with these particles. Using 3D Auto-refine in Relion 1.4, a reconstruction was obtained from 390000 particles resulting from 3D classification above (using highest resolution 3D class as initial model, low pass filtered to 20Å). Using the resulting parameters, the particles were further drift corrected per particle and dose weighted using the Particle Polishing feature(*44*). The B-factor weighing curve was fit by a polynomial (with a rationale that such a curve should be smooth) and used to generate new weighting parameters for Particle Polishing, with which 390000 particles were then polished. All further data processing was done using

the polished particles. Re-refinement of the 390000 particles after polishing yielded the map at about 4Å resolution (determined using gold standard FSC in the PostProcessing tab)(*45*). Raw particles were sharpened with a B-factor of -50, low pass filtered with Gaussian filter to 3Å and the refinement was continued for 10 more iterations (until convergence) with these particles (the rationale was that due to extremely low noise levels of K2 direct detector, this would yield more accurate alignments due to presence of more high resolution data in the images). This resulted in similar resolution but a reconstruction with visually sharper features (Fig S13). This reconstruction, after Modulation Transfer Function (MTF) correction and B-factor sharpening(*46*) yielded the 4Å reconstruction shown on Fig1 and shown without post processing in Fig2A and movie S2. Lastly, this reconstruction was tightly masked around Hsp90 region and refinement was further continued for 4 iterations (until convergence), with rationale that Hsp90 region is more coherent. This yielded a 3.9Å reconstruction with the best density for Hsp90 region (Shown in inserts on Fig 1B, 2B and Fig 5), at the expense of Cdk4 C-lobe and Cdc37 NTD density quality. Local resolution was estimated using ResMap(*47*).

Obtaining 3D classes for Cdc37 and Cdk4 N-lobe.

The 390000 polished particles were further sub-classified into four 3D classes. All four resulting reconstructions were better than at 10Å resolution, with Hsp90 density staying unchanged, but the densities on the periphery changing. One of the classes had a low-resolution density where Cdc37 M/C was placed later, but at this resolution the fit would be ambiguous. To obtain higher resolution reconstruction of this region, a local mask was generated around this region. The 390000 particles were then 3D classified into

four different classes without particle re-alignment, using the alignment parameters from 4Å reconstruction. Particles contributing to each of the four classes were grouped and a full 3D refinement with a spherical 200Å mask was performed with each of the four groups of particles using the same initial model, low pass filtered to 20Å. One of the classes (referred to as Cdc37 Reconstruction throughout the text and shown on Fig 3A) had a distinct density into which we fit Cdc37 M/C (in UCSF Chimera(*48*)). There was also a low-resolution density for the kinase N-lobe. To attain a better density for the kinase N-lobe, we re-did the local masked 3D classification as described for Cdc37 Reconstruction, but used the subtraction protocol described recently(*49*). Again, particles contributing to each of the masked classes were grouped and a full reconstruction with a spherical 200Å mask was performed for each of the groups, starting with identical initial models. Such a procedure generated the two kinase reconstructions (Blue Kinase reconstruction and Maroon Kinase reconstruction shown in Fig3 B), a reconstruction with Cdc37 M/C density (but no Cdk4 N-lobe density) and a reconstruction which had no extra densities in that region (similarly to the 4Å reconstruction). The last two reconstruction of this set were not show or used in this manuscript. All the reconstructions were filtered and sharpened using the PostProcessing tab in Relion. All the reconstructions were visualized using UCSF Chimera.

Processing of T4 Lysozyme tagged data.

Image stacks were dose weighted, drift corrected, binned to 1.22Å/pix and summed using new UCSF DriftCorr program. The particles were picked and the CTF was estimated the same way as in the main data collection. Rounds of 2D classification (300

classes, 50 iterations) followed by 3D classification (2 classes, 50 iterations) in Relion 1.4 were used to eliminate low quality particles (using 30Å low pass filtered reconstruction from the main data set as initial model). Using the final set of particles, 3D Auto-refine feature in Relion 1.4 was used to generate the final maps. The parameters of final reconstructions and post processing are reported in Table S1.

Model Building and refinement

Atomic model building and refinement the Hsp90/Cdc37/Cdk4 complex was performed incrementally in five stages: 1) *de novo* model-building for Cdc37, 2) structure refinement of the Hsp90/Cdc37 complex, 3) *de novo* model extension for Cdk4 in the presence of the refined Hsp90/Cdc37 complex, and 4) structure refinement of the Hsp90/Cdc37/Cdk4 complex. The atomic structure of Hsp90/Cdc37/Cdk4 complex was used in the modeling of other low-resolution maps.

Initial fitting of hHsp90/Cdk4 C-lobe model

The V-shape structure of Hsp90 was clearly identified from the 4Å reconstruction, in which it adapts the closed-state conformation of known Hsp90 structure. The hHsp90 homology model was derived from a close (~60% sequence identity) homologous structure from *Saccharomyces cerevisiae* (PDB: 2CG9 chain A and B), which also adapts a closed-state conformation. The unrefined hHsp90β model was first rigid-body fit into the map using UCSF Chimera (Fit In Map function), revealing good agreement with the density data, where most of the secondary-structure density features can already be explained. The Cdk4 C-lobe (residues 96-295) from PDB:3G33

was fit based on structural alignment to a CATH(*50*) domain 3orkA02. This CATH domain was obtained by downloading all the CATH protein folds and running COLORES program (Situs package)(*51*) on each, rigid body fitting it into the segmented globular region density (Fig 1B arrows and Fig S6). This resulted in an un-biased fit into the density. The initial hHsp90β homology model was built together with Cdk4 C-lobe using the Molecular Dynamics Flexible Fitting (MDFF) (*52*) in NAMD(*53*).

De novo building Cdc37-NTD into 4Å reconstruction using Rosetta.

With no homologues of known structure available for the Cdc37 N-terminal domain (Cdc37-NTD), we employed the Rosetta automated *de novo* model-building method (*54*) to register the sequence (residues 1-132) in the density. The density belonging to Cdc37-NTD was manually segmented guided by the initial hHsp90/Cdk4 C-lobe model using Chimera's "Volume Cleaner" tool. The method first places 9-mer fragments derived from local sequence into the density map, in order to simultaneously trace the backbone and assign sequence. High-confidence partial models are generated using Monte Carlo sampling to identify a set of placed fragments consistent with each other and with maximum agreement to the data. After two iterations of applying the procedure described above, the method converged on a partial model with residues ranging from 2-50 and 92-122. RosettaCM was used to complete the partial model through density-guided model rebuilding and refinement (*55*). To this end, *de novo* model-building of Cdc37-NTD was done in the segmented density alone. However, it was clear from our initial model that Cdc37 had extensive contacts with hHsp90 and

Cdk4 C-lobe in the map. Therefore, we carried out a further structure refinement in the context of Cdc37-NTD and hHsp90.

Refinement of Hsp90/Cdc37 into 3.9Å map using Rosetta

The starting model of hHsp90 and Cdc37-NTD was obtained as described in the previous paragraph. A split map approach was used to prevent and monitor models from data over-fitting, and for model selection; one of the half maps used for calculating "gold-standard" FSC was designated as the training map against which the model was refined, and the other half map was designated as the testing map which was used for evaluations. The training/testing map designations were strictly followed and consistent in all stages of refinement. Guided by the starting Hsp90/Cdc37 model, density from the Cdk4 and nucleotide was carefully removed from the training map using Chimera's "Volume Cleaner" tool.

The refinement procedure has five cycles of iterative backbone rebuilding; in each cycle, regions with poor fit to density or poor local geometry were automatically identified, and rebuilding focused on these regions. Backbone rebuilding of a residue identified as problematic is similar to what has been described in DiMaio et al.(*56*), where the rebuilding starts with replacing the coordinates of the current model with fragments at the residue position through Monte Carlo sampling, followed by Cartesian space minimization. The fragment with the best fit to the local density is selected; the backbone coordinates from the current model are replaced by the selected fragment. Each rebuilding cycle was followed by side-chain rotamer optimization and all-atom refinement with a physically realistic force field to ensure the regularity of the rebuilt

backbone. After the backbone rebuilding cycles, a "dual-space" all-atom refinement which alternates between torsion-space and Cartesian-space optimization was carried out, and was followed by a newly-developed "local relax" to ensure the convergence of side-chain rotamer optimization in a large protein complex. Following this procedure, ~5,000 independent trajectories (models) were run.

Model selection was done in three steps. First, the initial pool of models were picked by selecting 30% most physically realistic models accessed by the Rosetta all-atom force field, from which the top 20% most well fit-to-density models were selected using Rosetta all-atom electron density score ("elec_fast_dens"). Second, evaluating the fit-to-density of the initial pool of models against the testing map using the high-resolution shells (10-3 Å) of FSC; 50 models with low over-fitting ($FSC_{training}$ - $FSC_{testing}$ < 3%) and high correlation with the testing map were retained. Third, 10 out of 50 models were picked using Molprobity (*57*), sorted first by Molprobity score and then "Ramachandran favored" score. Lastly, a final model was selected among the 10 models through visual inspection in Chimera. Here, the above described model refinement/selection procedure was carried out with two iterations to reach a satisfactory model. Residues with poor fit to density were specified to correct for the next iteration refinement.

De novo model extension for the docked Cdk4 C-lobe (into 3.9Å map)

Starting with a docked configuration of the Cdk4 C-lobe (residues 96-295), *de novo* building of the upstream residues 86-95 (tube) was carried out using RosettaCM into the tubular density as described in the main text. This density has extensive contacts with the other two component proteins, Hsp90 and Cdc37-NTD. Thus, model building

into the tube density was done in the presence of Hsp90 and Cdc37-NTD. Density-guided conformation sampling was primarily focused on the tube and the residues of Hsp90 that were likely in contact with (residues 341-349 Hsp90 chain A and B), which combines Monte Carlo sampling of backbone fragments with Cartesian space minimization in the context of residues around the tube-like density. 50 low-energy models were selected by finding models with physically realistic energy using Rosetta all-atom energy, as well as good density-fit. Among the 50 low-energy models, one conformation was clearly favored and showed good agreement with the density. Next, we used the iterative backbone rebuilding procedure as described in the previous paragraph to further sample and optimize the tube residues, as well as the surrounding residues from Hsp90. Finally, the conformation again was favored and converged among the low-energy models.

Refinement of the Hsp90/Cdc37/Cdk4 complex in 3.9Å map

Refinement of the Hsp90/Cdc37/Cdk4 complex was done out using the same procedure described in the paragraph of refining the Hsp90/Cdc37 complex. However, due to the much worse resolution (~ 6 Å) of the density for Cdk4's C-terminal domain (residues 96-295, chain K) and Cdc37-NTD residues 56-91 (chain E), it was not necessary to further optimize the structure; thus, no fragment-based rebuilding was allowed in these residues. Three iterations of automatic model refinement/selection procedure were carried out. Furthermore, through visual inspection residues that showed poor density-fit were pinpointed and subject to the iterative backbone rebuilding on only those residues. With three more iterations of human-guided model refinement/selection, a satisfactory model was finally obtained. Next, heteroatoms including nucleotides (ATP),

Magnesium and phosphorylated-Serine were appended into the model. The intial ATP conformations were adapted from the yHsp90 crystal structure (PDBID: 2CG9). The model was refined using the Rosetta *relax* protocol with Cartesian space optimization, followed by the *local_relax*. The same model selection procedure described in the previous paragraph was used to select the final model of Hsp90/Cdc37/Cdk4 with heteroatoms. B-factors of each atom in the atomic model were refined in the full reconstruction using the approach from DiMaio et al.(*56*). Finally, we used the half maps to find a weight of density map that does not introduce over fitting. Using this weight, we did a *local_relax* in the 3.9Å map reconstructed from all the 390000 particles. The resulting model (hHsp90β 10-690, hCdc37 2-132, hCdk4 86-295) would be used as rigid body models for fitting into all the low resolution maps downstream.

Generating a model for residues 1-260 of Cdc37

Cdc37 crystal structure from PDB:1US7 was fit into the Cdc37 Reconstruction (not post processed, so, low pass filtered to ~7Å and no B-Factor sharpened) manually and then with UCSF Chimera "Fit In Map" tool. The model was truncated at residue 260, as there was no reliable density for the rest of the crystal structure. The Rosetta built model generated in the previous paragraph and the above fit crystal structure for residues 148-260 were loaded in Coot(*58*). The residues 133-147 were built in by hand into the Cdc37 Reconstruction and residues 245-260 (helix) were rotated as a rigid body. To relieve atomic clashes or bond length/angle distortions at the linker regions, the resulting model was subjected to "Cartesian space relax" protocol within Cdc37 Reconstruction

density map using Rosetta. Final model was selected using the combined score of Rosetta all-atom physically-realistic score and electron density score.

Generating a complete Cdk4 model (Blue and Maroon Kinase reconstructions)

Residues 5-85 (N-lobe) of Cdk4 were fit in Chimera as rigid body into the appropriate density in each of the reconstructions. Such fit N-lobe of Cdk4 was further tweaked in Coot in the context of model generated in the previous paragraph to join the Cdk4 chain and minimize clashes for each of the maps. To relieve atomic clashes or bond length/angle distortions at the linker regions, these models were subjected to "Cartesian space relax" protocol within corresponding density maps using Rosetta. Final models were selected using the combined score of Rosetta all-atom physically-realistic score and electron density score.

Fitting of T4 Lysozyme into the T4 Lysozyme reconstructions.

Hsp90/Cdc37/Cdk4 model was fit into each of reconstructions in UCSF Chimera. T4 Lysozyme (PDB:2LZM) was fit into the extra densities first by hand and then in UCSF Chimera. No further refinement was undertaken.

Figure preparation

All model and reconstruction figures were prepared in UCSF Chimera except Fig. 4B which was prepared with pre-release version of ChimeraX.

Supplementary materials.

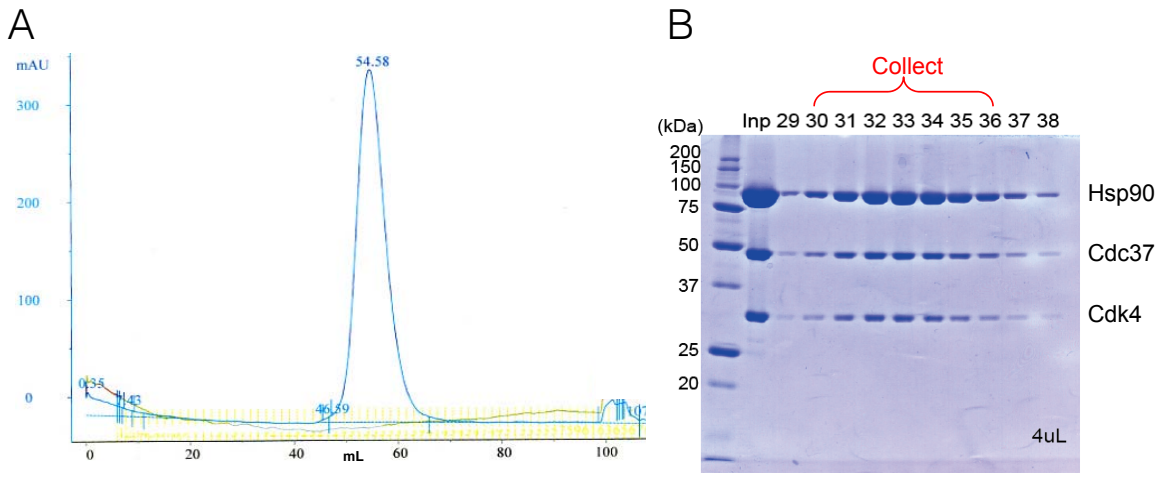

Fig. S1.

Purification of Hsp90/Cdc37/Cdk4 complex from Sf9 cells.

(A) Final sample is monodisperse on S200 Superdex gel filtration column. (B) The peak from the gel filtration ran on SDS-PAGE gel showing that all proteins are present in the final sample and are highly pure.

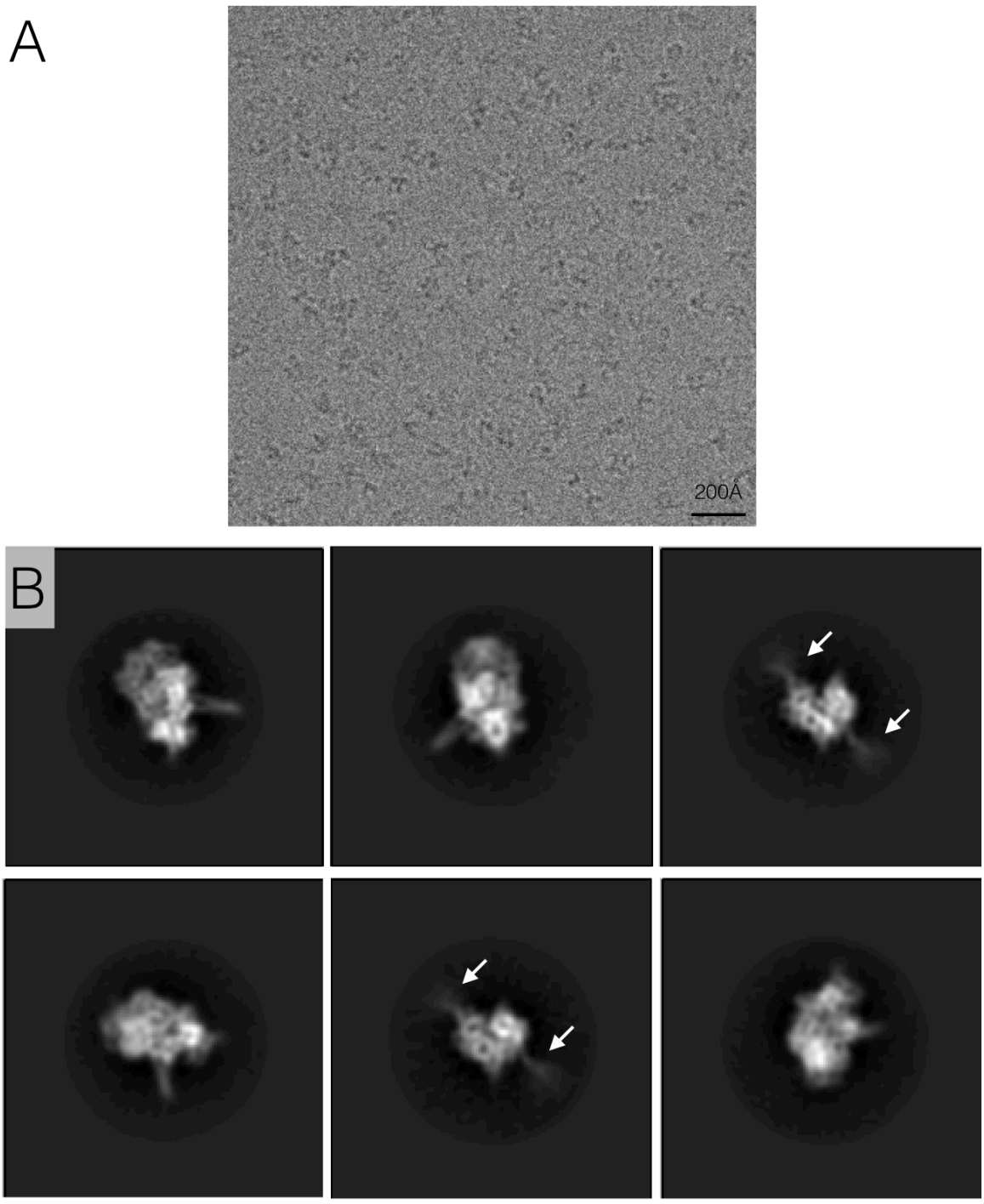

Fig. S2

Pre reconstruction assessment shows high quality data.

(A) A crop of unfiltered drift corrected image stack sum shows clearly visible particles.

(B) 6 classes were picked from a total of 300 reference free classes (Relion). The classes

clearly show secondary structure elements and the coiled coil protrusion. Marked with white arrows is the charged linker, which clearly becomes more diffuse the further it is from the center.

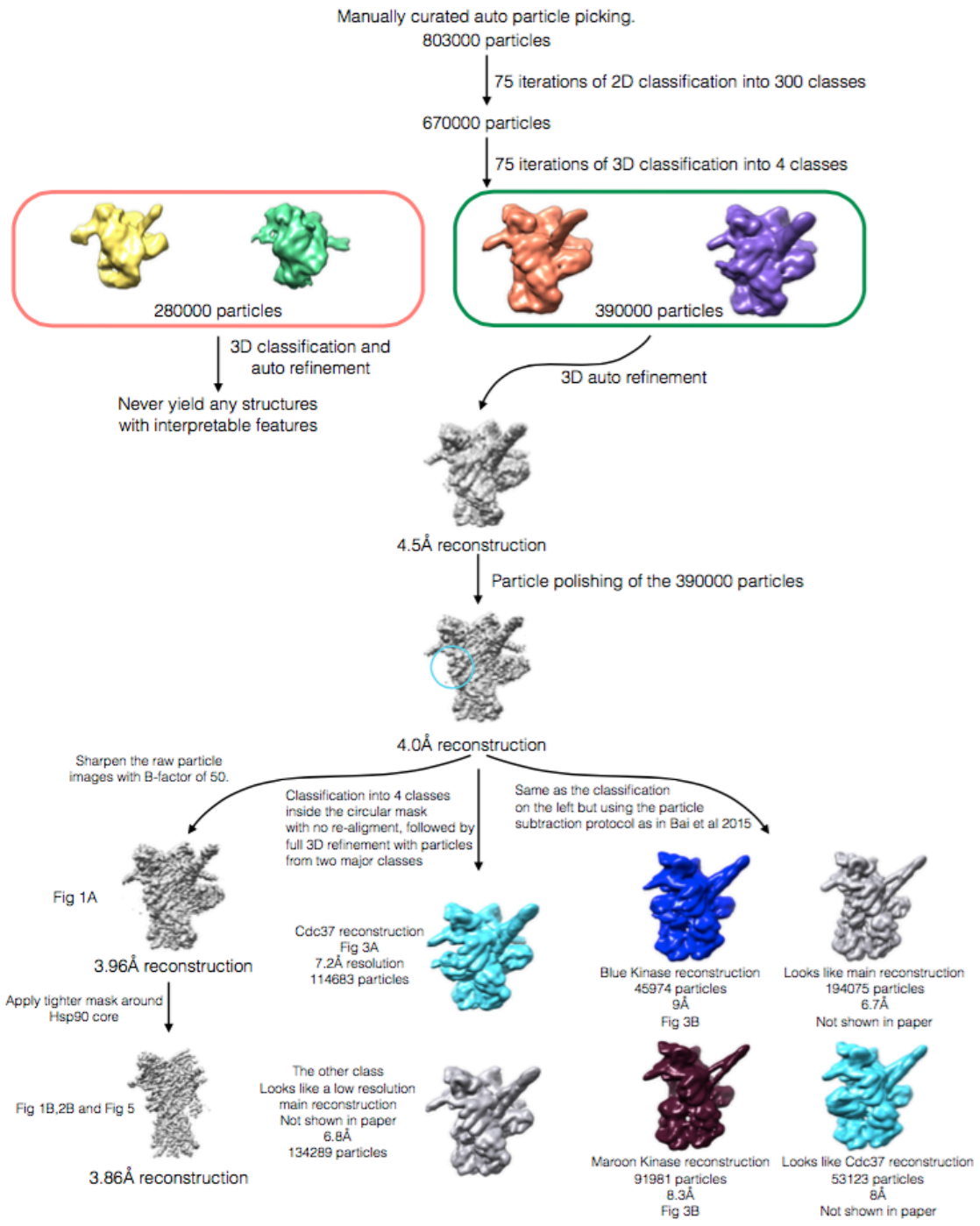

Fig. S3.

Flowchart of the EM processing.

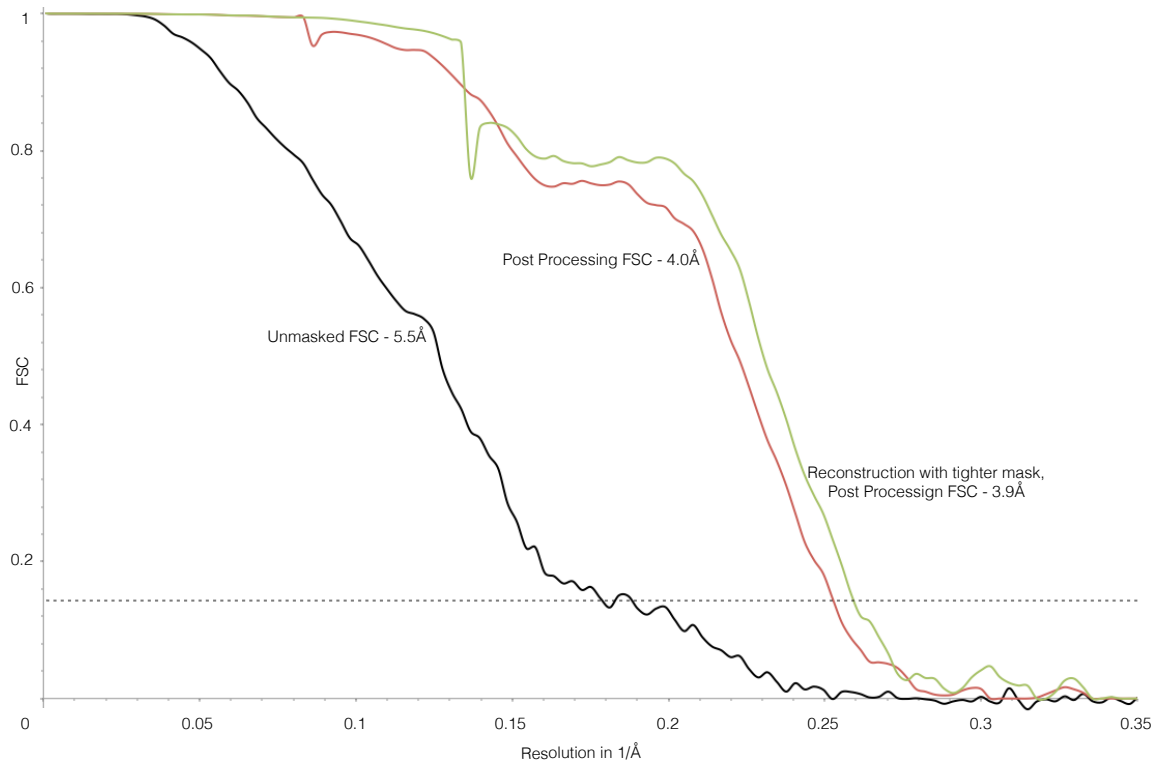

Fig. S4

Gold standard FSC of our highest resolution reconstruction.

In black is the unmasked FSC (ie 200Å spherical mask) of the reconstruction, crossing 0.143(dashed line) at 5.5Å. In red is the masked, corrected FSC of the same reconstruction, crossing the 0.143 threshold at 4.0Å, generated in the post processing node in Relion. In green is the corrected FSC for the 3.9Å reconstruction, which was performed utilizing a mask around Hsp90 region (See methods for more details).

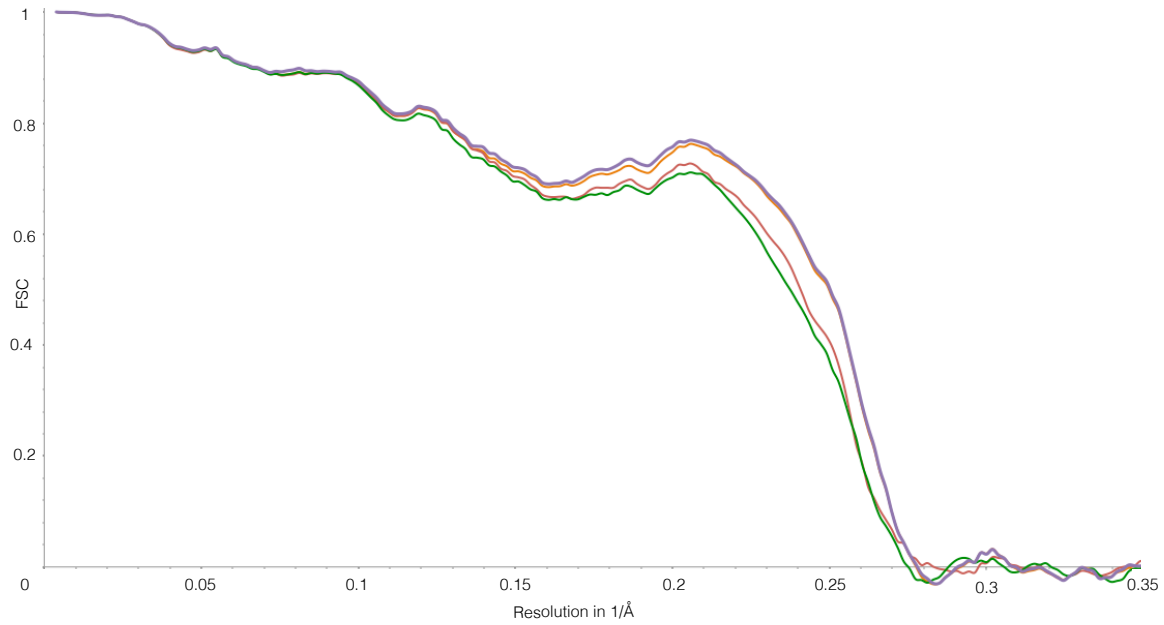

Fig. S5

Model vs map FSC shows no over fitting.

The difference between model vs the training map FSC (red curve) and model vs test map FSC (green curve) is small, signifying no over fitting. In orange is the FSC between the model refined into a half map and full 3.9Å map. In violet is the FSC of the final model vs 3.9Å map. The final map was refined into the map from full dataset of particles using weighting parameters from the half map refinements. (See methods for more details).

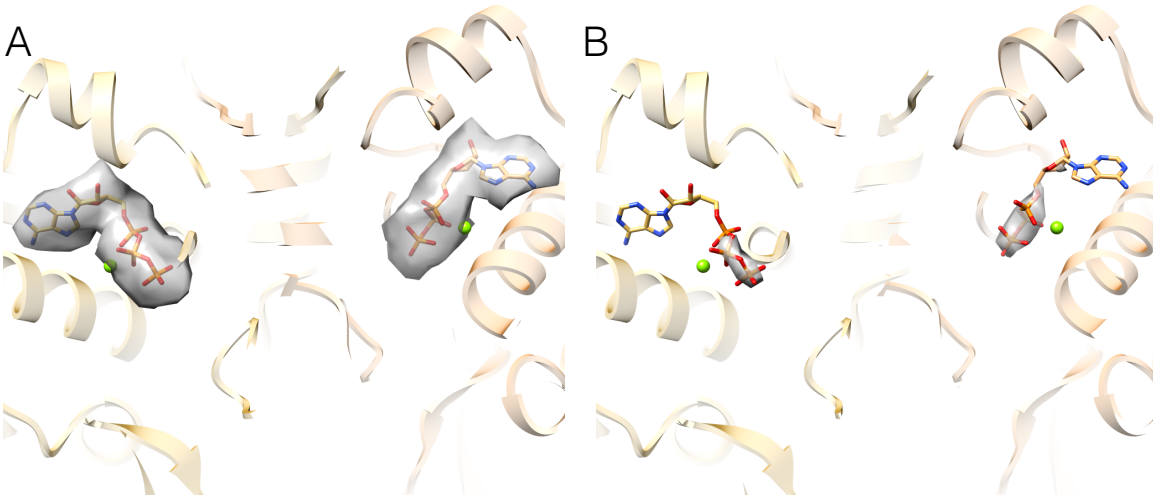

Fig. S6

There is a clear density for nucleotide in both Hsp90 monomers.

(A) View from the 4Å map showing the ATPs fitting perfectly into the density in both monomers. (B) The density for the γ-phosphate is the strongest density in the whole map.

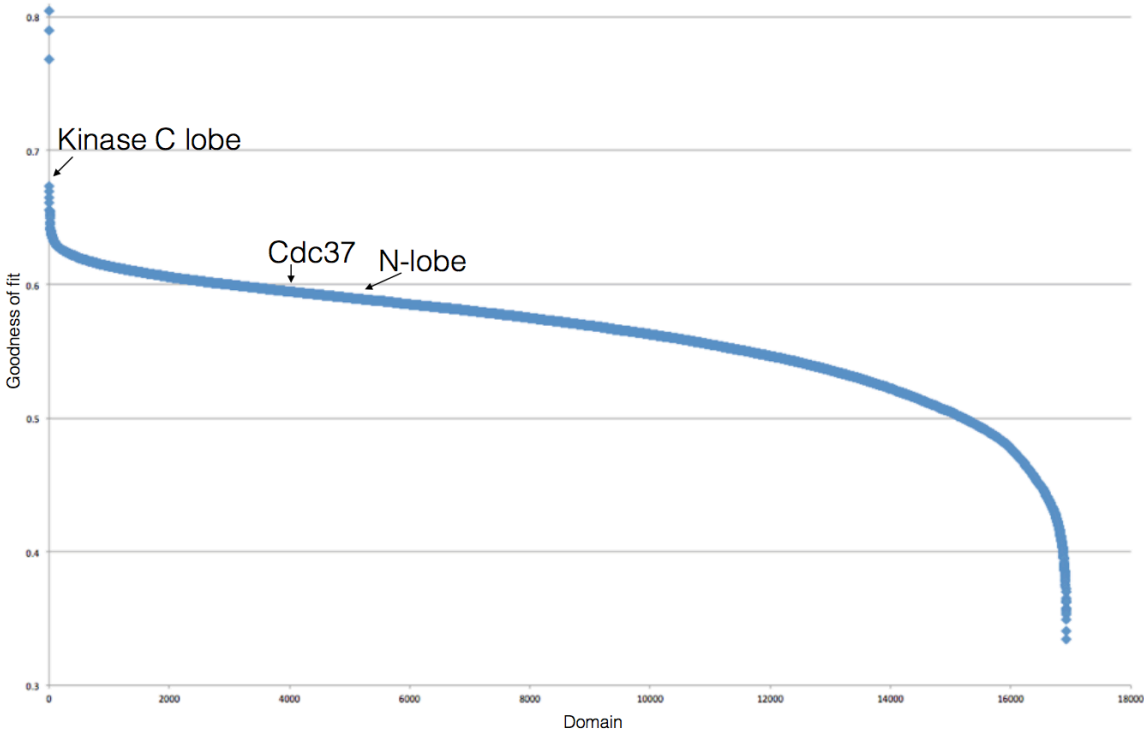

Fig. S7

Fits of different CATH domains into the globular density plotted by cross correlation.

The plot of the cross correlation coefficient vs CATH database domain, as output from COLORES program in SITUS package. Upon manual examination, the three points above 0.7CC are clearly artifacts. The CC values from kinase C-lobe, N-lobe and Cdc37 are marked with arrows.

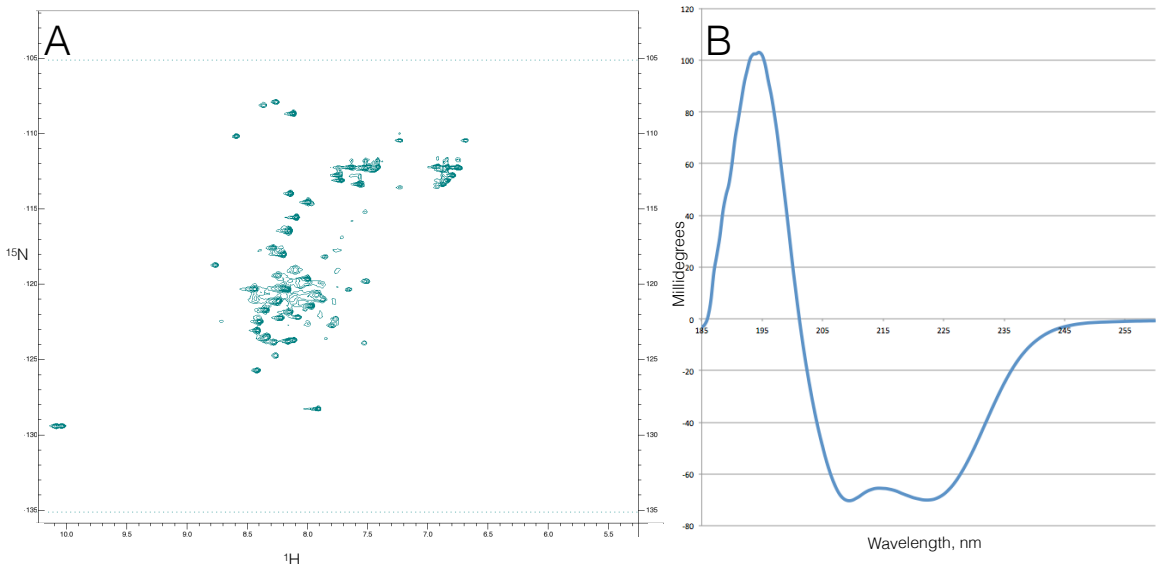

Fig. S8

CDC37 N-terminal domain is helical.

(A) NMR spectrum of N^{15}-H^{1} HSQC experiment performed on the CDC37 NTD, which is characteristic for either unfolded or helical proteins. (B) CD of the same protein fragment, showing spectrum characteristic of α-helix.

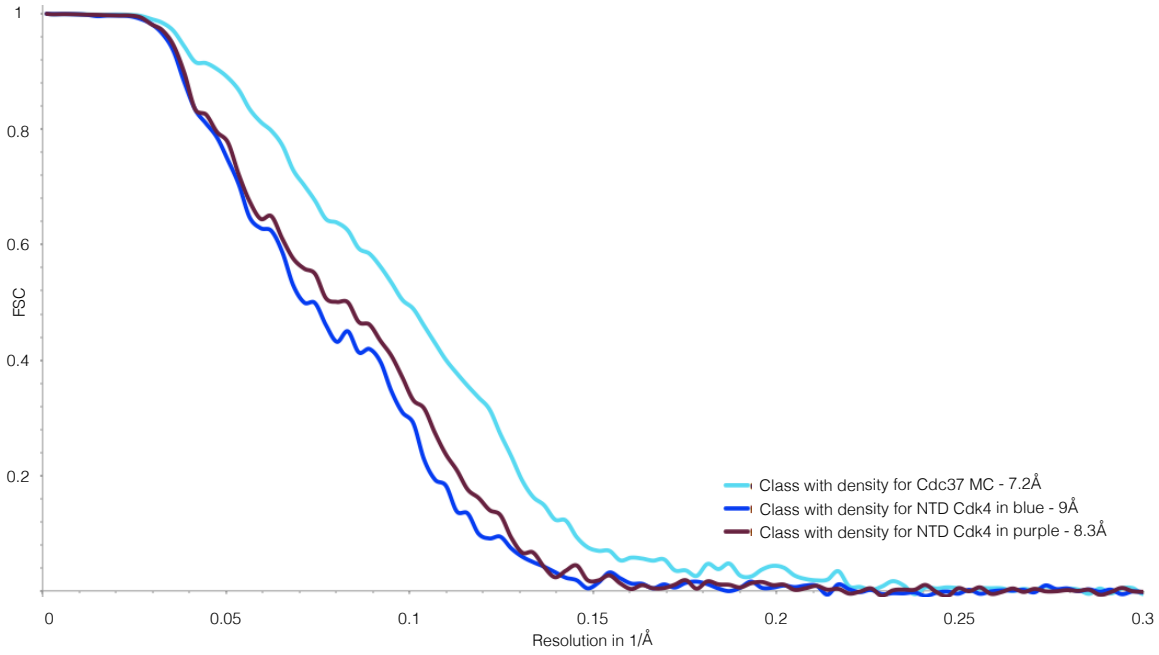

Fig. S9

Gold standard FSCs of the three alternate reconstructions.

Unmasked gold standard FSCs of the three reconstructions done after local 3D classifications, as discussed in the main text. Due to using only a spherical mask, the resolution estimates are quite conservative.

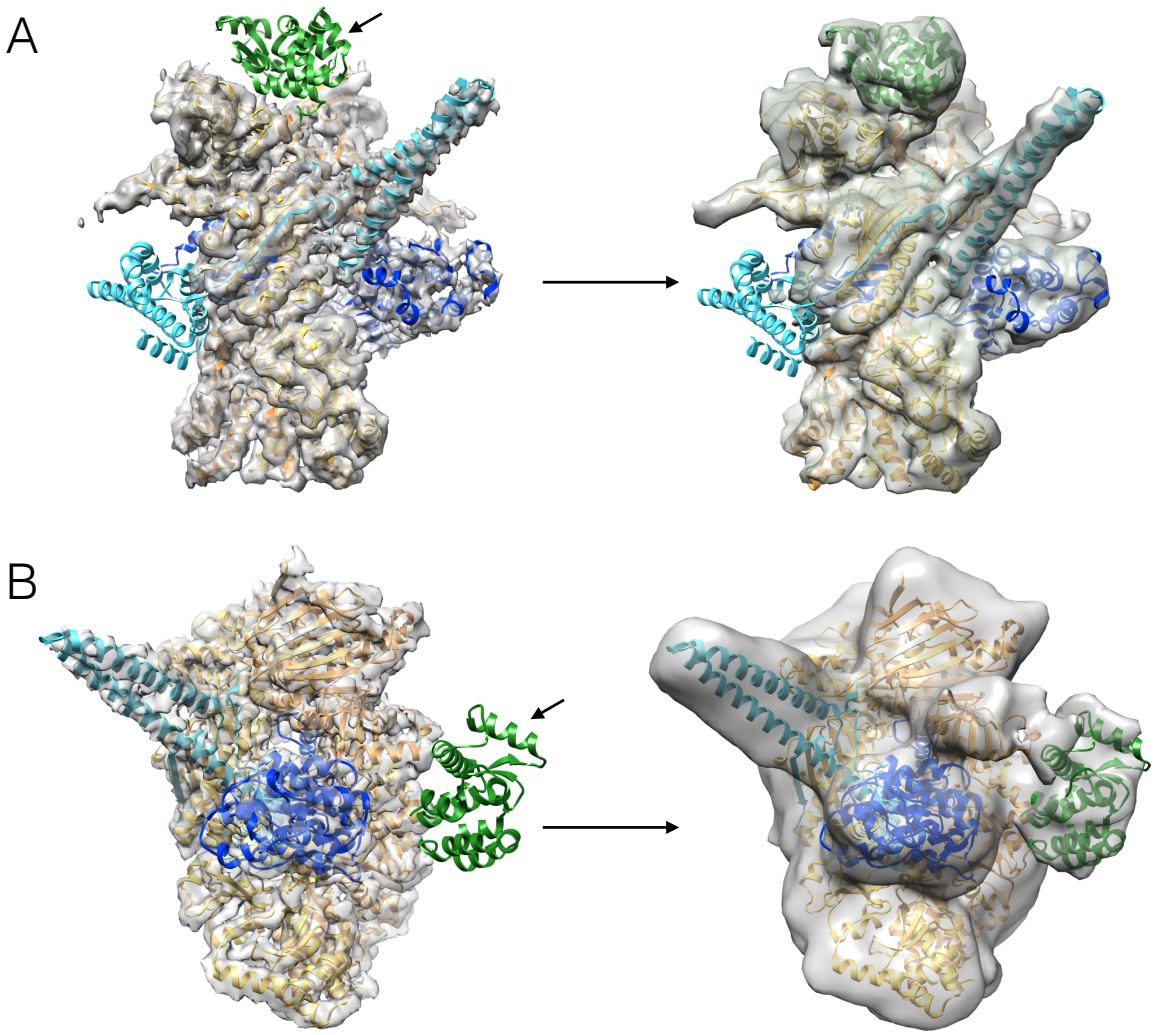

Fig. S10

T4 lysozyme tagging supports protein placement in our model.

(A) Cdc37 was tagged on its N terminus with T4 lysozyme. On the left is our model fit into the 4Å map, with lysozyme (PDB:2LZM) in green placed at its expected location as per construct(marked with an arrow). On the right is the reconstruction of the Hsp90/T4Lys-Cdc37/Cdk4 complex, clearly showing the new extra density in the expected location perfectly fitting lysozyme structure. (B) Everything as in A, but now Cdk4 was tagged with T4 Lysozyme at its C terminus. Again, reconstruction of Hsp90/Cdc37/Cdk4-T4Lys shows a clear new extra density for lysozyme.

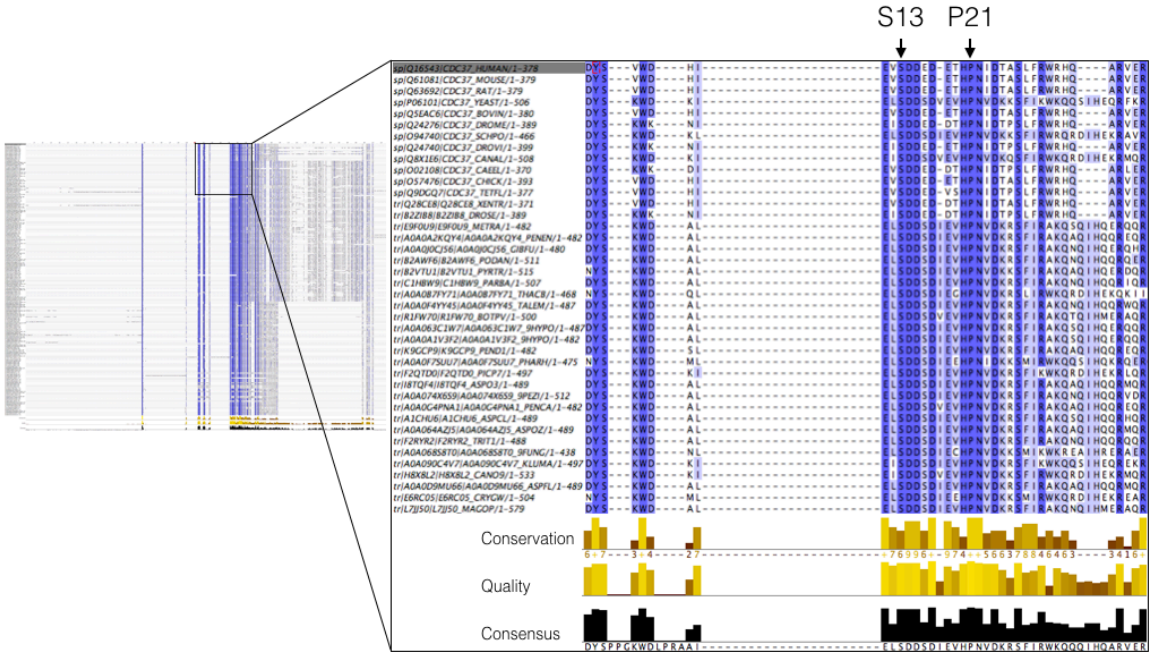

Fig. S11

Cdc37s very N terminus is extremely well conserved.

Sequence alignment of over 200 different Cdc37 protein sequences aligned using T-COFFEE server and visualized using JalView. The insert is showing a zoom view of the first 30 amino acids of 40 organisms, with the top sequence being human. Conservation in the region is over 90% for many of the residues.

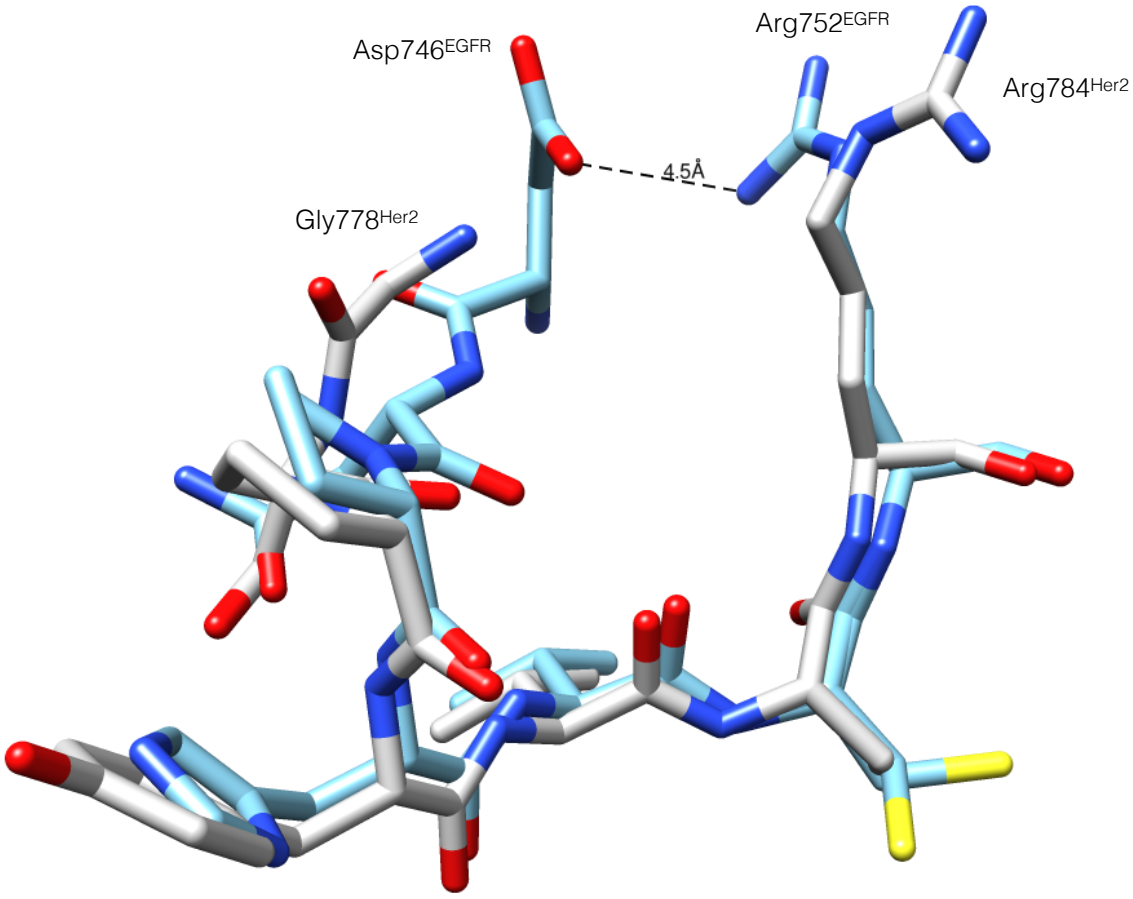

Fig. S12

αC-β4 loop in EGFR may be stabilized by an ionic interaction.

Overlay of the loop between Her2 and EGFR structures, with Her2 being in white and EGFR being in blue. Considering the overall flexibility of protein kinases, Asp746 in EGFR may electrostatically interact with Arg752, stabilizing the loop. This interaction would be absent in Her2 as Asp746 is replaced with Gly778. (PDB codes 3PP0 and 1M17)

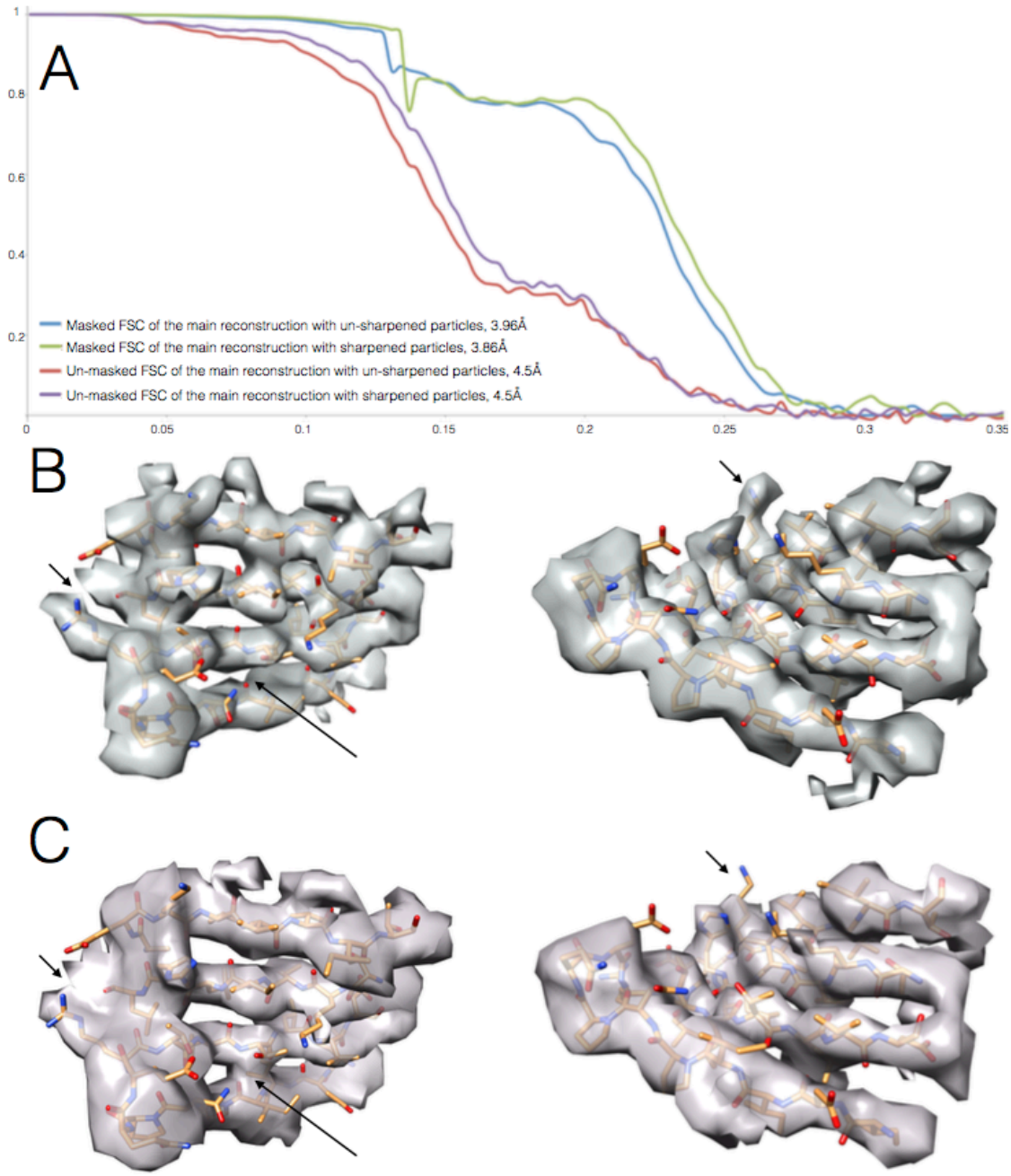

Fig S13.

The effect of B-factor sharpening of the raw images.

(A) FSCs of reconstructions from sharpened and un-sharpened particles. Both, the masked FSC and the un-masked are shown to demonstrate that the improved resolution is not a masking artifact. Both FSCs show that reconstruction done from the sharpened

particles is of a higher resolution. (B, C) In panel (B) are two views of the model fit in the reconstruction from the sharpened particles and in panel (C) are the same two regions from the reconstruction done with the un-sharpened particles. The arrows show subtle higher resolution features of the reconstruction done with the sharpened particles. The region depicted is a different view of the region shown in the bottom insert on Fig1B in the main text.

	3.9Å and 4Å reconstructions	Cdc37 reconstruction	Blue Kinase reconstruction	Maroon Kinase reconstruction	Reconstruction T4 at the Cdc37 N terminus	Reconstruction T4 at the Cdk4 C terminus
Data Collection						
Microscope	FEI Titan Krios				FEI Polara	
Voltage	300kV				300kV	
Detector	Gatan K2 Summit				Gatan K2 Summit	
Pixel size	1.315Å				1.22Å	
Total electron dose	44e/Å^2				40e/Å	
Dose rate	5.8e/Å^2/sec				6.7e/Å^2/sec	
Frame rate	5 per sec				5 per sec	
Total images acquired	3718				1634	1082
Defocus spread	1.4 - 3.8 µm				1 - 5µm	1 - 5µm
Total particles picked	802877				135142	85865
Reconstruction parameters						
Number of particles	388688	114683	45974	61981	29313	29146
Symmetry	C1	C1	C1	C1	C1	C1
Resolution(unmasked)	5.5Å	7.2Å	9Å	8.3Å	9.3Å	9.6Å
Resolution(masked)	3.9Å/4.0Å	4.7Å	7Å	6.23Å	7.8Å	-
Map sharpening B-factor	-90Å^2	-141Å^2	-200Å^2	-126Å^2	-438Å^2	-
Refinement parameters						
Model composition						
Non-hydrogen atoms	26298					
Protein residues	1612					
Nucleotides	2					
Ramachandran plot						
Favored	95.55%					
Allowed	99.50%					
Outliers	0.50%					
Rms deviations						
Bonds	0.0154Å					
Angles	1.04°					
Validation						
Molprobity score	1.34					
Clashscore, all atoms	2.48					
Good rotamers	99.93%					
Poor rotamers	0.00%					
Bad bonds	0.01%					
Bad angles	0.00%					
Cß deviations>0.25Å	0.00%					

Table S1.

Parameters for all the reconstructions discussed in the main text and refinement parameters for the final model refinement (omitting Cdc37 M/C and Cdk4 N-lobe) fit into the 3.9Å reconstruction.

Protein Fragment 1	Protein Fragment 2	Interface Area (Å$^{2)}$
Cdk4	Hsp90 A	639
	Hsp90 B	922
	Hsp90 NTD A	90
	Hsp90 MD A	225
	Hsp90 MD B	572
	Hsp90 CTD A	366
	Hsp90 CTD B	376
	Cdc37	1001
	Cdc37NTD	725
	Cdc37MC	300
Cdc37	Hsp90 A	654
	Hsp90 B	2000
Cdc37NTD	Hsp90 NTD A	230
	Hsp90 NTD B	67
	Hsp90 MD B	1608
Cdc37MC	Hsp90 MD B	337
Cdc37MC	Hsp90 CTD A	424

Table S2.

Buried surface area between the proteins in the complex, per domain, generated by submitting the final model into the PISA server.

37. J. H. Kim *et al.*, High cleavage efficiency of a 2A peptide derived from porcine teschovirus-1 in human cell lines, zebrafish and mice. *PLoS One* **6**, e18556 (2011).

38. D. S. Booth, A. Avila-Sakar, Y. Cheng, Visualizing proteins and macromolecular complexes by negative stain EM: from grid preparation to image acquisition. *J Vis Exp*, (2011).

39. G. Tang *et al.*, EMAN2: an extensible image processing suite for electron microscopy. *J Struct Biol* **157**, 38-46 (2007).

40. X. Li *et al.*, Electron counting and beam-induced motion correction enable near-atomic-resolution single-particle cryo-EM. *Nat Methods* **10**, 584-590 (2013).

41. M. Liao, E. Cao, D. Julius, Y. Cheng, Structure of the TRPV1 ion channel determined by electron cryo-microscopy. *Nature* **504**, 107-112 (2013).

42. A. Rohou, N. Grigorieff, CTFFIND4: Fast and accurate defocus estimation from electron micrographs. *J Struct Biol* **192**, 216-221 (2015).

43. S. H. Scheres, RELION: implementation of a Bayesian approach to cryo-EM structure determination. *J Struct Biol* **180**, 519-530 (2012).

44. S. H. Scheres, Beam-induced motion correction for sub-megadalton cryo-EM particles. *Elife* **3**, e03665 (2014).

45. S. Chen *et al.*, High-resolution noise substitution to measure overfitting and validate resolution in 3D structure determination by single particle electron cryomicroscopy. *Ultramicroscopy* **135**, 24-35 (2013).

46. P. B. Rosenthal, R. Henderson, Optimal determination of particle orientation, absolute hand, and contrast loss in single-particle electron cryomicroscopy. *J Mol*

Biol **333**, 721-745 (2003).

47. A. Kucukelbir, F. J. Sigworth, H. D. Tagare, Quantifying the local resolution of cryo-EM density maps. *Nat Methods* **11**, 63-65 (2014).

48. E. F. Pettersen *et al.*, UCSF Chimera--a visualization system for exploratory research and analysis. *J Comput Chem* **25**, 1605-1612 (2004).

49. X. C. Bai, E. Rajendra, G. Yang, Y. Shi, S. H. Scheres, Sampling the conformational space of the catalytic subunit of human gamma-secretase. *Elife* **4**, (2015).

50. I. Sillitoe *et al.*, CATH: comprehensive structural and functional annotations for genome sequences. *Nucleic Acids Res* **43**, D376-381 (2015).

51. W. Wriggers, Conventions and workflows for using Situs. *Acta Crystallogr D Biol Crystallogr* **68**, 344-351 (2012).

52. L. G. Trabuco, E. Villa, K. Mitra, J. Frank, K. Schulten, Flexible fitting of atomic structures into electron microscopy maps using molecular dynamics. *Structure* **16**, 673-683 (2008).

53. J. C. Phillips *et al.*, Scalable molecular dynamics with NAMD. *J Comput Chem* **26**, 1781-1802 (2005).

54. R. Y. Wang *et al.*, De novo protein structure determination from near-atomic-resolution cryo-EM maps. *Nature methods* **12**, 335-338 (2015).

55. Y. Song *et al.*, High-resolution comparative modeling with RosettaCM. *Structure* **21**, 1735-1742 (2013).

56. F. DiMaio *et al.*, Atomic-accuracy models from 4.5-A cryo-electron microscopy data with density-guided iterative local refinement. *Nature methods* **12**, 361-365

(2015).

57. I. W. Davis *et al.*, MolProbity: all-atom contacts and structure validation for proteins and nucleic acids. *Nucleic acids research* **35**, W375-383 (2007).

58. P. Emsley, B. Lohkamp, W. G. Scott, K. Cowtan, Features and development of Coot. *Acta Crystallogr D Biol Crystallogr* **66**, 486-501 (2010).

Chapter 2.

Investigations of *in vitro* interactions between Her2 and bRaf kinases and Hsp90/Cdc37.

Introduction.

All the members of EGFR family are dependent on Hsp90 prior to maturation, but only Her2 remains dependent on Hsp90 even after it has been transported to the plasma membrane(*1, 2*). The rapid degradation of Her2 in the absence of Hsp90 is mediated via CHIP and Cullin5 ubiquitin ligases, where upon GA treatment, Her2 is rapidly ubiquitinated and then degraded via the proteasome pathway(*3*). Indeed, Hsp90 co-immuno-precipitates with Her2 in cell lysates, but upon GA treatment this interaction is lost. It has been shown that the kinase domain of Her2 (Her2 KD) is responsible for the interaction with Hsp90(*4*). Her2-Hsp90 interaction is one of the strongest kinase-Hsp90 interactions, which is a desired characteristic for *in-vitro* studies(*5*). Curiously, there is also evidence for extracellular Hsp90 being involved in dimerization/heterodimerization of the extracellular domains(*6*). As with Cdk4, most questions about interactions between Her2 and Hsp90/Cdc37 were un-answered when I started working on it. Before work on Hsp90/Cdc37/Cdk4 complex I spent a couple of years trying to build an *in vitro* system from purified components, rather than co-purifying these proteins from cells. The rationale was that this would allow for more rigorous biochemical investigation of the system. Surprisingly, I could never get a strong enough interaction *in vitro* between these proteins so that it was unquestionably worth following up. Obtaining the Hsp90/Cdc37/Cdk4 structure answered main structural questions that I wanted to answer using *in vitro* Her2 system, therefore this project was not completed. However, I still think that it is useful to describe these experiments for those who may want to pursue work on Her2 and Hsp90 in the future. Potentially fruitful avenue of pursuit would be more biochemical investigation utilizing the kinase assay, potentially incorporating

insights learned from the published vSrc reconstitution work(*7*). I also co-purified the Hsp90/Cdc37/Her2 kinase domain complex from eukaryotic cells using the yeast expression system described in Chapter 1 and imaged it via negative stain EM. All evidence points to the fact that such purified system is identical to the Hsp90/Cdc37/Cdk4 complex already characterized and therefore future structural work on this complex is of dubious value.

During my work on this system a paper was published by Pearl group describing *in vitro* reconstitution of Hsp90/Cdc37/bRaf complex from purified components(*8*). Raf family kinases are known to depend on Hsp90, with cRaf (Raf-1) being the strongest client(*9*). bRaf is considered a weak client, and aRaf is independent when mature(*5*). Interestingly, bRaf V600E cancer driving mutant is a much stronger client than wt bRaf, so, this was the mutant I chose to work with. Also, for *E.coli* expression, 16 mutations were introduced on the surface to make the kinase soluble(*10*). The goal of this work was to look at bRaf-Cdc37 N terminal domain interactions by either crystallography or NMR, to potentially complement low resolution EM structure. I was able to reconstitute the complex, but the kinase proved to be fairly unstable precipitating during NMR data collection.

Results.

I started the project by trying to purify the kinase domain of Her2 (residues 684-1031) from *E.coli*, construct which was picked based on previous *in vivo* work but optimized via homology modeling based on EGFR crystal structure(*4*). In all expression conditions this construct would always aggregate and come out in the inclusion bodies. Co-expression with Hsp90 in *E.coli* did not alleviate the problem. After trying many

different refolding conditions, the condition which worked best was refolding on Ni beads during purification by diluting Tween 20. This yielded soluble kinase domain (Fig 1). Such purified domain didn't associate with either human or bacterial homologues of Hsp90, possessed no activity towards substrate peptide and always precipitated during concentration. The conclusion was that although this protein is soluble and workable it is in the state unfit for further assays.

Expression in Sf9 cells however, of the same kinase domain of Her2 (residues 704-1029) yielded clean, soluble protein, which was active and could be concentrated to high micromolar concentrations (Fig 2). Having this sample in hands, I attempted to assay the interactions between Her2 kinase domain and Hsp90 and/or Cdc37 via variety of different methods, with the hopes that some of them may capture the right regime of interactions. Starting first with non-equilibrium method of monitoring for co-elution on gel filtration column, I was not able to observe interactions between Her2 and Hsp90, or Cdc37, or Hsp90/Cdc37 complex after up to 3 hours incubations with or without ATP, with or without molybdate. (Fig 3) Including 1 hour 37C temperature jump (with ATP and molybdate) caused kinase aggregation (as monitored by appearance of void peak) still without complex formation. (Fig 4). Adding in Hsp70, Hsp40, CKII and Hop with ATP didn't yield complex either (trying to reconstitute previously observed complex with Chk1)(*11*). However, it seemed like there were Hsp90/Cdc37, Hsp90/Hsp70/Hop/Cdc37 and Hsp70/Cdc37 complexes forming, which might be interesting to follow up (See Materials and Methods). Although these experiments were done at 20-30uM protein concentrations, the fear was that due to non-equilibrium nature of the method I was missing a weak interaction, therefore I attempted to capture the interactions via a number

of different available equilibrium methods with either yeast homologue (Hsc82) via fluorescence or human Hsp90 homologue.

It has been observed that Hsp90 closure rate between monomers in response to AMPPNP is accelerated in the presence of the model substrate, therefore it was logical to attempt such an experiment with Her2 kinase domain (using Hsc82, as it is the closest homologue to human cytosolic Hsp90 which can be cysteine free)(*12*). At first a different plateau was observed in response to higher concentrations of Her2, indicating higher population of closed Hsc82. However, upon comparison with matching amounts of BSA, it was observed that this effect was not specific to Her2 (Fig 5). Another assay was previously established in the lab to monitor for client binding based on the reduction in exchange rate between monomers of Hsp90 upon binding of the substrate, as monitored by reduction in FRET between fluorophores on different arms of the Hsp90 dimer(*13*). However, neither Cdc37 (human homologue), nor Her2 reduced the rate of monomer exchange (Fig 6).

Fearing that we might still be missing a very weak interaction, or that Her2 binding may be asymmetric and/or not having an effect on Hsp90's closure rate, I established a kinase assay for Her2 using commercially available substrate peptide. Again, Sf9 expressed Her2 kinase domain had robust and reproducible kinase activity (Fig 7A). However, the rate of kinase activity with 10uM Hsp90 and Cdc37 each was only 1.5 fold faster than the rate of Her2 kinase domain with 30uM BSA (Fig 7B). Thinking that the system may be similar to GR, I tried incubating the kinase with Hsp70/Hsp40 to see if it would lead to reduction in kinase activity. However, this was not observed (Fig 8).

Taking into consideration that Her2 kinase domain is a strong client *in vivo* from published work meant that somehow we were missing an essential piece required for the interaction, which was not recapitulated by either pure Hsp40/Hsp70/Hop as in the GR system, or by phosphorylated Cdc37, or by heat shock. To test this hypothesis, I went ahead and added Sf9 purified Her2 kinase domain to Rabbit Reticylo Lysates, and assayed if there was complex formation via Anti His IP followed by a Western Blot for Cdc37 and Hsp90 (native rabbit Cdc37 and Hsp90). Indeed, this experiment worked, where His-tagged Her2 kinase domain was able to robustly interact with Cdc37/Hsp90 (Fig 9). Interestingly, adding Hsp90 inhibitor, Radicicol had no effect, but sodium molybdate and EDTA seemed to strengthen the interaction when ATP wash weakened it, indicating that although this system cannot recapitulate in vivo effects of inhibitor caused dissociation, it still has an ATP dependence. Although this system was working and can be explored further for biochemical assays, it was too small of the scale for structural work.

Inspired by the success of Hsp90/Cdc37/Cdk4 co-expression in insect cells I attempted to replicate these results with Her2 kinase domain. Indeed, such co-expressed Her2 kinase domain, purified with molybdate, yielded a stable Hsp90/Cdc37/Her2 kinase domain complex (Fig 10). Proteins purified this way were phosphorylated, acetylated and tri methylated as seen by phospho-specific gel staining and mass spectrometry. (Fig 11). Interestingly, Her2 kinase in context of the complex had no activity as compared to being purified alone. (Fig 12). I was able to take the same construct and co-express it in the yeast system, as described before to high purity. Trying to learn about how the kinase remodeling happens during the cycle progression, I attempted to dissociate the complex.

Surprisingly, under no conditions was I able to dissociate the kinase from Hsp90/Cdc37 (Fig 13). Imaging such prepared complex under negative stain EM followed by reference free 2D classification yields classes that at low resolution look indistinguishable from Hsp90/Cdc37/Cdk4 complex prepared in Sf9 cells or yeast. (Fig 14).

I was able to get a stable complex of Hsp90/Cdc37/bRaf in vitro from purified components. (Fig 15). Interestingly, this was without phosphorylation on Cdc37, and 1h incubations at 4C with nucleotides, inhibitors or nucleotide analogues had no effect. By negative stain EM the complex looks much more heteregenous than the sample from eukaryotic cells (Fig 16). Also, one can see that on gel filtration, when comparing eukaryotic complex with human Hsp90 as purified from bacteria, the complex is actually more compact. However, when comparing the Hsp90/Cdc37/bRaf complex to Hsp90 alone, Hsp90 is more compact. This indicates a different state.

With the goal of studying interactions between the kinase interacting part of Cdc37 (N terminal domain) alone with the kinase by NMR, I assayed interactions between bRaf and Cdc37 residues 1-128. Indeed, although weaker, I was able to get a robust interaction based on gel filtration (Fig 17). However, when followed up by NMR, the kinase precipitated over time, causing Cdc37 to precipitate with it causing disappearance of peaks on proton-N15 HSQC. Utilizing ThermoFluor assay I searched for optimum buffers to increase bRaf solubility (Fig 18). Interestingly, sodium sulfate had a pronounced stabilizing effect. bRaf purified with sodium sulfate was considerably more stable, not precipitating during the purification. However, Cdc37 failed to interact with bRaf in this buffer. This may benefit from further optimization.

Discussion.

It is a fundamentally important question, why client kinase-Hsp90/Cdc37 interactions are readily observable in cells or as purified from eukaryotic cells but are so difficult to reconstitute *in vitro*. There are a number of potential explanations for this. Although I have tried utilizing Hsp40/Hsp70/Hop system, which has worked for GR, there are potential differences between numerous Hsp40 and Hsp70 homologues, and I could have been using the wrong ones. Alternatively, it may be not an Hsp40/Hsp70 family member that is necessary. More and more evidence points to extreme importance of allosteric regulation in kinases. Potentially in cells, via interactions with substrates or regulatory proteins the kinases populate the Hsp90 interacting state more often. Recent work from Buchner lab shows an important distinction between Hsp90α and Hsp90β, with the first one not being able to associate *in vitro* with vSrc but the second one making such an interaction.(*7*) This is very interesting as there is only a handful of differences between the two homologues, therefore it would be interesting to follow up and narrow in on the exact residues responsible for the difference. In my assay *in vitro* I have used Hsp90α homologue, therefore this could explain the absence of interactions. Finally, phosphorylation on both, Hsp90 and Cdc37, is known to be very important for these interactions and although I was able to add Cdc37 phosphorylation on serine 13, phosphorylation on other residues was missing. Hsp90 was also not phosphorylated. There is evidence that phosphorylation needs to be dynamic, so, just having appropriate sites phosphorylated may not be enough(*14*).

Surveying kinase domain structures from different families and in different states, it is apparent that structurally they are very similar(*15*). Therefore, it is unsurprising that

at negative stain resolutions I do not see differences between the complex with Her2 and the complex with Cdk4 (Chapter 1). It is very likely that once the kinase makes an interaction with Hsp90/Cdc37 system, in that state, disregarding what kinase specifically it is, the structure will be the same. The main differences lay in the dynamics of breathing motions between the two lobes, rather than differences in the binding site. Therefore you may find that some kinases bind more or less readily than others, but once they bind to Hsp90/Cdc37, especially when trapped with molybdate, they all are in the same state. Therefore I do not believe following up structural work on Hsp90/Cdc37/Her2 kinase domain as expressed in Sf9 is a worthwhile pursuit. There could be important structural differences however in context of other domains of the kinase, and this may be an interesting area of further investigation. One could imagine for example that extra domains in the kinase, or motifs, like juxtamembrane region for example, make interactions with the unfolded kinase N lobe in the context of quaternary complex, and it could be beneficial to visualize this state.

bRaf system offers a very different glimpse into Hsp90-kinase interactions as the complex seems to be considerably different than the ones prepared from eukaryotic cells. This could be for a couple of reasons. First, this may represent the loading complex, the one which interacts with the kinase while Cdc37 is making crystal structure like interactions (see model in Chapter 1 or Chapter 3). However, the interactions seem to be fairly weak for structural studies by electron microscopy, therefore some way to stabilize them is needed before proceeding forward. The other possibility is that bRaf prepared in such a way is making non physiological interactions due to being in a severely destabilized state. Therefore, the interactions at the level of Cdc37 are interesting and

likely relevant, but how relevant are the interactions in the context of quaternary complex, due to missing post translation modifications, ATP dependence, etc, is questionable.

Although Her2 and bRaf projects were not completed I think important insights into the kinase-Hsp90 interactions, how they fit into Hsp90 ATPase cycle and affect kinase activity were still learned. Much of the results underlie the fact that binding between these two proteins should be studied on the backdrop of extremely intricate ATP cycle of both of the proteins. Therefore there are many modes of interactions between these two, in different conformational states and with different affinities, all depending on where in the cycle you look at it. Any future projects should be very mindful of this point.

Methods and Materials.

Expression and purification of Her2 kinase domain from E.coli.

Her2 kinase domain (residues 684-1031) was cloned into pet151 D-Topo vector. BL21 DE3Star cells were transformed with the above. Grown shaken at 37C in LB with carbenecilin (50-100mg/L) to OD of 0.8 and then induced with 1mM IPTG (0.23g/L) and grown shaken at 37C for 4 more hours. Cells were spun down and frozen.

Solubilize cell pellet in ice cold Her2 Lysis buffer (50mM Tris pH 8, 0.1mM EDTA, 5% Glycerol, 100mM NaCl, 15mM BME), about 20 mLs per liter of cells. Emulciflex at 20000 psi for 15 minutes. Spin down at 30000g for 30 minutes. Discard the supernatant, resuspend the pellet in 20 mLs of the unfolding buffer (6M Guanidine HCL, 50mM Tris pH 8, 20mM Imidazole, 100mM NaCl, 15mM BME). Dounce homogenize for 30 cycles. Let sit for 30-60 minutes. Spin down at 30000g for 30 minutes. Incubate the supernatant with 2mLs (bed volume) of QIAGEN NiNTA beads for 2h, rotating at 4C. Wash with 15CV of the unfolding buffer. Then wash with 10 CV of Refolding buffer (20mM Tris pH 8, 150mM NaCl, 15mM BME, 0.1% Tween 20). Let the beads sit in the buffer O/N at 4C. Elute with 15 mLs of Elution buffer (20mM Tris pH 8, 150mM NaCl, 15mM BME, 0.01% Tween 20). Dialyze against 1L of Dialysis Buffer (20mM Tris pH 8, 150mM NaCl, 15mM BME). Collect, concentrate and freeze. Can get about 20uM.

Expression and purification of Her2 kinase domain from Sf9 cells.

Her2 kinase domain (residues 704-1025) in pFastBac HTB insect cell vector was a gift from Ron Bose lab. 1L insect cell pellet was solubilized in 30mLs of Buffer A (50mM HEPES pH8, 150mM NaCl, 20% Glycerol, 1% Tween 20, 15mM BME, protease inhibitors), then emulciflexed at 15000psi for 10 minutes. Spin the lysate down at 30000g

for 30 minutes. Incubate the supernatant for 1h at 4C with 1mL of QIAGEN NiNTA beads prewashed in Buffer A. Wash with 35mLs of Buffer B (50mM HEPES pH8, 100mM KCl, 20% Glycerol, 0.05% Tween 20, 15mM BME). Wash with 10mLs of Buffer C (50mM HEPES pH8, 1M KCl, 20% Glycerol, 0.05% Tween 20, 15mM BME) Wash with 10mLs of Buffer B + 10mM Imidazole. Repeat with 10mLs Buffer B + 20mM Imidazole. Elute into 10mLs of Buffer B with 200mM Imidazole. Concentrate down to 5mLs and then load 16/60S200 column pre equilibrated in Buffer D (50mM HEPES pH8, 150mM NaCl, 20% Glycerol, 5mM DTT, 0.01% Tween 20). Collect peak at about 90mls, concentrate (down to about 200uM) and flash freeze.

Hsc82 Closure assay with Sf9 Her2.

The assay was done on the plate reader, Labeled Hsc82 (One with Alexa525, another with Alexa647) was kindly provided by Timothy Street. Reaction volume was 80ul, final concentration was 250nM of Hsc82 dimer. Hsc82 A525 at 500nM concentration was mixed with equal amount of Hsc82 A647 and incubated for 30 minutes for monomer exchange to happen. This mix at 500nM labeled dimer concentration was then used downstream for closure assays. The reactions were mixed in with Her2 at different concentrations (0uM 5uM, 10uM, 15uM, 20uM, 25uM, 30uM) with MgCl2 to a final concentration of 10mM. The reactions were equilibrated at room temp for 60 minutes. 60uL of each reaction was added to the 384 well plate, 2uL of 52uM AMPPNP was added to each reaction, mixed, and then read out by exciting at 550nm, reading at 670nm with cutoff at 570nm every 30 seconds for 120 minutes at 25C in the plate reader.

Hsc82 monomer exchange assay with Sf9 Her2.

Use Hsc82 labeled with Alexa dyes as above. Reaction ran in the plate reader, final

volume is 80uL. Mix labeled Hsc82 at 1uM monomer with each other and incubate at room temp for 30 minutes. Then mix in 30uM of Her2 or Cdc37 and incubate further at room temp for 30 minutes. Then add unlabeled Hsc82 (40uM dimer) to initiate the reaction. The plate reader set up was as before, reads were every 30 seconds for 30 minutes.

Analytical gel filtration assaying for Sf9 Her2 interactions with human Cdc37 and or human Hsp90α.

Reaction volume was 60uL, Hp90 was at 10uM dimer, Her2 and Cdc37 were each at 20uM. Reactions were incubated at room temp for 30 minutes before running, but gel filtration was at 4C. The column used was PC3.2 S200. The incubation/running buffer was 50mM HEPES pH8, 150mM NaCl, 10% Glycerol, 0.01%Tween 20, 5mM DTT.

Experiments on figure 4 were done a little bit different. Hsp90 (10uM dimer), Cdc37(20uM) and CK2 (0.7U) were incubated in 30mM HEPES pH 8, 150mM KCl, 10mM MgCl2, 10mM ATP, 5mM DTT, 10% Glycerol, 0.01% Tween 20 at 30C for 1h to phosphorylate Cdc37. At this point sodium molybdate was added to a final concentration of 20mM and then Her2 was added to a final concentration of 20uM. This mix was incubated at 30C for 180 minutes. Aliquots of the mixture were ran on gel filtration at 1h and 2h. The rest of the reaction after 2h was shifted to 37C, and incubated for another 80 minutes, then ran on the PC3.2 S200. The column was equilibrated in 30mM HEPES pH8, 150mM NaCl, 10mM KCl, 10mM MgCl2, 5mM DTT, 10% Glycerol, 0.01% Tween 20, 20mM Na2MoO4.

Also, did a variation of the experiment described in Arlander et al, where 10uM Hsp90 dimer, 10uM Cdc37, 10uM Hsp70, 5uM Hsp40, 5uM HOP, 2U of CK2 were

incubated at room temp for 1h in 30mM HEPES pH8, 50mM KCl, 5mM MgCl2, 5mM ATP, 5mM DTT, 10% Glycerol, 0.01% Tween 20. Then added Her2 to a final concentration of 10uM and further incubated for 3h. Ran aliquots of the reaction on PC3.2 S200 column at 20, 90 and 180 minutes in the same buffer as above but without ATP. Hsp70, Hsp40, HOP were kindly provided by Elaine Kirschke.

Kinase Assay.

Make 2X Kinase Mix (2uM Her2 kinase, 100uM Substrate Peptide, 50mM HEPES pH8, 150mM NaCl, 20% Glycerol, 5mM DTT, 0.01% Tween 20) and 2X Reaction Buffer (50mM HEPES pH8, 150mM NaCl, 20mM MgCl2, 100uM ATP, 0.01% Tween 20, 20uCi of P32 ATP per 70uL reaction). Add 10uL of Reaction buffer to 10uL of Kinase Buffer to start the reaction. Run for the desired time. If doing time series, start multiple equivalent reactions at the same time in 96 well plate by using multi channel pippetter. Usually would do 0(had 1uL 0.5M EDTA to start), 3, 6, 9, 12, 15, 18 minutes. Quench the reaction with 10uL of 0.5M EDTA. After quenching spot 5uL of each reaction on P81 phospho-paper. Wash the paper by rocking in 50mLs of 1% Phosphoric Acid for about 10 minutes. Repeat 8-10 times. Then rinse the paper in 100% acetone for couple of minutes, then leave to dry. Expose phopshoscreen O/N then image on typhoon machine. Kinase concentrations and can vary, and extra proteins, like Hsp90, Cdc37, BSA, Hsp40, Hsp70, etc can be added to the 2X Kinase Mix for desired time before starting the kinase reaction.

Using His tagged Sf9 Her2 as bait in Rabbit Reticulo Lysates (RRL).

3uL of Sf9 expressed Her2 at 94uM were added to 45 uL of RRL from Promega (to a final concentration of 5uM). At this point sodium molybdate, ATP, EDTA or

Radicicol could be added to appropriate concentrations to bring the final volume to 50uL. Reactions were incubated at 30C for 45 minutes, then placed on ice. 30uL of Sigma monoclonal anti His antibody tethered to agarose (AntiHist beads) were washed two times in 10mM PIPES pH7.2, 50mM NaCl, 0.5% Tween 20. Such washed beads were incubated with the above 50uL reactions for 30 minutes at 30C. 500uL of 10mM PIPES pH 7.2, 50mM NaCl, 0.5% Tween 20 (low salt buffer) was then added to each reaction, reaction was spun down at 1000g for 1 min and supernatant discarded. The beads were then wash 3 times with 200ul of either low salt buffer, medium salt buffer (same as low salt, but 150mM NaCl), or high salt (same as low salt but 500mM NaCl). After last wash beads were resuspended in 50uL of SDS Loading buffer incubated at 65C for 10 minutes and, spun down and 5uL of was ran on the gel. Western blots were done using standard procedures using Santa Cruz HRP conjugated anti-His antibody or Cell Signaling #4874 anti Hsp90 antibody.

bRaf expression and purification.

Growth and induction.

1) Set up a 50mL O/N culture in LB+antibiotic (kan in my case, 50mg/L). Make media. Don't autoclave if M9, otherwise autoclave.

2) Next morning, add antibiotic(kanamycin) to growth media. Spike ~10mLs of O/N culture per liter of growth media. Shake at 37C, 180rpm.

3) When the cells are about 1 hour away from reaching OD of 0.6, shift the temperature of incubator to 17C. Induce cells with 0.23g/L of IPTG when the culture is around OD0.6 (around 1 for TB). Take about 3 hours to reach the right density in LB or TB, about 6-7 hours in M9. Shake at 17C O/N. (about 18h induction time)

4) Spin the cells down at 4000g for 15 minutes. Collect the cell pellets and freeze by placing into the -80 freezer.

Buffers.

Lysis Buffer: 100mM HEPES pH7.0, 250mM NaCl, 0.75% Igepal, 5% Glycerol, 25mM Imidazole, 5mM MgCl2, protease inhibitors.

Ni-NTA Wash Buffer: 20mM HEPES pH7.5, 200mM NaCl, 25mM Imidazole, 5mM MgCl2, 1mM DTT.

GF Buffer: 20mM HEPES pH7.5, 200mM NaCl, 5% Glycerol, 1mM DTT.

Purification.

Keep everything cold!

1) Solubilize the cell pellet in about 35 mLs of cold Lysis Buffer. This is for 3L of M9 media cell pellet (OD and spin down is 1.7), yields about 40mls of solubilized pellet solution. Scale appropriately.

2) Lyse the cells using the Emulciflex, 15000psi for 10-15 minutes. Can probably use other means of lysis, this is what works for me.

3) Spin down at 30000g for 1h. Collect the supernatant.

4) While spinning, washed the the Ni-NTA superflow resin (Qiagen) with about 15-20 bed volumes of Lysis buffer. Usually use about 1mL bed volume per 1L cell culture.

5) Incubate the clarification spin supernatant with the washed Ni-NTA resin for about 2h at 4C.

6) Wash the resin with 5x bed volume of Lysis Buffer+25mM Imidazole(50mM total).

7) Wash the resin with 10x bed volume of Ni-NTA wash buffer.

8) Elute the resin into 5x bed volume of Ni-NTA wash buffer+500mM Imidazole.

9) Concentrate the elution or load straight onto the S200 column pre-equilibrated in the GF buffer. The kinase crashes out over time and during concentration, so, need to minimize concentration steps (ie load 5 mLs onto 16/60S200 or 10mLs onto 26/60S200), also, spin before the gel filtration and also, load through the filter. This step most likely can be optimized, ie add glycerol, etc.

10) There is usually a large void peak and then a peak at about 0.7 bed volume of S200 gel filtration column. Collect that peak, concentrate, aliquot and flash freeze.

An example of yields, 3L of cells grown in M9 media(spun down at OD of 1.7) yielded about 500uL at 345uM. 5L of M9 media with extra glucose and biotin/thiamin yielded ~1mL at about 470uM.

P.S. His tag can be cleaved after Ni-NTA elution step, by dialyzing ON with added protease into GF buffer. However, a lot of protein crashes out. Still good yields afterwards.

Eukaryotic CDC37 Expression and Purification From *E.coli* (full length or NTD*)*

Lysis Buffer(need 500 mLs):

50mM Tris pH 7.5, 500mM NaCl, 20mM Imidazole, 5mM BME

Cleaving Buffer(need 4L):

20mM Tris pH 8, 100mM NaCl, 1mM DTT

Buffer A(need 500mLs):

10mM Tris pH8, 1mM DTT

Buffer B(need 500mLs):

10mM Tris pH8, 1M NaCl, 1mM DTT

Buffer 4(need 1L):

50mM Potassium Phosphate pH8, 200mM NaCl, 1mM DTT

Use LB, Bl21DE3Star cells, Induction is at 37C for 4h, induce at 0.8, 1mM IPTG.

1) Add Lysis Buffer to the pellet (about 20mLs of buffer per 1L of LB pellet). Resuspend with spatula and pipette so that there are no clumps.

2) Emulciflex at 15000 psi for about 15 mins

3) Spin down at 30000g for 30 mins

4) While spinning, wash 10mLs (bed volume) of Qiagen High Flow Ni beads in Buffer 1 (20 bed volumes)

5) Incubate the washed beads + spin sup from step 3 at 4C for about 1h.

6) Load the biorad gravity column. Wash without about 10 bed volumes of buffer 1.

7) Elute with 50mLs of Lysis Buffer + 500mM Imidazole.

8) Add 2 tubes of TEV (what amount??) and dialyze O/N into 4L of Cleaving Buffer.

9) Wash the S200 GF with Buffer 4 O/N.

Next day.

10) Wash 10/300 MonoQ column. (buffer A then Buffer B then equilibrate with 5CV of Buffer A)

11) Dilute the dialyzed protein 1:1 with Buffer A to lower the NaCl concentration (now, total volume is 100mLs)

12) Load the MonoQ at 2-3 ml/min

13) Wash the column (usually about 3CV, so that UV stabilizes)

14) Run gradient to 100% of BufferB over 20 CV(steps 12-14 are part of the MonoQ method)

15) Collect peak/peaks. Concentrate to 5mLs(10mls if running 26/60 S200).

16) Load pre-equilibrated S200 with the above protein and run at the appropriate flow rate (1 ml/min for 16/60, 2.5ml/min for 26/60)

17) Collect peak/peaks, run a gel, concentrate and flash freeze.

Eukaryotic Cytosolic Hsp90 Expression and Purification from *E.coli*

Buffer 1(need about 500mLs for 6L prep):

50mM Potassium Phosphate(KPO4) ph8, 500mM NaCl, 30mM Imidazole, 5mM B-ME.

Buffer 2(need 50mLs):

50mM Potassium Phosphate ph8, 400mM NaCl, 500mM Imidazole, 5mM B-ME.

Buffer 3(need 4L):

10mM Tris pH8, 200mM NaCl, 1mM DTT

Buffer 4(need 1L):

50mM Potassium Phosphate pH8, 200mM NaCl, 1mM DTT

Buffer A(need 500mLs):

10mM Tris pH8, 1mM DTT

Buffer B(need 500mLs):

10mM Tris pH8, 1M NaCl, 1mM DTT

Use LB, Bl21DE3Star cells, Induction is at 37C for 4h, induce at 0.8, 1mM IPTG.

1) Add Buffer 1 to the pellet (about 20mLs of buffer per 1L of LB pellet). Resuspend with spatula and pipette so that there are no clumps.

2) Emulciflex at 15000 psi for about 15 mins

3) Spin down at 30000g for 30 mins

4) While spinning, wash 10mLs (bed volume) of Qiagen High Flow Ni beads in Buffer 1 (20 bed volumes)

5) Incubate the washed beads + spin sup from step 3 at 4C for about 1h.

6) Load the biorad gravity column. Wash without about 10 bed volumes of buffer 1.

7) Elute with 50mLs of Buffer 2.

8) Add 2 tubes of TEV (what amount??) and dialyze O/N into 4L of Buffer 3.

9) Wash the S200 GF with Buffer 4 O/N.

Next day.

10) Wash 10/300 MonoQ column. (buffer A then Buffer B then equilibrate with 5CV of Buffer A)

11) Dilute the dialized protein 1:1 with Buffer A to lower the NaCl concentration (now, total volume is 100mLs)

12) Load the MonoQ at 2-3 ml/min

13) Wash the column (usually about 3CV, so that UV stabilizes)

14) Run gradient to 100% of BufferB over 20 CV(steps 12-14 are part of the MonoQ method)

15) Collect peak/peaks (usually two peaks, at 30% and 40% BufferB, peak one is good). Concentrate to 5mLs(10mls if running 26/60 S200).

16) Load pre-equilibrated S200 with the above protein and run at the appropriate flow rate (1 ml/min for 16/60, 2.5ml/min for 26/60)

17) Collect peak/peaks(usually peak at 0.55CV and 0.63CV, first peak is the good one), run a gel, concentrate and flash freeze.

Figures.

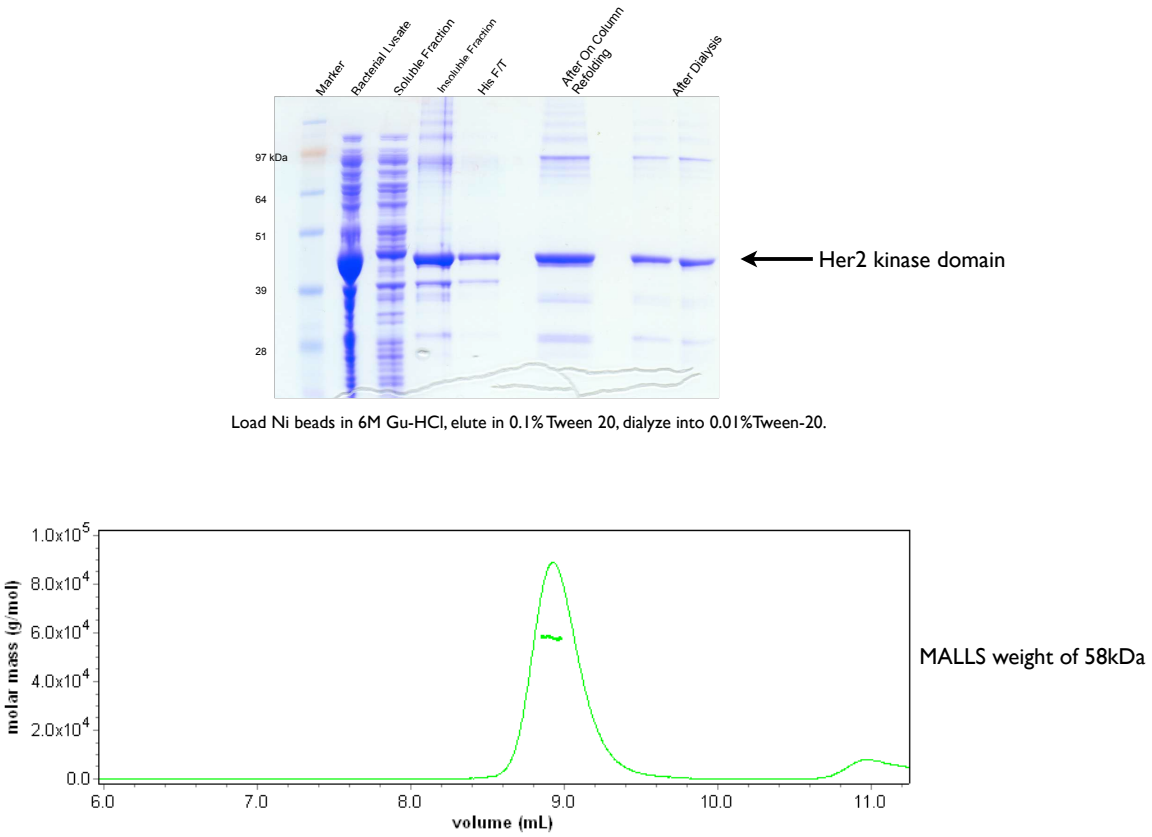

Figure 1. *E.coli* purification of Her2 kinase domain.

Top panel shows the SDS PAGE gel of different steps of purification. The panel on the bottom shows a run on SEC-MALLS. Although the mass is off, which is most likely due to baseline being off during estimation, one can see that the kinase domain was a monodsiperse peak.

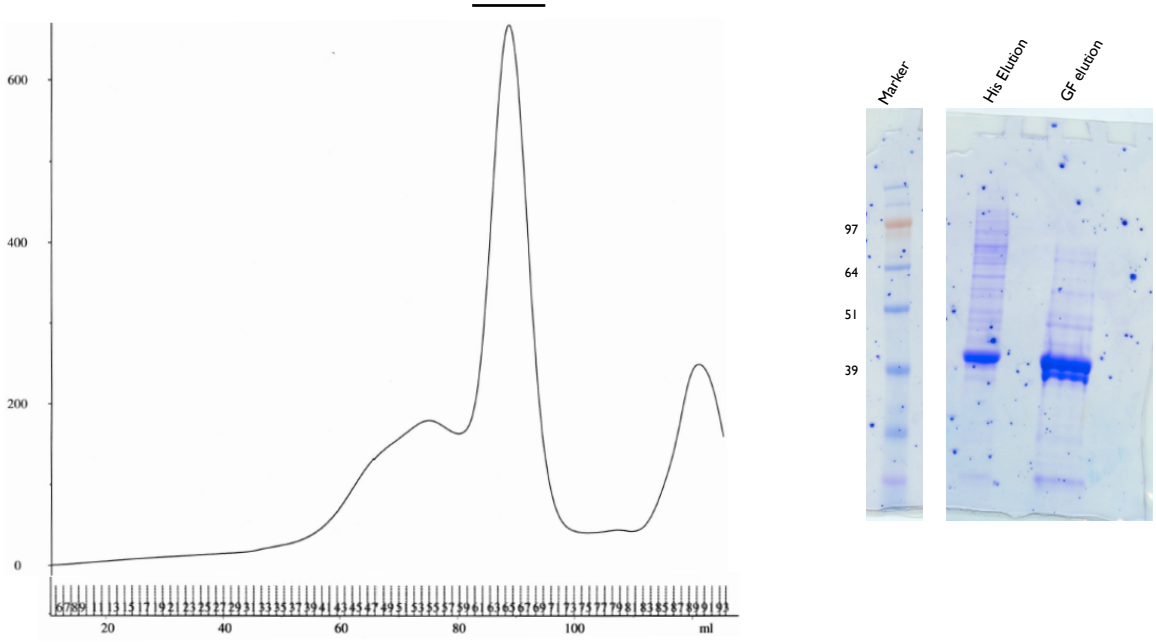

Figure 2. Purification of Sf9 expressed Her2 kinase domain.

On the left is the 16/60 S200 trace with the peak collected indicated by a black line. The gel on the right shows the overall purity of the final product.

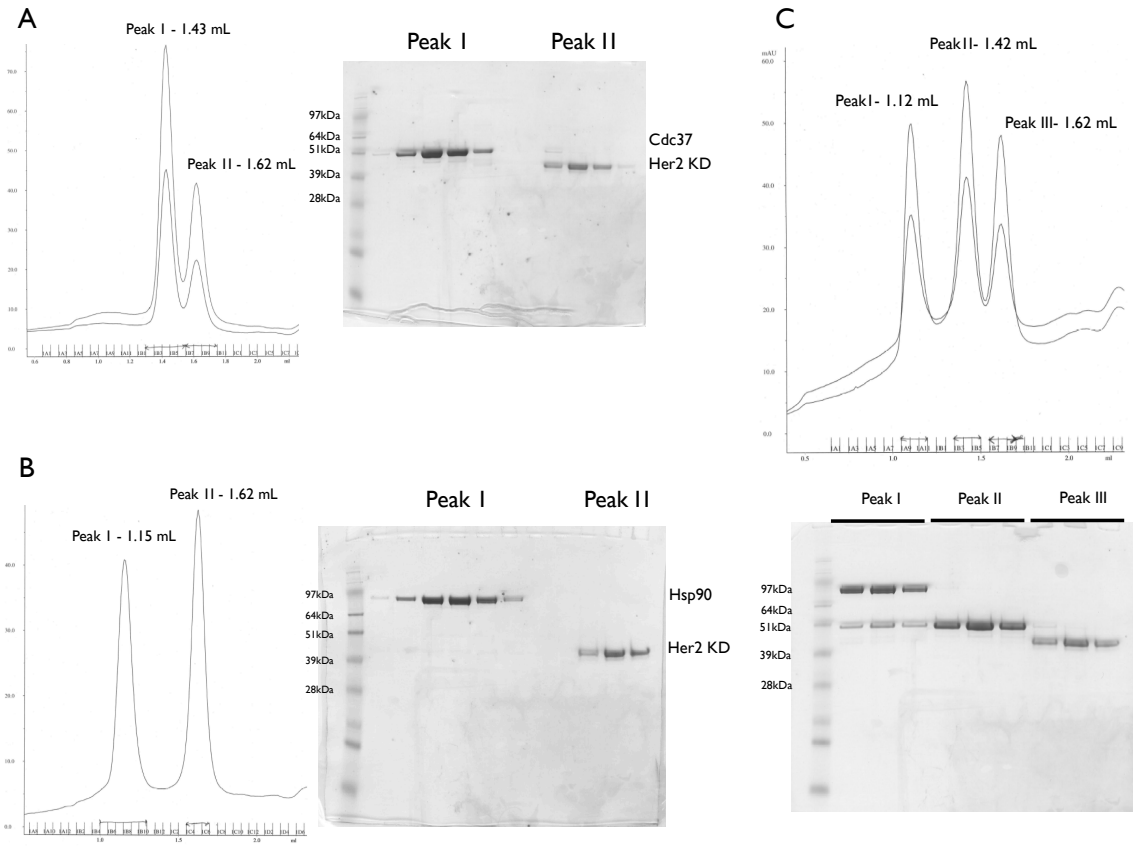

Figure 3. Assaying for Her2 kinase domain interactions with Hsp90/Cdc37 by co migration on the S200 gel filtration column.

(A). Human Cdc37 (Peak 1) was incubated with Her2 kinase domain (Peak 2) at 30C for 1h. (B) Human Hsp90α (Peak 1) was incubated with Her2 kinase domain (Peak 2) at 30C for 1h. (C) All three proteins were incubated together under the same conditions.

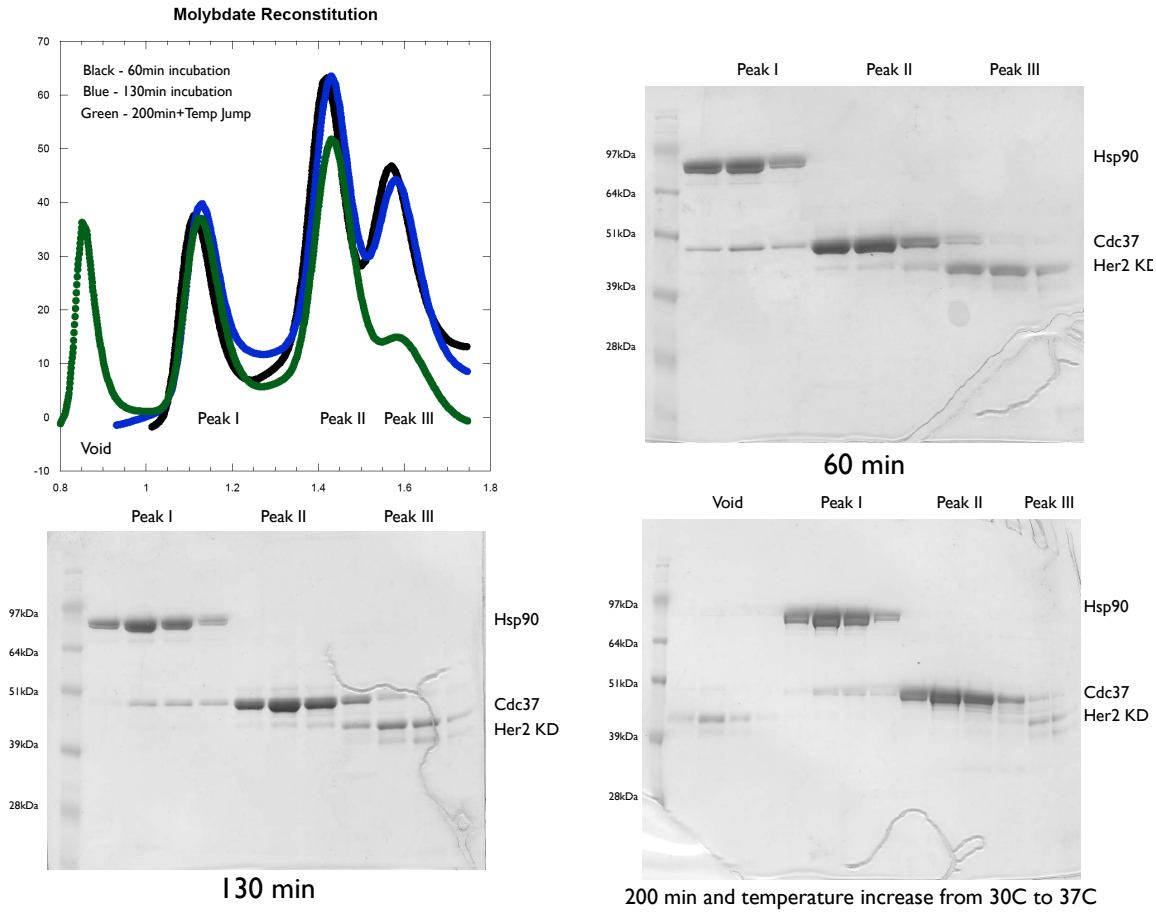

Figure 4. Effects of molybdate and temperature jump on the interactions between Hsp90/Cdc37/Her2 kinase domain.

Proteins were incubated for different times at 30 or 37C with 20mM Sodium Molybdate present. Peak 1 if Hsp90-Cdc37 complex, Peak 2 is excess Cdc37 and Peak 3 is free Her2 kinase domain. Void is aggregated Her2 kinase due to temperature jump.

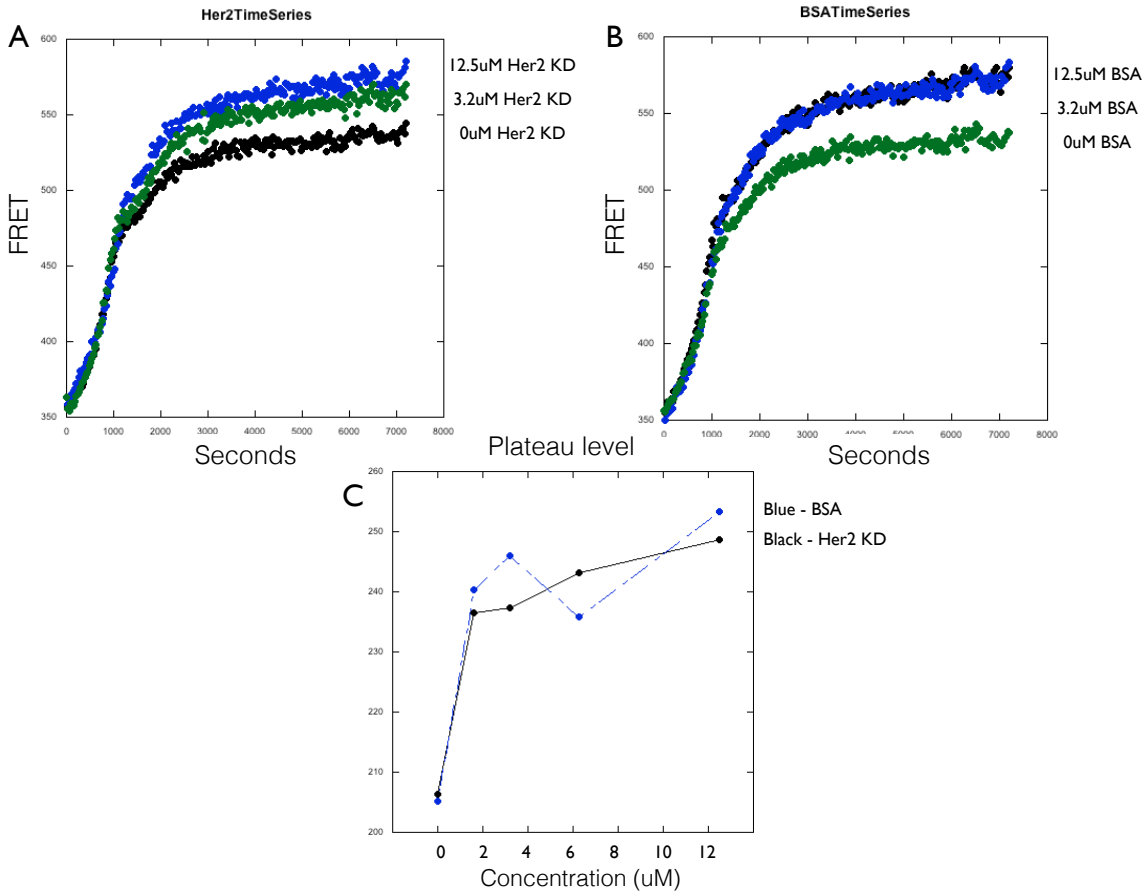

Figure 5. Effects of Her2 on closure rates of Hsc82 vs BSA.

Top left panel is the change in FRET indicating closure in response to AMPPNP addition by Hsc82 at different concentrations of Her2 kinase domain. Panel on the right is the same, but BSA was added instead of Her2. Bottom panel shows plateau levels from fit data, demonstrating that BSA and Her2 change the plateau level the same.

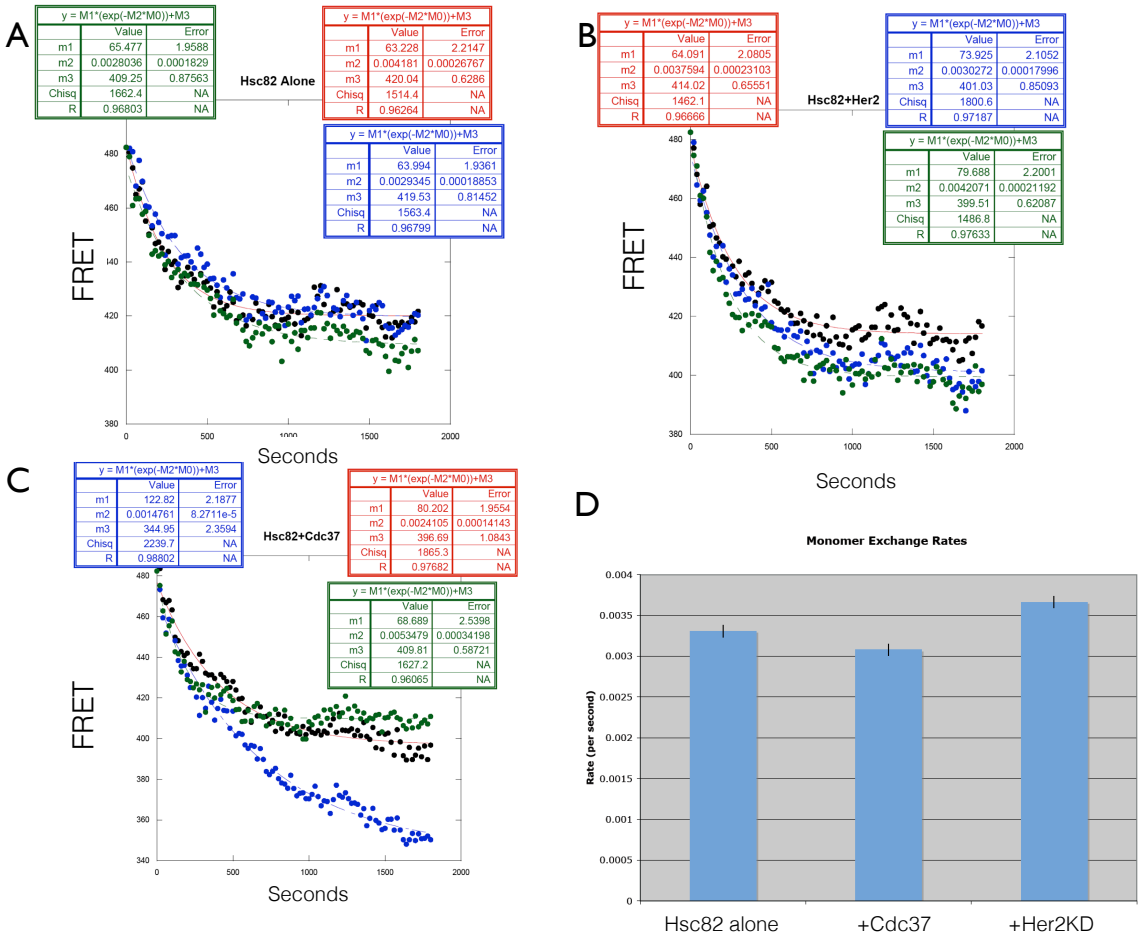

Figure 6. Effects of Cdc37 or Her2 kinase domain on monomer exchange of Hsc82 as monitored by change in FRET.

Top left panel displays three different experiments of monomer exchange by Hsc82 alone. Boxes indicate fitting parameters. Top right panel shows monomer exchange rates of Hsc82 with Her2 added, in triplicate. Bottom left panel is the same, but with Cdc37 added. Bottom right panel shows the mean rates of exchange for the three experiments. No difference is observed.

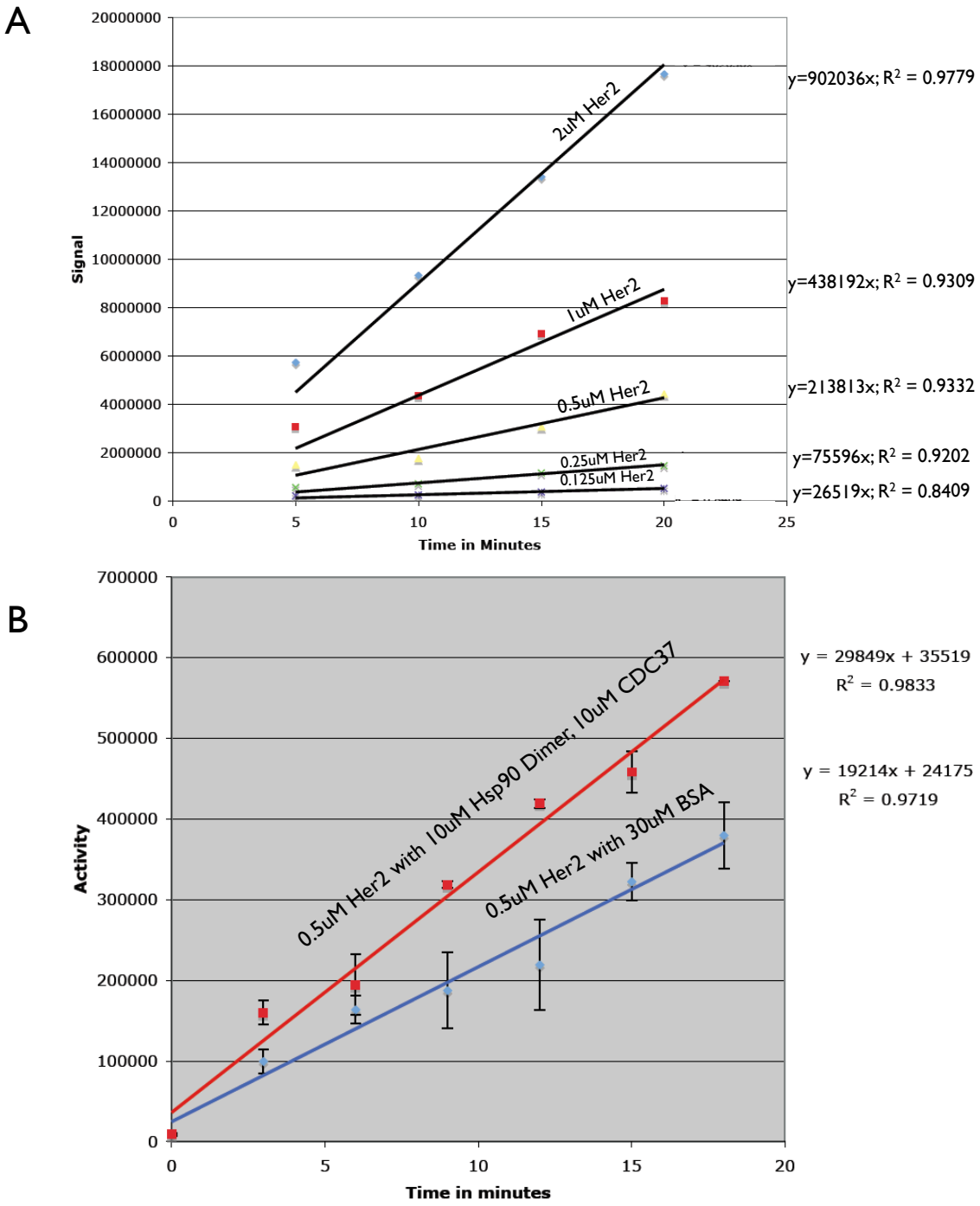

Figure 7. Kinase assay of Her2 kinase.

(A) Accumulation of phosphorylated product over time at different kinase concentrations. As expected the rate of the reaction (slope of the fitted line) doubles upon doubling the kinase concentration. (B) Kinase reaction performed with 20uM BSA or Hsp90. There is

a 50% increase in kinase rate upon addition of Hsp90/Cdc37 vs BSA. Importantly, Cdc37 alone or Hsp90 alone under the same conditions showed no increase.

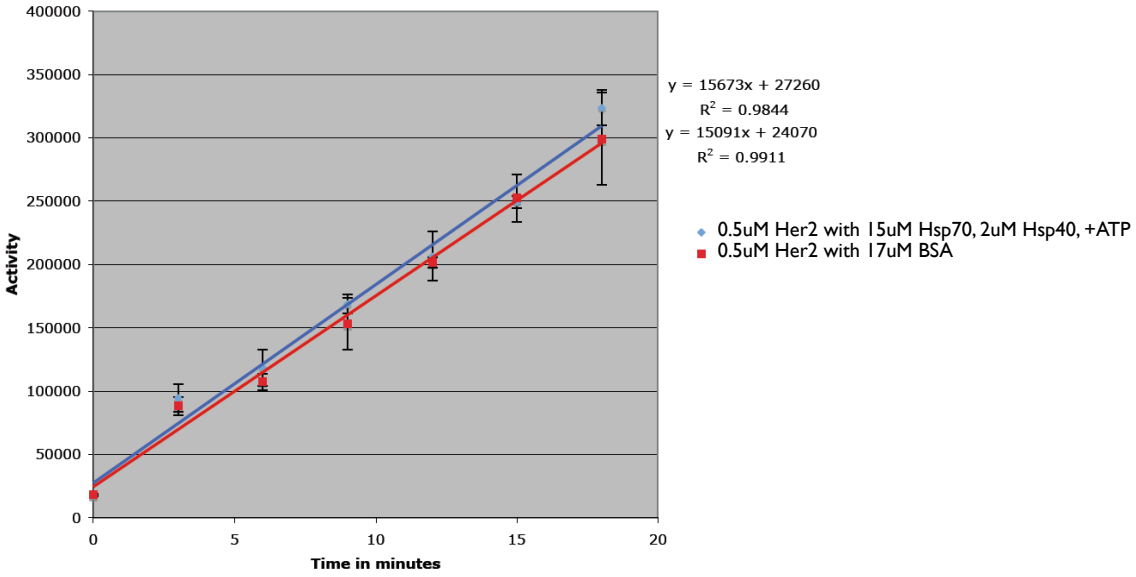

Figure 8. Effects of Hsp40/Hsp70 on Her2 kinase activity

Her2 kinase domain was incubated with indicated amount of Hsp70/Hsp40 or with BSA for 30 minutes, and then the kinase activity was performed.

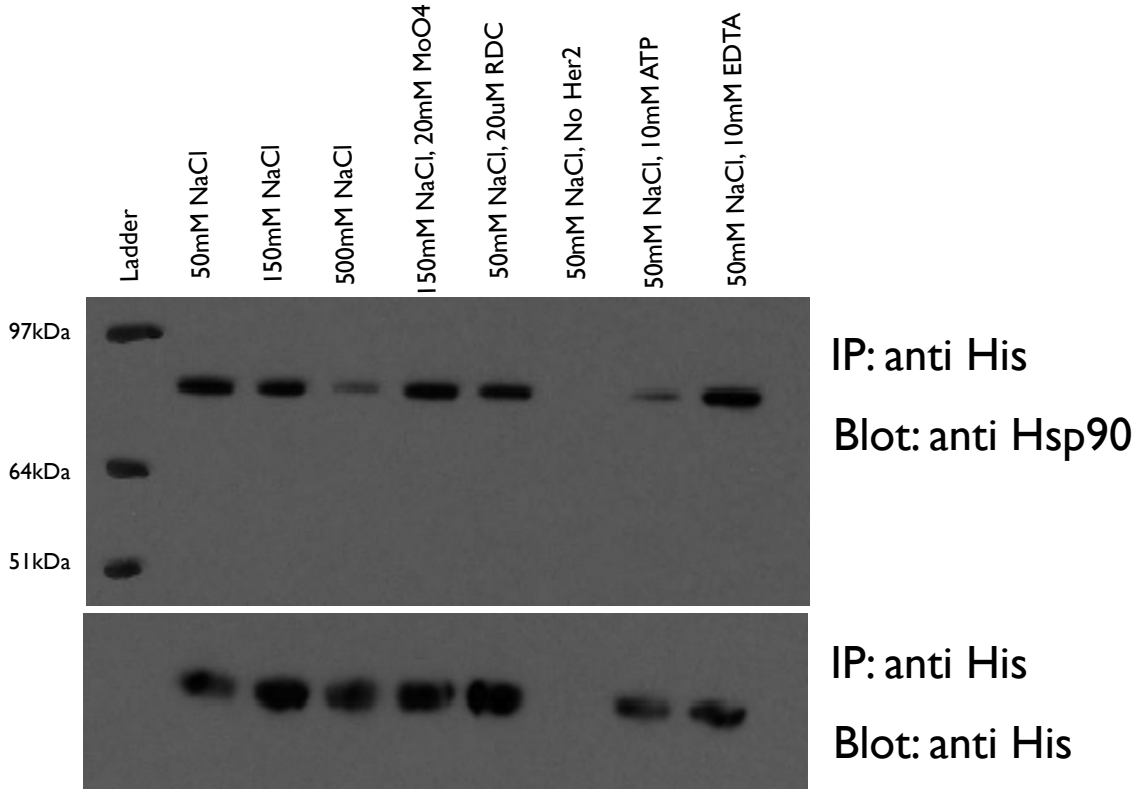

Figure 9. Hsp90/Cdc37/Her2 IPs from Rabbit Reticulo Lysates.

Her2 kinase had a His tag on it.

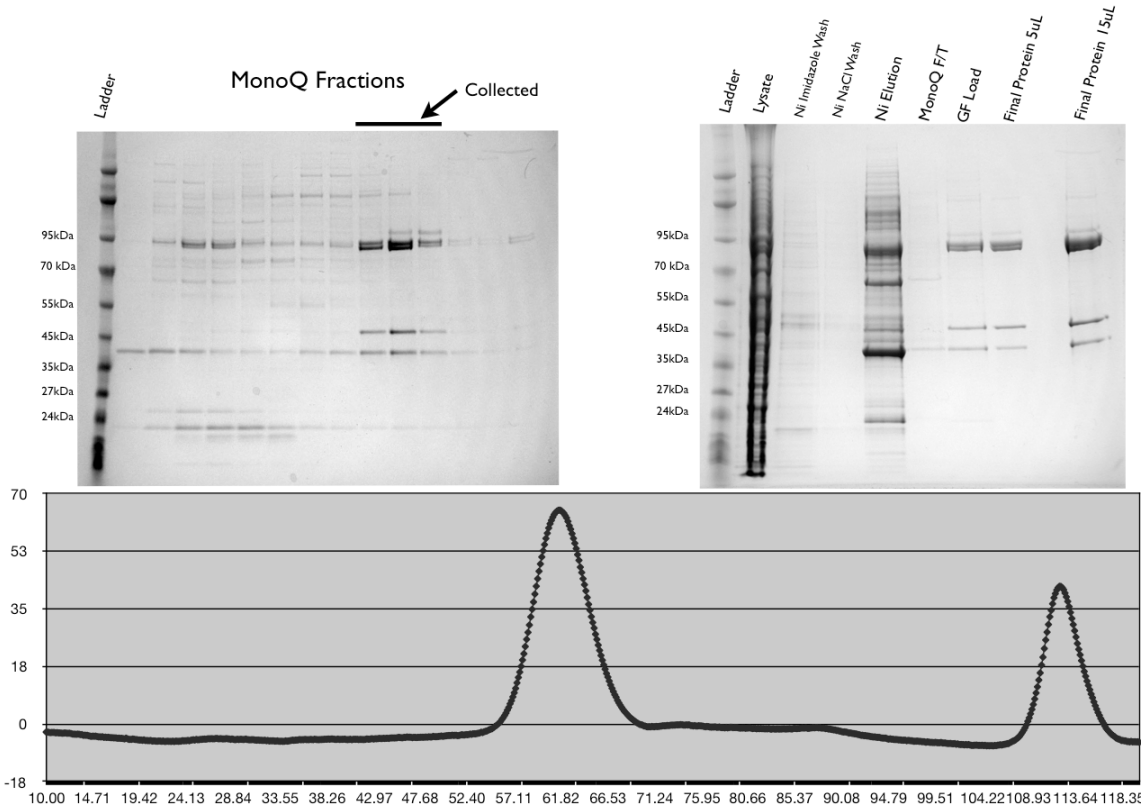

Figure 10. Purification of Hsp90/Cdc37/Her2 kinase domain complex from Sf9 cells co-expressing the three proteins.

Top left is the gel of ion exchange column, top right is the gel with different aliquots during purification and also with the final concentrated complex. The bottom is the chromatography trace (16/60 S200) of the complex. Purification protocol is the same as purification of Hsp90/Cdc37/Cdk4 from yeast except lysis is at 15000psi on Emulciflex.

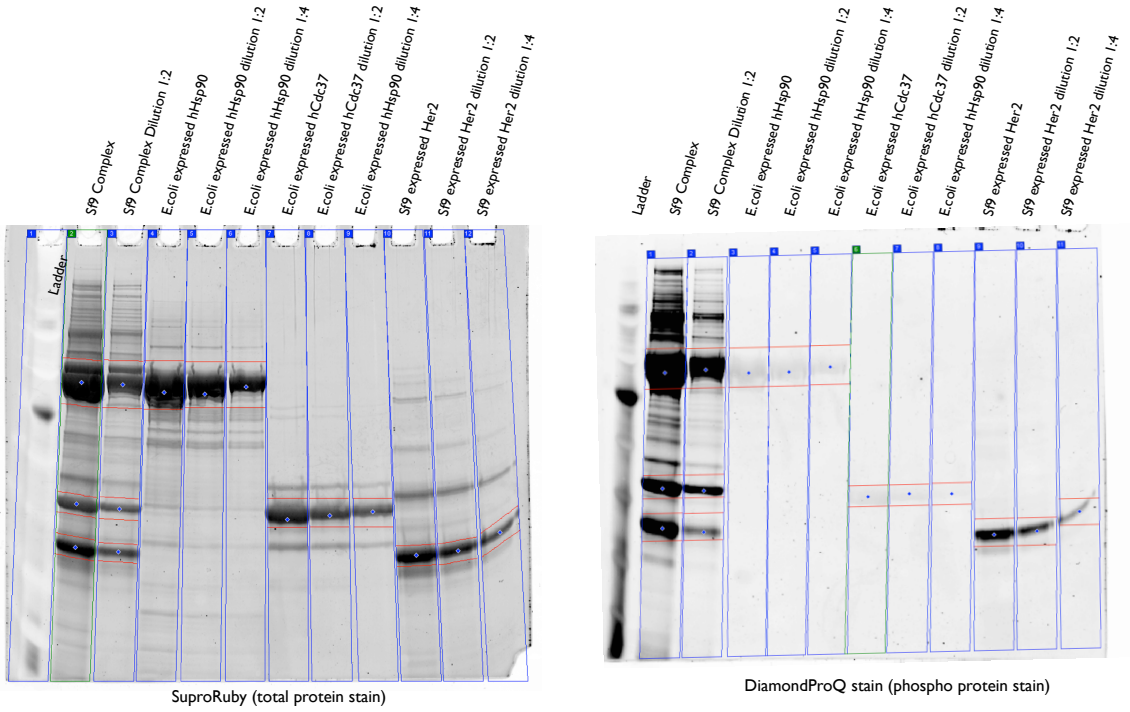

Figure 11. Looking at phosphorylation state of Hsp90/Cdc37/Her2 complex

Gel on the left is total protein as stained by Sypro Ruby (similar sensitivity to silver stain). Two dilutions of Sf9 prepared complex are on the left, followed by dilutions of Hsp90 and Cdc37 prepped from *E.coli* and Her2 kinase domain prepped from insect cells. The gel on the right is the same as on the left but stained with phosphor specific stain. It clearly shows that all proteins from insect cells are phosphorylated. Her2 is phosphorylated in the complex to a higher degree than when prepped alone.

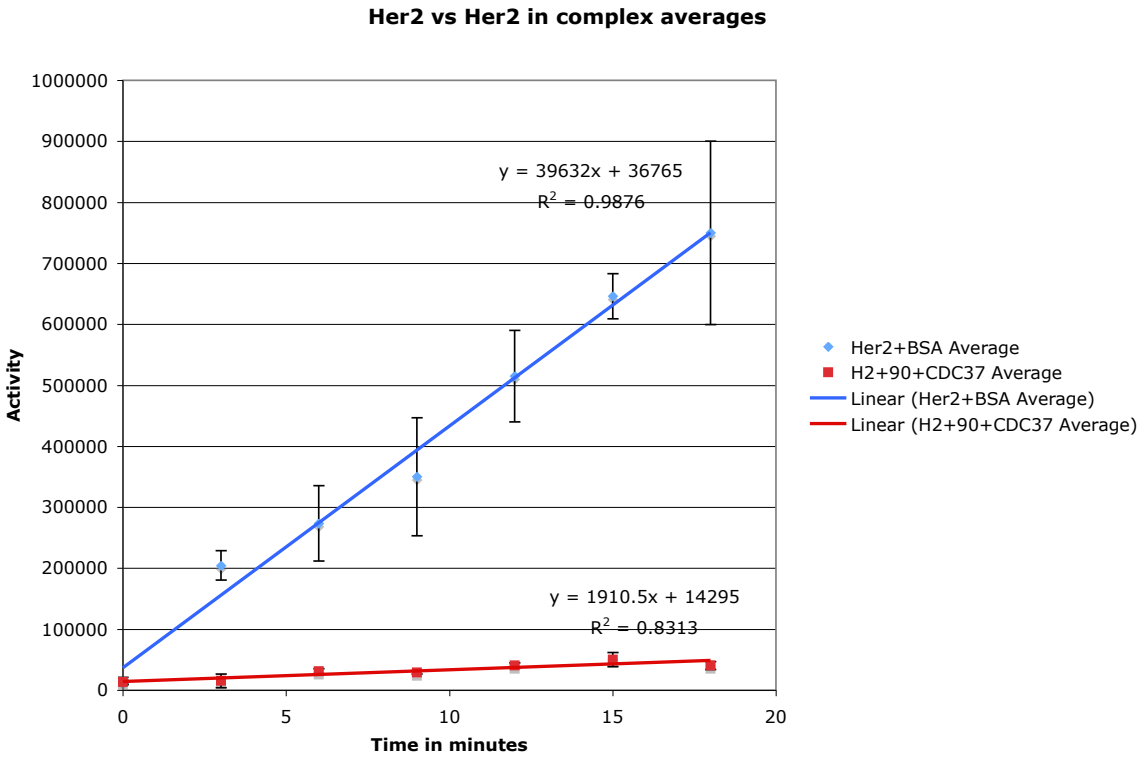

Figure 12. Comparison of kinase activity of Her2 kinase domain prepped alone vs prepped in complex with Hsp90 and Cdc37. Triplicate experiments. Equations on the chart indicate fit parameters with the slope being the kinase rate.

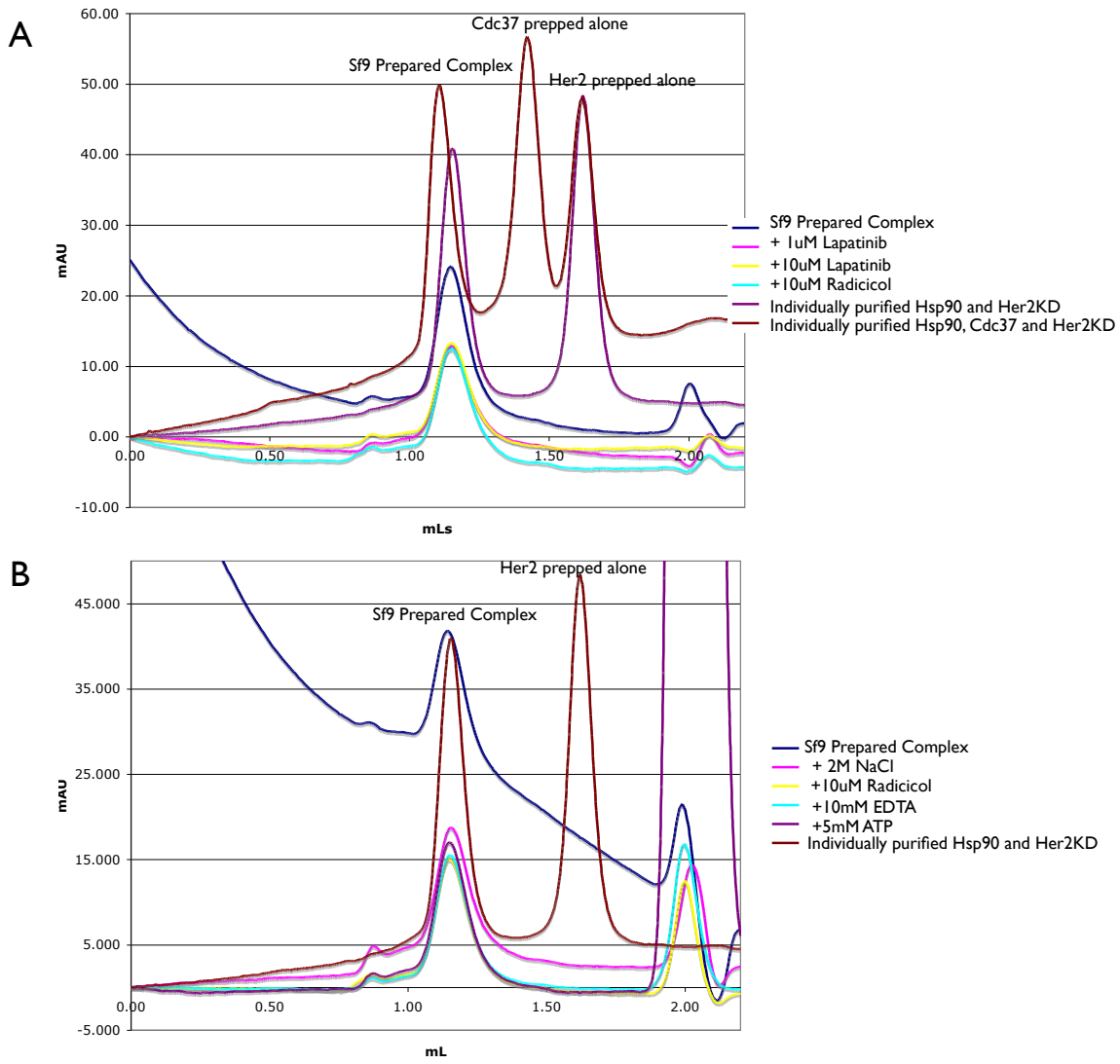

Figure 13. Sf9 co-expressed Hsp90/Cdc37/Her2 kinase domain complex is resilient to dissociation. Purified complex after dialyzing out molybdate, was incubated at 30C for 1h with indicated reagents and then loaded on PC3.2 S200 analytical column. Under no conditions was dissociation observed. Individually expressed Hsp90 and/or Cdc37 and /or Her2 were run also run on the same column for comparison.

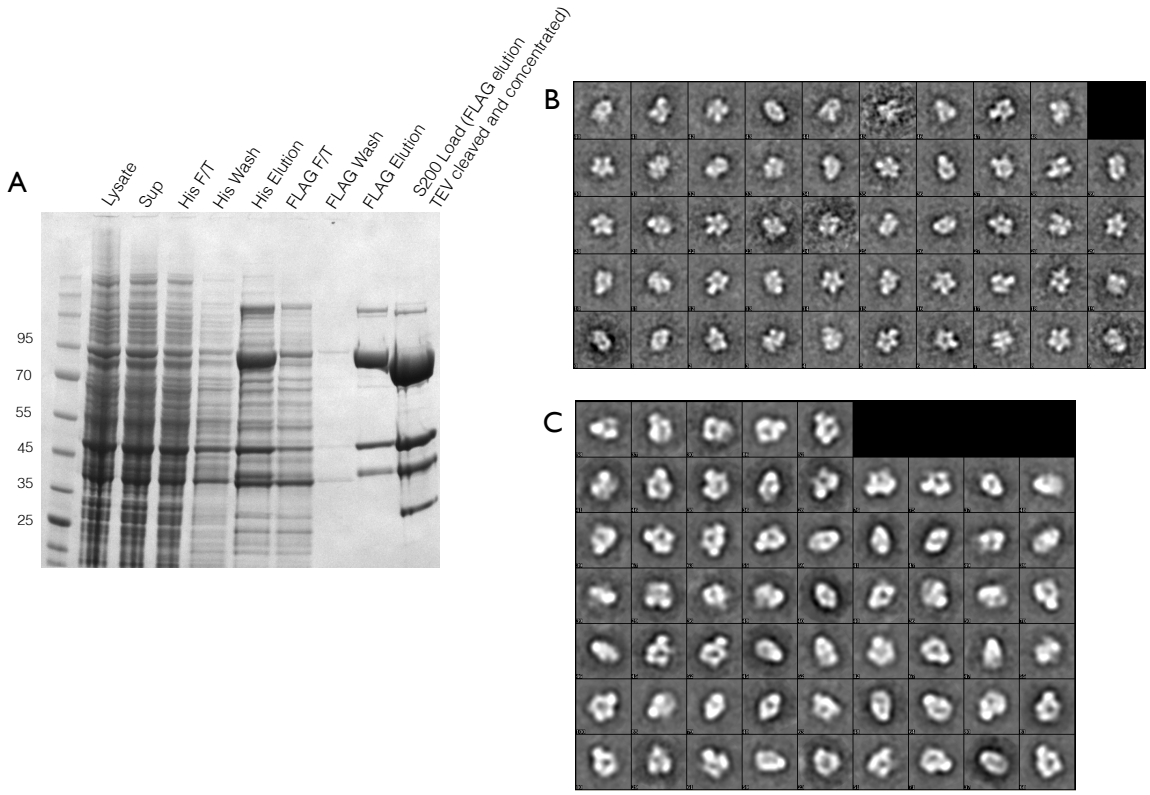

Figure 14. Co-expression of Hsp90/Cdc37/Her2 kinase domain in *Saccharomyces cerevisiae* yields pure and abundant complex, which under negative stain looks the same as Hsp90/Cdc37/Cdk4 complex. (A) SDS-PAGE gel of different steps along purification, indicating highly pure complex even before final gel filtration step. (B). 2D class averages of ~1000 particles of such expressed Hsp90/Cdc37/Her2 complex. (C) 2D class averages of ~3000 particles of Hsp90/Cdc37/Cdk4 complex expressed in yeast, shown for comparison.

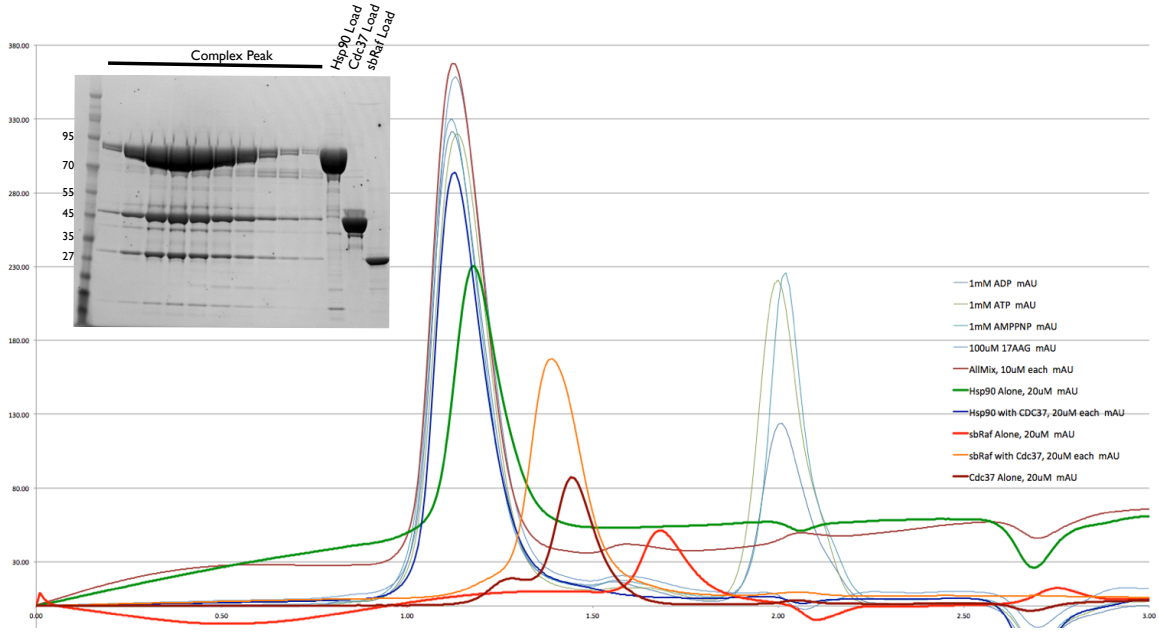

Figure 15. Assembly of Hsp90/Cdc37/sbRaf complex in vitro from individually purified samples and effects of nucleotide/Hsp90 inhibitors on it. The brown color trace (tallest peak) is the complex between three proteins, SDS-PAGE of which is displayed on the left. Individually run Hsp90 (green), Cdc37 (maroon) and sbRaf (red) are overlaid for comparison. Complex between Cdc37 and sbRaf alone, without Hsp90 was also observed (yellow trace). Quaternary complex formed with nucleotides/inhibitor traces are all light blue, thin traces. No dissociation is observed.

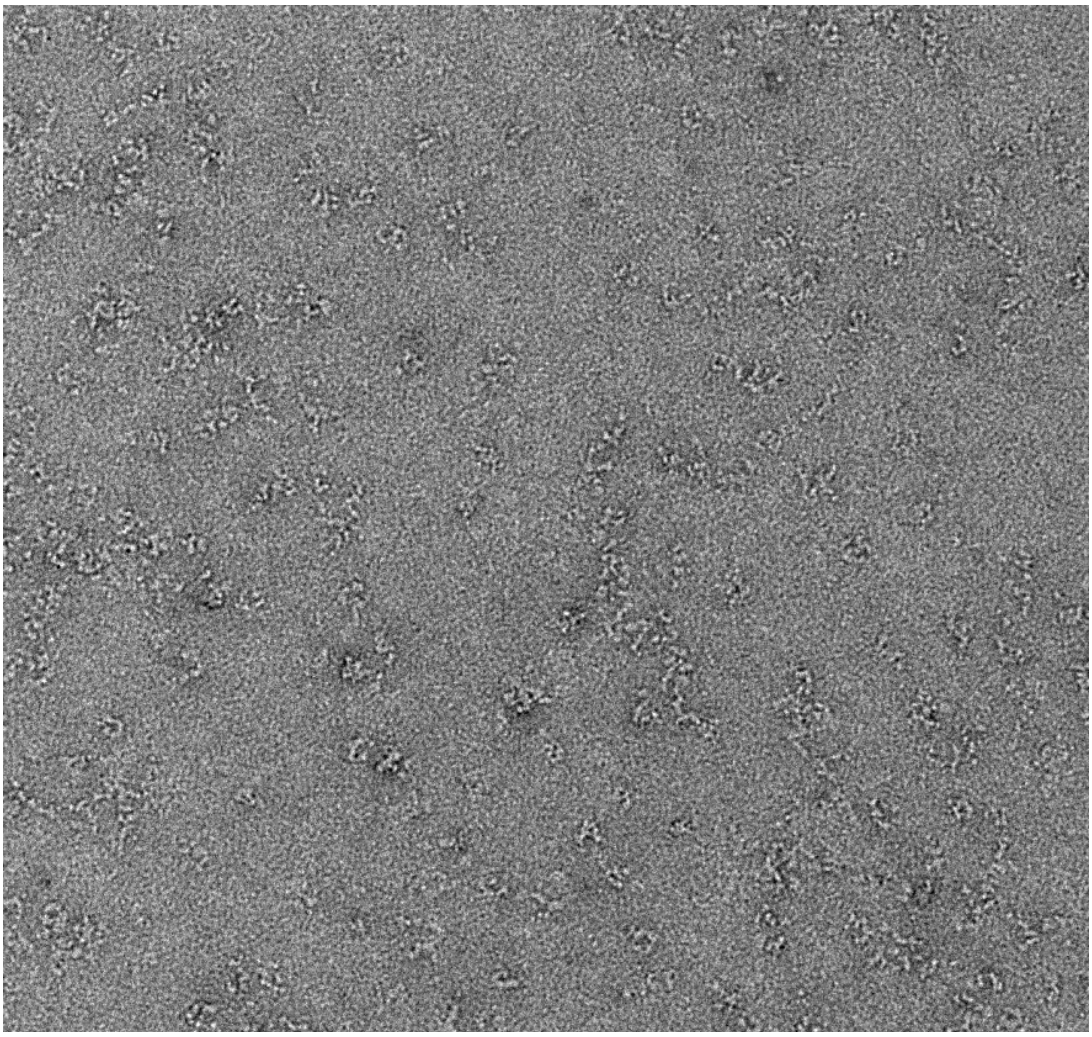

Figure 16. Hsp90/Cdc37/bRaf complex under negative stain EM.

It is apparent that the sample is considerably more heterogeneous than eukaryotic complexes. This could be to a worse binding affinity with most complexes dissociating at low concentration required for negative stain EM.

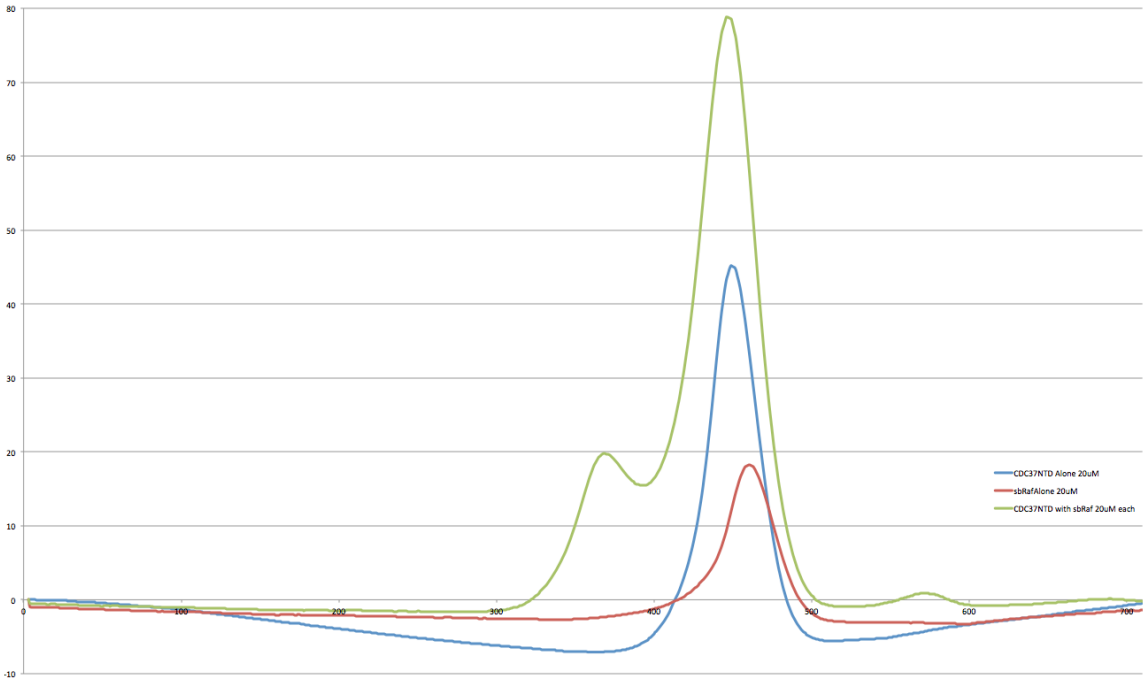

Figure 17. N terminal domain of Cdc37 is enough to form complex with sbRaf.

Cdc37 N terminal domain (residues 1-128) were incubated with sbRaf on ice for 1 h and then ran on PC3.2S200 column (green). For comparison Cdc37 N terminal domain alone and sbRaf alone were also loaded on the column (blue and red traces). One can see that the interaction is weaker than with the full length Cdc37 but still clearly observable on gel filtration.

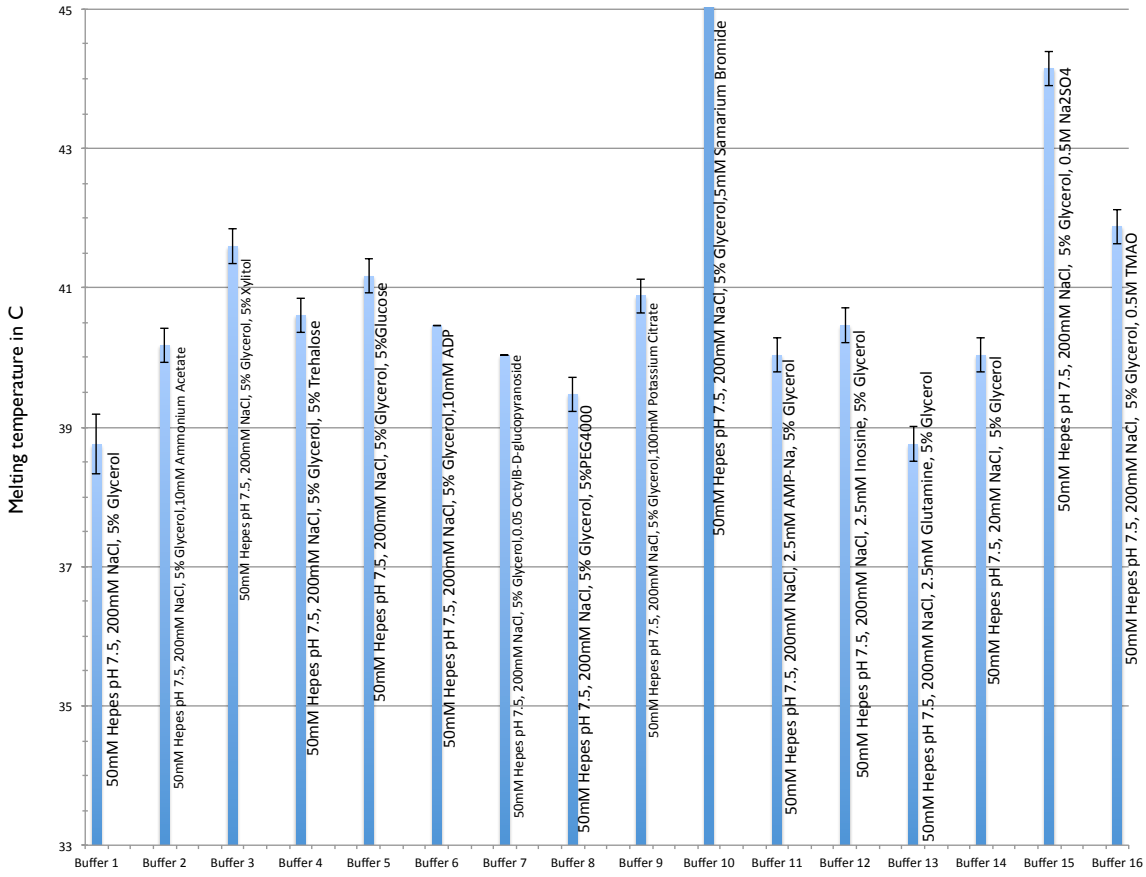

Figure 18. Buffer optimization of sbRaf in preparation for NMR. Melting temperatures of sbRaf as read out by the inflection point of SYPRO Orange fluorescence as temperature was changed. A number of additives significantly stabilized the kinase, but Sodium Sulfate had the most reproducible and robust effect.

Acknowledgments.

I would like to thank Timothy Street for all the help with plate reader, fluorimeter and for providing mutant Hsc82 for fluorescent labeling. I would also like to thank Elaine Kirschke for providing me with Hsp70, Hsp40 and Hop. I would like to thank Mariano Tabios for Sf9 cell expression and I would like to thank Ron Bose for Sf9 Her2 kinase domain construct.

References.

1. C. S. Gerbin, R. Landgraf, Geldanamycin selectively targets the nascent form of ERBB3 for degradation. *Cell Stress Chaperones* **15**, 529-544 (2010).
2. A. Citri *et al.*, Hsp90 recognizes a common surface on client kinases. *J Biol Chem* **281**, 14361-14369 (2006).
3. P. Zhou *et al.*, ErbB2 degradation mediated by the co-chaperone protein CHIP. *J Biol Chem* **278**, 13829-13837 (2003).
4. W. Xu *et al.*, Sensitivity of mature Erbb2 to geldanamycin is conferred by its kinase domain and is mediated by the chaperone protein Hsp90. *J Biol Chem* **276**, 3702-3708 (2001).
5. M. Taipale *et al.*, Quantitative analysis of HSP90-client interactions reveals principles of substrate recognition. *Cell* **150**, 987-1001 (2012).
6. S. Tsutsumi, L. Neckers, Extracellular heat shock protein 90: a role for a molecular chaperone in cell motility and cancer metastasis. *Cancer Sci* **98**, 1536-1539 (2007).
7. E. E. Boczek *et al.*, Conformational processing of oncogenic v-Src kinase by the molecular chaperone Hsp90. *Proc Natl Acad Sci U S A* **112**, E3189-3198 (2015).
8. S. Polier *et al.*, ATP-competitive inhibitors block protein kinase recruitment to the Hsp90-Cdc37 system. *Nat Chem Biol* **9**, 307-312 (2013).
9. L. F. Stancato *et al.*, Raf exists in a native heterocomplex with hsp90 and p50 that can be reconstituted in a cell-free system. *J Biol Chem* **268**, 21711-21716 (1993).
10. J. Tsai *et al.*, Discovery of a selective inhibitor of oncogenic B-Raf kinase with

potent antimelanoma activity. *Proc Natl Acad Sci U S A* **105**, 3041-3046 (2008).

11. S. J. Arlander *et al.*, Chaperoning checkpoint kinase 1 (Chk1), an Hsp90 client, with purified chaperones. *J Biol Chem* **281**, 2989-2998 (2006).
12. T. O. Street, L. A. Lavery, D. A. Agard, Substrate binding drives large-scale conformational changes in the Hsp90 molecular chaperone. *Mol Cell* **42**, 96-105 (2011).
13. T. O. Street *et al.*, Cross-monomer substrate contacts reposition the Hsp90 N-terminal domain and prime the chaperone activity. *J Mol Biol* **415**, 3-15 (2012).
14. C. K. Vaughan *et al.*, Hsp90-dependent activation of protein kinases is regulated by chaperone-targeted dephosphorylation of Cdc37. *Mol Cell* **31**, 886-895 (2008).
15. A. P. Kornev, S. S. Taylor, Defining the conserved internal architecture of a protein kinase. *Biochim Biophys Acta* **1804**, 440-444 (2010).

Chapter 3.

Conclusions, or

How Hsp90 and Cdc37 lubricate kinase molecular switches.

This chapter is the draft of a review on recent developments in Hsp90/Cdc37/kinase interactions from our and other labs.

Abstract.

Hsp90/Cdc37 chaperone system interacts with and supports 60% of the human kinases. A large number of these kinases are key oncoproteins, and their interactions with Hsp90/Cdc37 machinery are crucial for their normal and malignant activity. This effect has been exploited with many Hsp90 drugs currently in clinical trials, without however much structural understanding of Hsp90-Cdc37-kinase interactions. Recent advancements in cryoEM and biochemical methods yielded new levels of understanding of these interactions at molecular level. Due to meta-stable native states many kinases rely on Hsp90/Cdc37 system long after initial folding. These interactions potentially allow for rapid kinase response to key signals but prevent unwanted spurious activity.

Protein kinases are widely recognized to be key players in regulation of the cell cycle, cell signaling and early organism development (*1, 2*). Dysregulation of their normal function leads to a variety of human disease including cancer, and consequently protein kinases have become key therapeutic targets over the past decade (*3*). During early work on the remarkable transforming power of vSrc kinase in chick embryos, two additional proteins were discovered that closely associated with vSrc, polypeptides of size 80 kDa and 50 kDa, which are now recognized to be molecular chaperone Hsp90 and its co-chaperone Cdc37 (also referred to as p50)(*4*). Since then, Hsp90 has been shown to be a key molecular chaperone for ~10% of the proteome with substrate proteins (known as clients) highly enriched for those involved in signaling and regulation, including kinases, nuclear steroid receptors, ubiquitin ligases, amyloid proteins and others (*5, 6*). Although initially in the shadows, in the past 10 years Cdc37 been found to be a key player single handedly connecting Hsp90 chaperone system to the kinome. New advances in biophysical methods (*7*) and in *in vitro* reconstitution of Hsp90/Cdc37/kinase interactions(*8*) recently yielded mechanistic and molecular insights into the role Cdc37 plays between Hsp90 and kinases. In this review we will discuss these recent advancements and their implications for kinase regulation.

What is a client kinase?

Although historically kinases have been broken into binary client and non client categories, recent results affirm the view that most if not all kinases depend on and interact with Hsp90/Cdc37 system, and the question should be not if a kinase is a client, but how strong of a client the kinase is with the strength of dependence being a

continuum. However, before elaborating more fully on this point we should discuss the two main ways scientists have been fishing for Hsp90/Cdc37 kinase clients.

Due to low stabilities of large number of kinases, studies of kinase interactions with Hsp90/Cdc37 system have been predominantly limited to either cellular or cell lysate experiments. In this context, kinases have been classified as clients if, one, they co-immunoprecipitate with Hsp90/Cdc37 and two, kinase activity, read out indirectly via activity of the appropriate phosphorylation cascade goes down in response to inhibition of Hsp90's ATP cycle (Fig 1). It turns out that such loss of activity can be attributed to the fact that kinase levels plummet and/or kinases aggregate in response to Hsp90's inhibition, rather than Hsp90 providing direct activation. After inhibition of Hsp90 for longer than 20 hours this is observed for almost all the kinases, and is due to Hsp90/Cdc37 playing an important role in early folding, much as anticipated for a molecular chaperone. This is experimentally observed as failure of synthesis of new kinases in response to Hsp90 inhibition, direct interactions of recently translated kinases from cell lysates or Hsp90/Cdc37 "activating" severely misfolded kinase in vitro (probably due to prevention of aggregation). Explicit examples of theses are EGFR (*9*), ErbB3 (*10*), Ire1 (*11*), LCK (*12*) and Chk1 (*13*). Again, this is observed even for kinases that are sometimes referred to as non-clients.

On the other end of the spectrum are kinases that historically are thought of as clients. Upon Hsp90 inhibition, levels of these kinases plummet much faster than protein synthesis inhibition, due to rapid ubiquitination followed by degradation via proteasome. Such kinases are constitutively addicted to Hsp90/Cdc37, even when mature as has been shown explicitly for ErbB2 (Her2), where kinase population at the plasma membrane still

gets rapidly degraded after Hsp90 inhibition (*10*). Interestingly, closely related kinases can lie at the different ends of the interaction strength spectrum, with a single point mutation being able to convert one into another, for example EGFR/ErbB2 (*14*), cSrc/vSrc (*15*), Cdk2/Cdk4 (*16*) and aRaf/cRaf (*17*). Many groups have used such client/non-client pairs to discover an Hsp90-interacting signal sequence or motif but their findings were generally only applicable to a single kinase or family, with no truly general feature among clients.

In 2012 Lindquist lab heroically investigated physical interactions between all the human kinases and Hsp90/Cdc37 system in a quantitative manner (*18*). They observe 60% of human kinome interacting with Hsp90/Cdc37, with clients present among all the kinase families. However, even with the data for all the kinases in human cells, the authors failed to identify a global sequence determinant for Hsp90/Cdc37 interactions. Instead, the only unifying feature observed was that client kinases are generally less thermally stable than non clients. This strongly suggested the need for detailed biochemical/biophysical investigation.

Recent work by Boczek et al is a rare example of rigorous *in vitro* investigation of interactions between Hsp90/Cdc37 and a constitutive client, vSrc (*19*). This study is insightful for a number of reasons. First, it is the only work where in a reconstituted *in vitro* system from purified components authors show that human Hsp90β (and not α) together with Cdc37, in ATP dependent manner are able to safeguard vSrc from being inactivated at 30C temperature. Second, via mutational analysis authors show that the strength of interactions between Src and Hsp90/Cdc37 can be varied in a continuous manner from weak/early client cSrc all the way to constitutive client vSrc. This delineates

the fact that fundamentally the same physical feature is responsible for interactions with Hsp90/Cdc37 in early folding clients and in the constitutive clients.

The fact that mature kinases, long post folding depend on Hsp90/Cdc37 clearly falls outside simplistic canonical chaperone model of initial folding, raising a question of what kinase structural state is being recognized by Hsp90/Cdc37. Also, observation that minimal sequence variations should be able to eliminate this post-folding need for Hsp90 also raises the question of why this dependence has persisted.

Structural hallmarks of client kinases.

The kinase domain has been definitively shown to be both necessary and sufficient for interaction with Hsp90/Cdc37 (*9*). This is curious, as barring order/disorder transition at the activation loop and movement of the αC helix, structurally, eukaryotic kinase domains are all very similar (Fig 2A). Most recent data along with the failure to find a general client sequence motif, would argue that the relevant interaction surfaces are present in both clients and non-clients, and it is the propensity to display these surfaces that is the determinant.

First line of evidence for this hypothesis comes from observation that clients are less thermally stable. Mutation analysis of bRaf by Taipale et al 2012 and Src by Boczek et al 2015 both show that mutations which destabilize kinase domain also make for stronger Hsp90/Cdc37 clients. This is also true for kinase stabilization by drugs/nucleotides, where drug/nucleotide bound kinase clients become less dependent of Hsp90/Cdc37, regardless of whether the drugs are active-site inhibitors or allosteric modulators(*20*). Moreover, Boczek and colleagues observe a higher rate of state

transitions by molecular dynamics of mutants that interact stronger with Hsp90/Cdc37.

Second, recent NMR work by Gelis lab shows that even historically non-client kinases interact with Cdc37, albeit very transiently (*21*). Interestingly, addition of Cdc37 alone to bRaf kinase leads to partial kinase unfolding. The residues which loose structure are the same as the ones that interact with Hsp90 alone (extremely weakly). Importantly, drug bound bRaf interacts transiently with Cdc37 and doesn't unfold, indicating that change in kinase dynamics alone, without change in sequence can shift the kinase along the client strength axis.

Third, a recent cryoEM structure of an Hsp90-Cdc37-Cdk4 complex by our group shows the kinase in an unfolded conformation, completely split between the lobes by Hsp90/Cdc37 (Fig2C) (*22*). Cdc37 interacts with αE helix via backbone hydrogen bonds, recognizing a fold and not a specific sequence. Furthermore, sequence alignment shows that there is no significant difference in the Hsp90 interacting residues between clients and non-clients, with kinases generally being hydrophobic in that region.

Taken together, the most consistent interpretation is that client kinases are more dynamic (less stable) than non-clients. That is, Hsp90/Cdc37 must be recognizing a non-native, partially unfolded state with the two kinase lobes being separated. Client kinases are those where the energy of this partially unfolded state is close to that of its functional state such that it is significantly populated at organism temperatures. This allows Cdc37 to bind and to further unfold the kinase, splitting it at the lobes and presenting regions which now can stably bind to Hsp90, as in the cryoEM structure. This mode of molecular motion, opening between the two lobes, although not as extreme as in the cryoEM structure has been observed in molecular dynamics by Shaw group on EGFR (Fig

2B)(*23*), and by our group running rotamerically induced perturbations on Cdk kinases (unpublished data).

How does Cdc37 interact with client kinases and promote Hsp90 function?

Cdc37 binds kinase clients without Hsp90, but Hsp90 interacts only extremely weakly without Cdc37, therefore Cdc37 constitutes an independent kinase binding unit (*8, 21*). Early analysis of protein fragments have identified Cdc37 middle domain (residues 148-276) as a proteolytically stable Hsp90 interacting domain, Cdc37 N terminal domain as the kinase interacting domain and a C terminal domain of unclear function (Fig 3A)(*24*). In the cryoEM structure, conserved His 20 Pro 21 Asn 22 motif in Cdc37 perfectly mimics type 1 β-turn within the αC-β4 loop in kinase native structures, packing against αE helix of the kinase. This interaction prevents the N lobe from making its cognate interactions with the C lobe, stabilizing a separated, partially unfolded state, and allows Hsp90 to clamp around β4- β5 strands of the N lobe (Fig 3B). Thus, Cdc37 may be playing an equivalent role to Hsp70 with the glucocorticoid receptor, where Hsp70 stabilizes a partially unfolded GR and then presents this state to Hsp90 (*25*). However, the analogy isn't perfect as our data suggests that transition to a closed Hsp90 results in active GR, whereas the observed closed Hsp90:Cdc37 complex must be fully inactive.

Studies of Cdc37 interaction with bRaf by NMR are largely consistent with what is seen in the cryoEM structure. However, in addition to very N terminus, authors also observe a number of residues at the very C terminal helical region of Cdc37, constituting a hydrophobic patch, which experience a new chemical environment upon binding to

bRaf (Fig 3A). Speculatively, this region may provide αC like helix for the N lobe to interact with stabilizing the unfolded conformation. In the cryoEM structure this region of Cdc37 is unresolved, indicating a high level of flexibility in the quaternary complex. Mutating residues in this hydrophobic patch in human cell lines abolishes binding of Cdc37 to client kinases. This is interesting as there are previous reports of C terminal domain of Cdc37 being dispensable in yeast for function (*26*). It may be the case that a mutated C terminal region plays a dominant negative role, or there may be some differences between yeast and human systems.

Both cryoEM and NMR identify the remainder of the Cdc37 N terminal domain as an antiparallel coiled coil, consisting of about 60 residues. It is unclear why such a long coiled coil would be required to make interactions with the kinase clients. NMR studies were done without Hsp90 present, indicating that quaternary interactions are not required to stabilize the coiled coil. One possibility is that during Hsp90's cycle, Cdc37 needs to move around while still being attached to both, Hsp90 and the kinase, and the long coiled coil allows this. Alternatively, this may be a docking site for a binding partner, as the coiled coils in ClpB serve as a binding site for Hsp70(*27*).

The kinase binding site on Hsp90 seen by cryoEM is the same as client binding site on bacterial Hsp90 for its client, showing a high degree of conservation(*28, 29*). This region of Hsp90, between the middle and C-terminal domains, has recently been shown to be asymmetric (*30*). Current work indicates that there is a correlation between asymmetry at the M-C interface of Hsp90 and a differential hydrolysis rate of the two monomers, providing an exciting connection between client binding, establishment of asymmetry and asymmetric hydrolysis(*31*). It should be noted however that in cryoEM

structure of the complex, Hsp90 closely resembles a symmetric state.

Cdc37 interactions with Hsp90.

The first Hsp90-Cdc37 interaction interface was revealed in 2004 (*32*). In that work authors crystallized middle and C terminal domains of human Cdc37 interacting with the N terminal domain of yeast Hsp90. That structure is consistent with prior fragmentation assays and also explains how Cdc37 can inhibit Hsp90's ATPase. Cdc37 interactions displace the catalytic water and also prevent the region called the "lid" on Hsp90 N terminal domain from coming over the bound ATP. However, docking such bound Cdc37 to full-length Hsp90 would require a rotation of the Hsp90's N terminal domain to prevent clashes, and would also prevent dimerization of N terminal domains of Hsp90, thought to be required for ATP hydrolysis (Fig 4). Although crystal structure like interactions have been observed by NMR (*33*), work by Eckl and colleagues on *C.elegans* homologues of Hsp90 and Cdc37 demonstrates that Cdc37 binds the middle domain of Hsp90, implying that Cdc37 may bind at multiple sites (*34*).

In the cryoEM structure of Hsp90-Cdc37-Cdk4, although all the proteins are human homologues, Cdc37's middle domain is bound to the middle domain of Hsp90, a radically different interaction than the crystal structure (Fig 4). Cdc37 contributes a strand to a β-sheet at a previously unappreciated interaction site on Hsp90's middle domain, filling a groove. The new β -strand connects Cdc37's globular middle domain with the coiled coil of the N terminal domain. The N terminal domains of Hsp90 are dimerized and would clash with Cdc37 if bound as in the crystal structure. Five very N terminal residues of Cdc37 are making interactions with the closed N terminal domains of Hsp90,

further stabilizing the closed state (Fig 3B). Finally, there is an extensive patch of ionic interactions between the Cdc37 N terminal region and Hsp90 middle domain, consistent with the reported salt dependence of Cdc37-Hsp90 interactions.

We propose that Cdc37 likely binds Hsp90 at two distinct interfaces, one on the N terminal domain, as in the crystal structure, and one on the middle domain, as seen in the cryoEM structure, and transitions between these sites during the cycle (Fig 5). With this model, preferential interaction with the middle domain of *C.elegans* homologues is due to a different conformational equilibrium of the *C.elegans* Hsp90, rather than idiosyncratic feature of *C.elegans* Hsp90-Cdc37 interactions. Molecular details of this transition however are unclear at this point, indicating a clear need to capture an Hsp90:Cdc37:kinase complex in an open Hsp90 state (perhaps analogous to that observed with Hsp90:Hsp70:and GR).

Regulation of Hsp90/Cdc37/kinase interactions.

Both Hsp90 and Cdc37 are intricately regulated by phosphorylation. Cdc37 can be phosphorylated on residues Tyr 4 and Tyr 298 by the Yes kinase (*35*) and on Ser 13 by CKII kinase (*36*). Notably, both of these kinases are also Hsp90 clients. The effects of Tyr 4 phosphorylation is unclear, but it was shown that phospho mimics at Tyr 298 lead to impaired Cdc37-kinase binding. This site is in the C terminal domain of Cdc37, corroborating recent NMR results of this domain's involvement in some step of kinase binding.

Best understood phosphorylation site on Cdc37 is Ser 13 with it being predominantly in a phosphorylated state in cells. Phospho-mimic or phospho-null

mutations fail to produce functioning vSrc in yeast, potentially indicating that this regulatory mark has to change for the Hsp90 cycle to progress (Fig 5) (*37*). In the Hsp90-Cdc37-Cdk4 cryoEM structure, Cdc37 Ser 13 is clearly phosphorylated and this phosphorylation stabilizes a kinase interacting state of the N terminus of Cdc37 in context of Hsp90. The phosphate is interacting with 3 positively charged residues, potentially explaining why phospho mimetic substitution fails to recapitulate the functional effects of phosphorylation. This role is consistent with bRaf having a slower in vitro off rate from Hsp90/Cdc37 in the phosphorylated Ser 13 state vs dephosphorylated Cdc37 (*8*). Importantly however, NMR data showed no differential patterns of interaction between Cdc37 and bRaf due to Ser13 phosphorylation. This may mean that the effect is most pronounced in context with Hsp90, and/or that in vitro system is probing the interaction at a different state of Hsp90.

Although general phosphatases can dephosphorylate Cdc37 alone or in the presence of a kinase, in context of quaternary complex with Hsp90 even overnight incubations with phosphatase yield no dephosphorylation. However, PP5 phosphatase has the unique ability to rapidly dephosphorylate Cdc37 even in the context of the whole complex. This is due to a TPR domain on PP5, which interacts with Hsp90 via its C terminal MEEVD motif (Fig 5). A recent crystal structure of PP5 phosphatase with a Cdc37 peptide in its active site identified a number of mutations which render PP5 catalytically dead. The authors show that such mutations cause client kinases to stay bound with Hsp90/Cdc37/PP5 complex, indicating that Ser 13 dephosphorylation is likely important for kinase release(*38*). Based on the Hsp90/Cdc37/Cdk4 structure, it is clear that the N terminus of Cdc37 would have to undergo a conformational change to be

accessible for dephosphorylation. At the moment however, the nature of any such change is unknown.

What are the functional consequences of kinase - Hsp90/Cdc37 interactions?

As discussed previously, the canonical interpretation of the Hsp90/Cdc37 system is that it helps fold, stabilize and activate its kinase clients. However, clear cut evidence for such activation as decoupled from simple stabilization, on late/constitutively dependent kinases is missing. In a number of reports on ErbB2 (*39, 40*) and Ire1 (*41*), where authors carefully and promptly monitored activity of the appropriate signaling cascade in response to Hsp90 inhibitor, an opposite effect was observed, with the kinase actually getting activated. Also, canonical activation of the kinase leads to Hsp90 dissociation, and Hsp90 inhibitor induced activation is synergistic with canonical activation, indicating that this aspect of kinase regulation by Hsp90 is physiologically relevant. Taken together with the Hsp90/Cdc37/Cdk4 structure, in which the kinase is clearly inactive, this indicates that Hsp90/Cdc37 system likely serves to repress the kinase activity for the constitutively dependent clients. Upon dissociation, clients get activated then ubiquitinated and degraded. Interestingly, corollary to the kinase being degraded there seems to be an exchange of Hsp90 for Hsp70 in the kinase complexes, indicating a hand off and potentially a transition through a quaternary complex akin to the recently visualized Hsp90/Hsp70/Hop/GR complex (*25*).

It is apparent why having an extra inhibitory regulator for strongly proliferative/oncogenic kinases would be beneficial for metazoans. Hsp90/Cdc37 system may serve as an extra layer of protection against malignant growth, keeping kinases in an

inactive state, but always ready to be activated by the appropriate signal. What is harder to explain, is why this state is structurally an unfolded state rather than a more canonical "αC helix out" inactive state (Fig2A)? In a number of experimental systems Hsp90 was able to buffer structurally destabilizing mutations associated with new functions arising during evolution, and one possibility may be that constitutively addicted kinases are examples of such clients(*42, 43*). It is an unfolded state because it can be, an aimless feature of evolution, a random consequence of acquiring a new function, like a new substrate. However, there are constitutive kinase clients as far back as fungi, raising a question of why wouldn't these kinases evolve away from potentially burdensome chaperone dependent state over the millions of years.

An exciting possibility (no matter how speculative) is that for some kinases, ie clients, a partially unfolded native state has been evolutionarily selected for as an important structural feature. This would fit beautifully with the job that some of the most important kinase family members are tasked with. Rather than being processive machines, some kinases are more akin to switches or even computers, integrating intracellular and extracellular inputs and producing proliferative signal if and only if the conditions are right. Inputs can be phosphorylation marks or binding interactions. Having multiple inputs/modifications, it may be beneficial to be in a structurally uncommitted state (ie partially unfolded state), so that one doesn't have to climb out of a considerable energy well to undergo a conformational change to interact with the binding partner (Fig 6). Also, such a state may lower the activation barrier when changing between states (say active and inactive), via being a partially unfolded intermediate, process termed "cracking"(*44*). Finally, as the active state depends on precise arrangement of "spines"

running through the kinase domain(*45*), partially unfolded native state would be by default an inactive state, providing the extra layer of protection from cancer as discussed above.

Concluding remarks.

Advancements in two different areas have allowed for rapid progress in the structural understanding of Hsp90/Cdc37/kinase interactions. First, construction of a solubilized mutant of bRaf kinase which is marginally stable but still purifiable from *E.coli* has allowed rigorous *in vitro* biochemical investigations of the Cdc37/kinase interactions and also studies by NMR. Second, advancements in cryoEM allowed for direct structural investigation of Hsp90/Cdc37/kinase complexes isolated intact from eukaryotic cells. These advances have for the first time permitted the visualization of how the three proteins come together statically and in solution, providing a foundation for developing unifying mechanistic models and guiding further experimentation with the goal of understanding chaperone-mediated kinase regulation in health and disease.

These results also raise fundamental questions about nature of the "native" state, protein folding and chaperones. Traditionally, one tends to think of proteins as being confined to a distinct, well defined native state(s), and the chaperone system as only being used to aid initial folding or recover from denaturing stresses. However, studies with Hsp90 are requiring that both of these views be significantly broadened. That is, the equilibrium between native and partially folded states may have been exploited evolutionarily by co-opting the chaperone systems to provide an additional layer of regulation or coordination with the state of the cell. More specifically, client kinases (ie,

majority of kinases in humans) should be thought of as being intermediate between well folded and intrinsically disordered proteins, spending most of their life in a malleable, partially unfolded state, ready to respond to the right signal. For these proteins folding is not a narrow funnel, a directional one way road, but a more fully explorable and sophisticated energy landscape. Chaperones would therefore not only facilitate the early folding events, once in a lifetime of a kinase, or deal with non-functional aggregates, but also carefully guide kinases throughout their function. The current data suggest that such behavior is not unique to kinases, but likely applies to other signaling families, like steroid receptors. Fundamental understanding of such partially unfolded states in light of evolution, although challenging, will lead to new ways of thinking about proteins and structure-function relationship, and therefore demands examination.

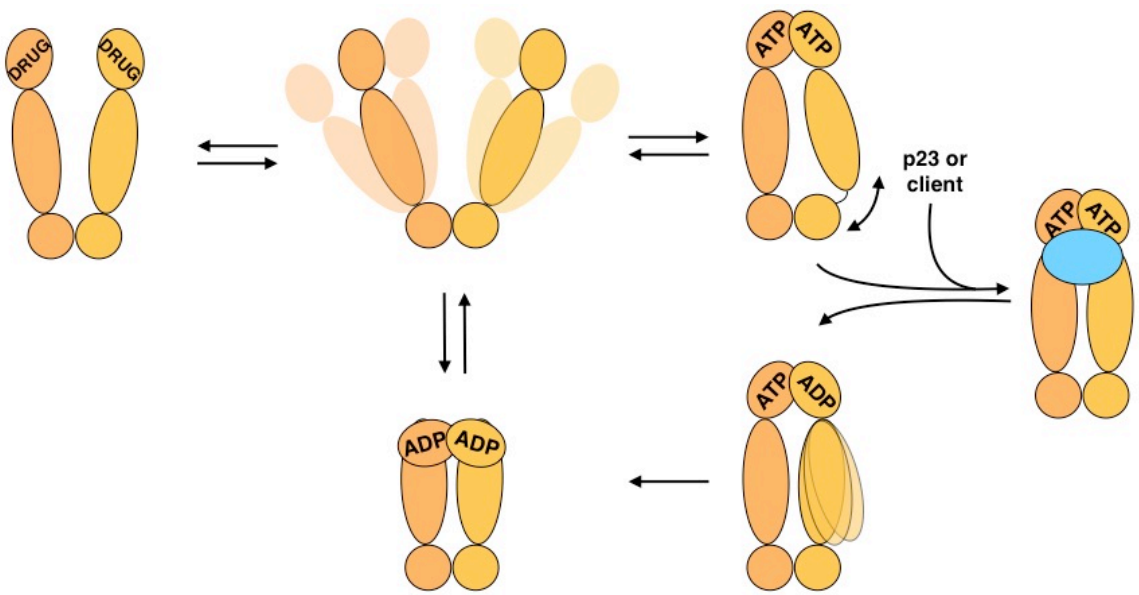

Figure 1. Hsp90 ATPase cycle.

Hsp90 is an ATPase and its catalytic ability is essential for its activity. Homologues differ in their ATPase rate with human cytosolic Hsp90 being almost undetectable but yeast cytosolic homologues being quite robust. Variety of co-chaperones like Aha1 or p23 can modulate Hsp90's ATPase with important functional consequences. Over the years, via a combination of techniques our lab and others have captured Hsp90 in drastically different conformations. Without nucleotides or inhibitors Hsp90 exists in equilibrium of states from very open to almost completely closed. ATP binding biases this equilibrium towards a closed state, with different homologues responding differently, for example yeast cytosolic Hsp90 almost completely shifting to the closed state and human Hsp90 populating it only transiently. Process of closure seems to be the rate limiting step for hydrolysis. This ATP bound state used to be thought of as symmetric, but recent work on mitochondrial homologue of Hsp90 TRAP1 shows asymmetry at the interface between middle domain and C terminal domain, potentially formed due to strain build up. Co-chaperones like p23 or clients (depicted as blue oval in the diagram), like kinases in

conjunction with Cdc37, stabilize the symmetric state. Upon hydrolysis of one ATP, the strain is released potentially forming a symmetric state. Current work from our lab indicates that hydrolysis can actually lead to a switch in asymmetry, not depicted here, with the asymmetric homologue always hydrolyzing first. Upon hydrolysis of ATP by the second monomer, Hsp90 forms a transient compact ADP state before releasing the nucleotides and returning to the apo state equilibrium. Multiple Hsp90 inhibitors target the conserved nucleotide binding pocket like geldanamycin, radicicol, 17AAG, ganetespib and others. Structurally such binding seems to bias the Hsp90 towards more compact state, which is however not as compact as ATP or ADP bounds states. *In vivo* inhibitor treatment usually leads to release of the client, but it is important to realize that inhibition of Hsp90 is not the same as its absence, as Hsp90 stalled at some point in its cycle may still have effects on clients due to simple binding.

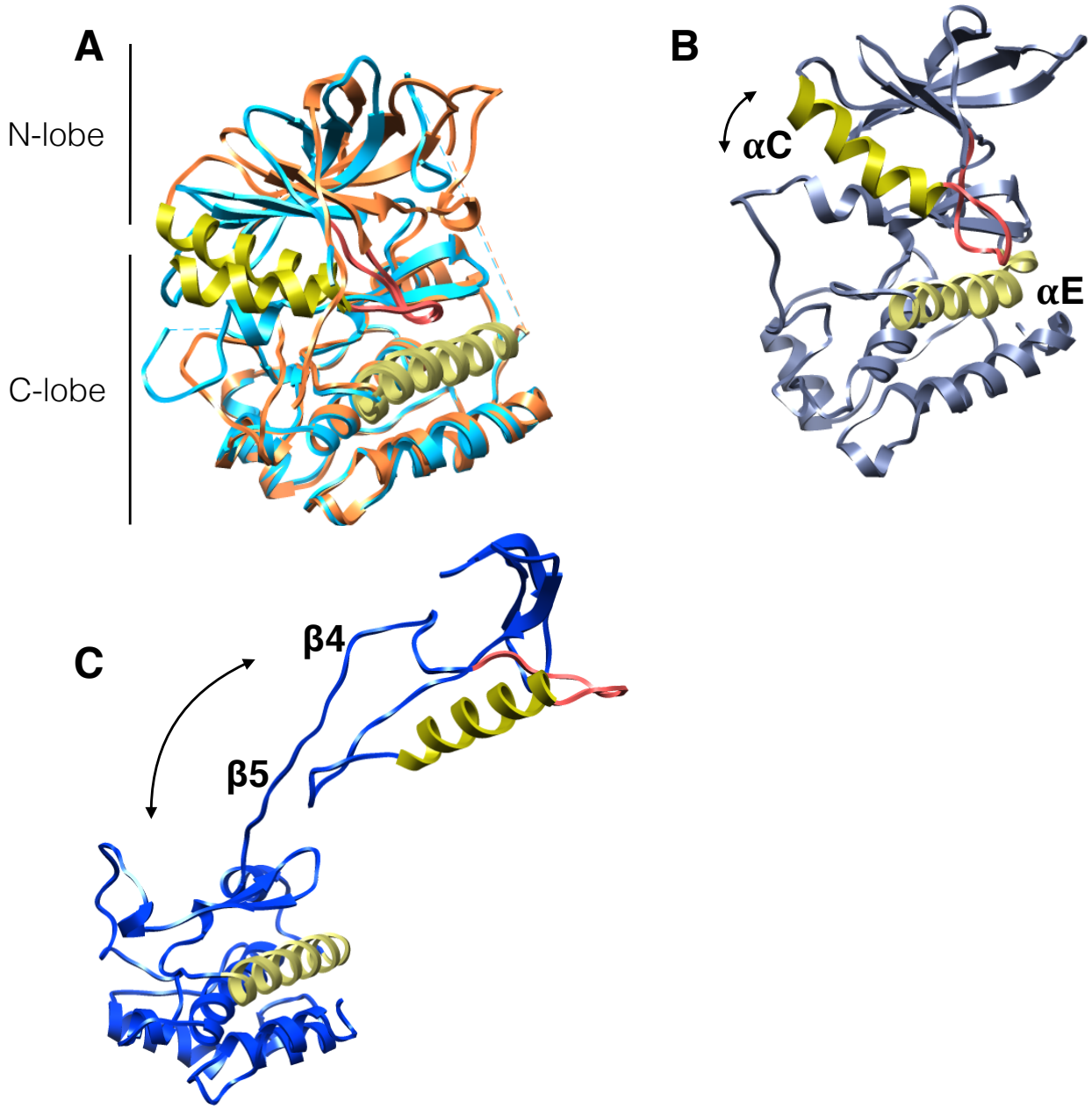

Figure 2. Kinase domain architecture and dynamics.

(A) Structures of EGFR in the active state (light blue, PDB:2ITP) and the inactive state (brick, PFB:2GS7). One can appreciate small shift in αC helix between states. (B) Snapshot from 12us all atom modeling on EGFR from Shaw group displaying opening between kinase lobes. (C) Cdk4 kinase structure as it is in the cryoEM complex of

Hsp90/Cdc37/Cdk4 (PDB:5FWL) showing dramatic unfolding between the kinase lobes and unraveling of β4- β5 strands. αC helix in all structures is in lime color, adjacent αC-β4 loop is in red. The proteins have been aligned by the αE helix (asparagus color helix in C-lobe). Arrows show the direction and relative magnitude of N-lobe motion in relation to C-lobe.

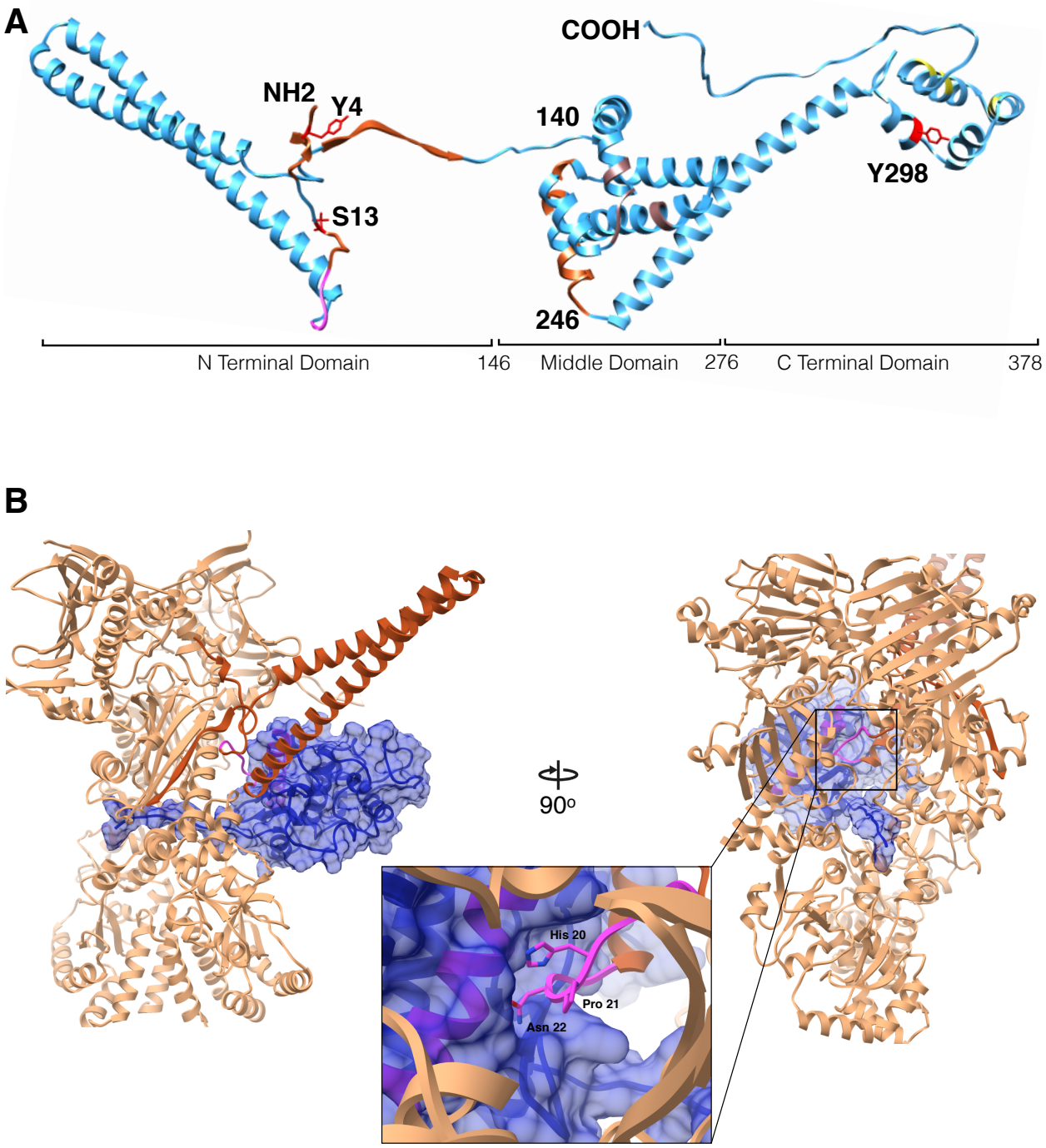

Figure 3. Cdc37 architecture and interactions with Cdk4 kinase in context of Hsp90.

(A) Cdc37 structure combined from different studies. Residues 1-260 are from cryoEM structure (PDB:5FWL), 261-293 from Hsp90-Cdc37 domain crystal structure (PDB:1US7) and 294-378 from the ensemble solution NMR structure (PDB:2N5X).

Brick color indicates regions interacting with Hsp90 in Hsp90/Cdc37/Cdk4 complex, pink is the kinase interacting loop (HPN motif), chocolate color are Hsp90 interacting residues as in the crystal structure and in yellow are residues implicated in additional interactions with bRaf kinase by NMR. Y4, S13 and Y298 are known to be phosphorylated and are marked in red. (B) Interactions between Cdc37 and Cdk4 in context of Hsp90. Only Cdc37 N terminal domain is depicted for clarity (brick) interacting with the αE helix on Cdk4 (pink helix within blue surface) with the loop harboring HPN motif on Cdc37 (pink, zoomed in). Kinase (omitting residues 1-85) depicted as blue transparent surface, threads β4- β5 strands through the lumen of Hsp90 with Hsp90 clamping around them at its middle domain-c terminal domain junction.

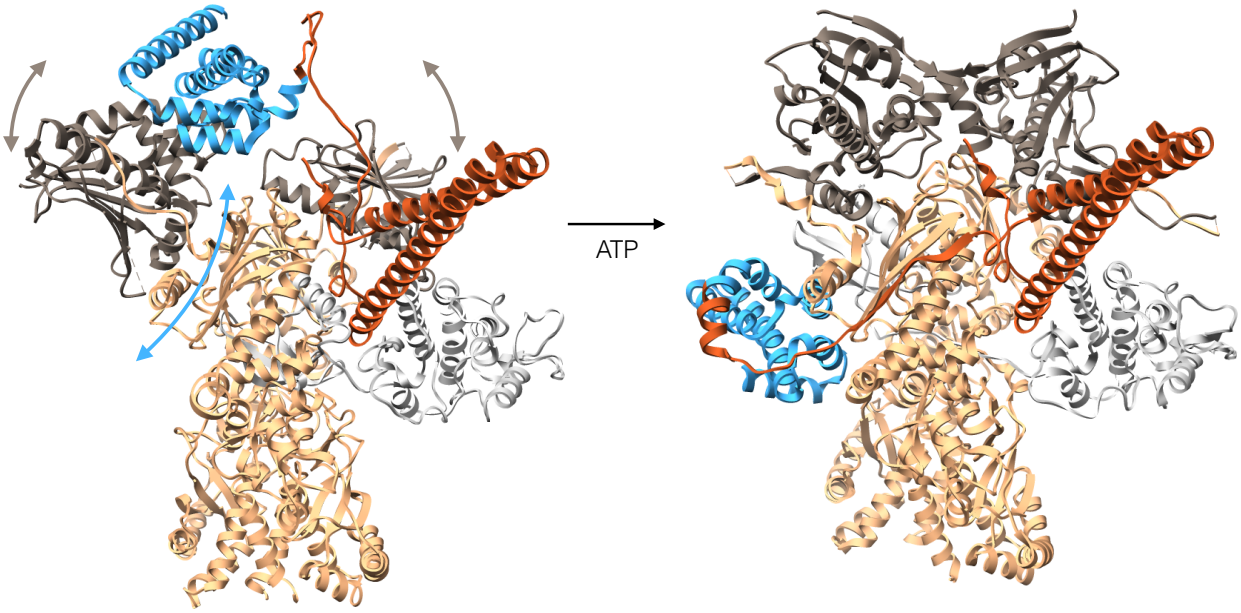

Figure 4. Conformational rearrangements of Cdc37 during Hsp90 cycle.

On the left is a modeled quaternary complex between Hsp90-Cdc37-Cdk4 where Cdc37-Hsp90 interactions are preserved as in the crystal structure of the fragments (PDB:1US7). Cdc37 middle domain is colored in blue with the N terminal domain in brick, Hsp90 is in tan with N terminal domains in charcoal and Cdk4 kinase is in light gray. In this state Hsp90's N terminal domains are parted, and the domain of the monomer on the left had to undergo a rotation as to avoid clash between Hsp90's middle domain and Cdc37's middle domain. Kinase is partially open at the lobes. Upon ATP binding to Hsp90 N terminal domains, these undergo closure displacing Cdc37 down to the middle domain and stabilizing the kinase in the unfolded state, resulting in the cryoEM structure (domain motions are depicted with arrows). Structure on the left corresponds to state (b) in Fig 4 and structure on the right corresponds to state (c) in Fig 4.

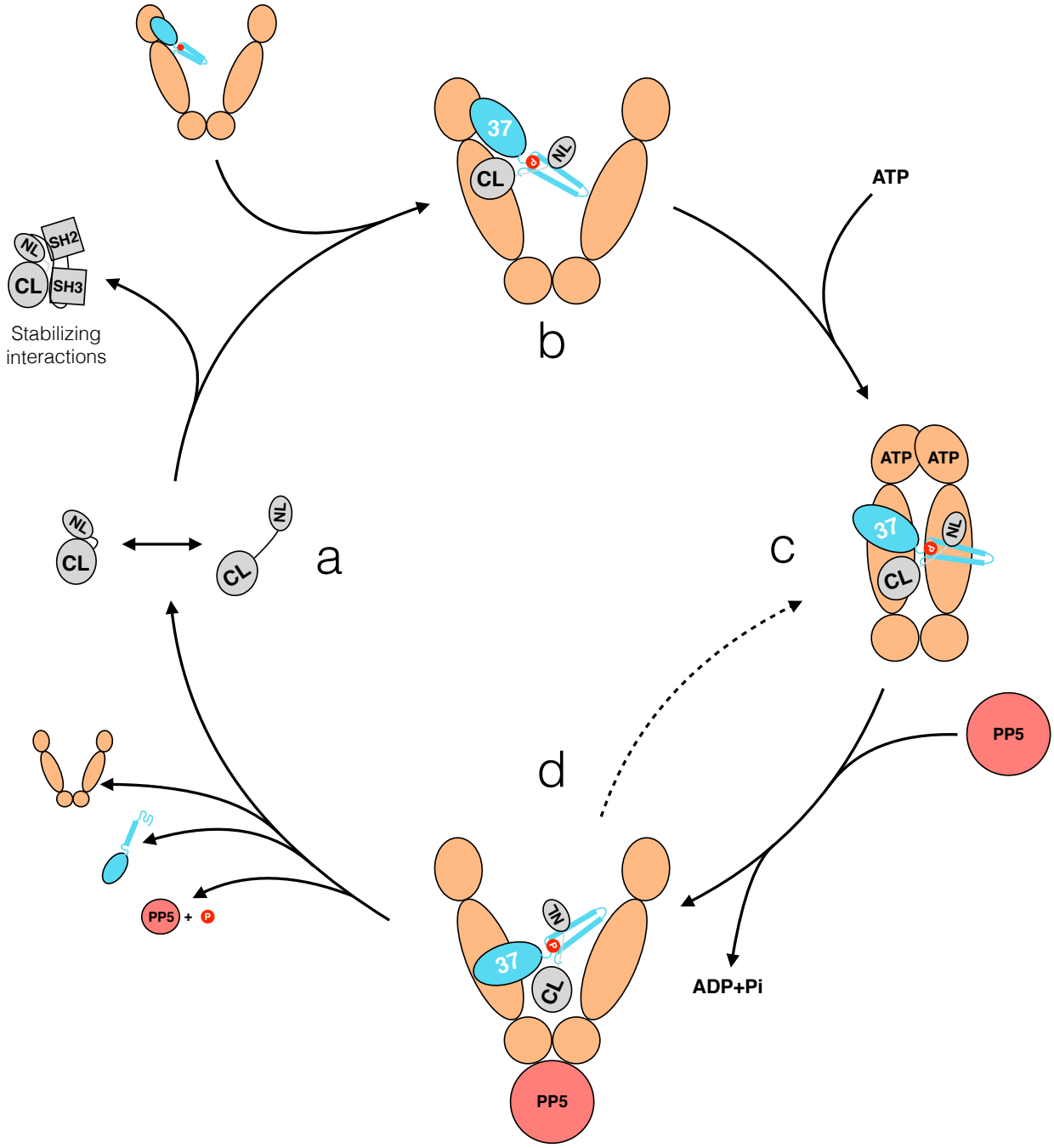

Figure 5. Hsp90-kinase cycle.

Kinases sample partially open states (CL- C-lobe, NL – N-lobe) as depicted in (a). If the kinase spends too much time open at the lobes, ie early folded state or constitutive client, Cdc37 while on Hsp90 (due to high concentration of Hsp90 in relation to Cdc37) wedges

in between the two kinase lobes with its N terminal domain, further unfolding the kinase resulting in state (b). Based on NMR, C terminus of Cdc37 also makes some kinase interactions at this point. Cdc37 interacts with the N terminal domain of an open Hsp90, utilizing the contacts as in the crystal structure. This is a modeled state (Fig 3). Upon binding ATP, Hsp90 undergoes closure, clamping around unfolded kinase β4-β5 strands, and Cdc37 migrates to the middle domain (state c). Upon ATP hydrolysis by Hsp90 (potentially sequential, with an asymmetric state in between), Hsp90 opens, giving a chance for the kinase to fold (state d). If this was an initial folding interaction for the "non client", or there is a stabilizing binding partner present nearby for the constitutive client, the folded N lobe outcompetes Cdc37 for the C lobe, dissociating the kinase from the complex. However, if there are no stabilizing interactions, Hsp90 may re bind ATP and enter another cycle (dashed line). This way, the kinase is safely held in a partially folded inactive state, always ready to interact with an appropriate binding partner, checking for its presence with the frequency of Hsp90's ATPase. Dynamic phosphorylation/dephosphorylation by Yes and CKII kinases, and PP5 phosphatase add a layer of regulation.

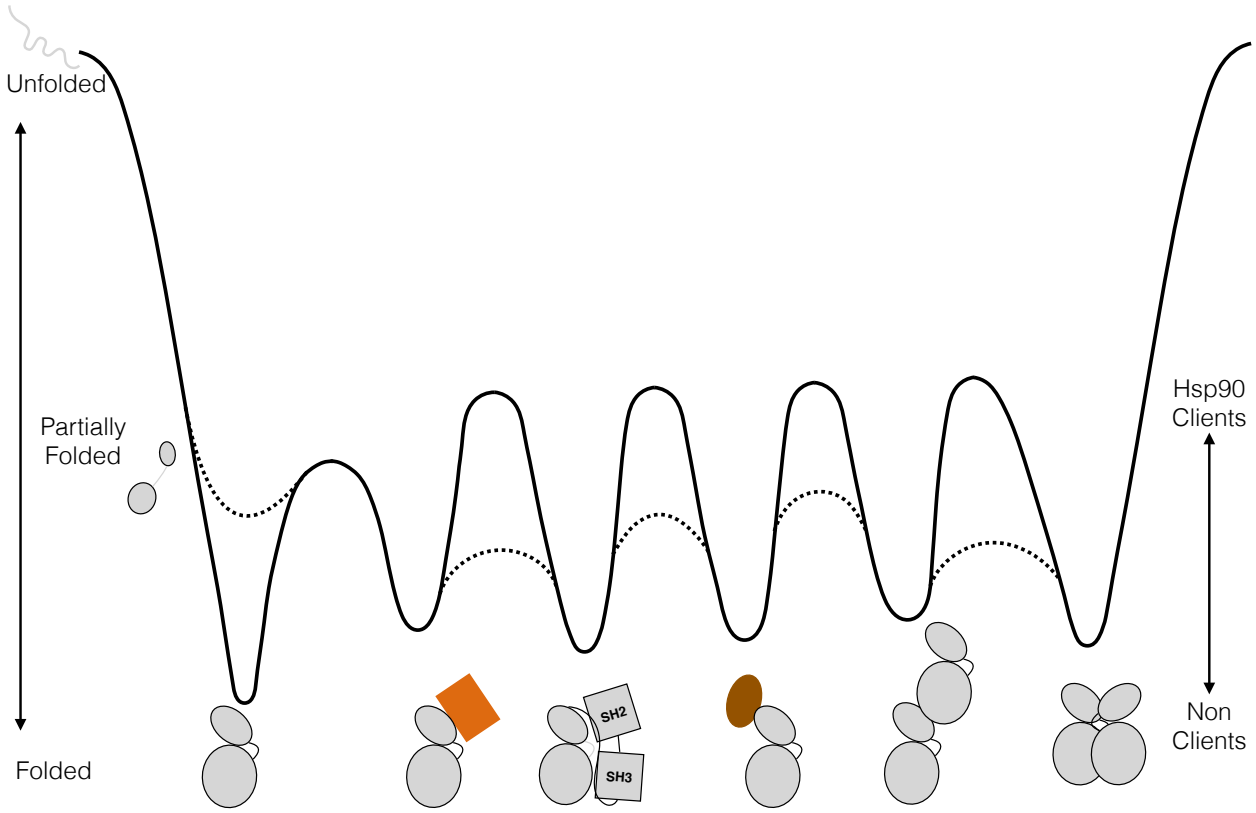

Fig 6. Imagined kinase energy landscape.

In solid black line is the energy landscape of the kinase system without Hsp90/Cdc37. In this case the kinase would have a very stable native state and high energy barriers transitioning between states in complex with different partners/domains, severely impacting the rate of transitions. In dashed line is the energy landscape with Hsp90/Cdc37 system. Now the native state is de-stabilized/partially folded and this allows easier transition into interacting states. Also, being in a partially unfolded state may speed up transitions between states, via a process termed "cracking". Hsp90/Cdc37 may also actively catalyze such transitions.

References.

1. S. S. Taylor, M. M. Keshwani, J. M. Steichen, A. P. Kornev, Evolution of the eukaryotic protein kinases as dynamic molecular switches. *Philos Trans R Soc Lond B Biol Sci* **367**, 2517-2528 (2012).
2. J. A. Endicott, M. E. Noble, L. N. Johnson, The structural basis for control of eukaryotic protein kinases. *Annu Rev Biochem* **81**, 587-613 (2012).
3. J. Zhang, P. L. Yang, N. S. Gray, Targeting cancer with small molecule kinase inhibitors. *Nat Rev Cancer* **9**, 28-39 (2009).
4. J. Brugge, W. Yonemoto, D. Darrow, Interaction between the Rous sarcoma virus transforming protein and two cellular phosphoproteins: analysis of the turnover and distribution of this complex. *Mol Cell Biol* **3**, 9-19 (1983).
5. L. M. Gierasch, A. Horwich, C. Slingsby, S. Wickner, D. Agard, in *Series in structural biology Vol. 6*. (World Scientific, New Jersey, 2016), pp. 1 online resource (vii, 319 pages).
6. M. Taipale, D. F. Jarosz, S. Lindquist, HSP90 at the hub of protein homeostasis: emerging mechanistic insights. *Nat Rev Mol Cell Biol* **11**, 515-528 (2010).
7. Y. Cheng, Single-Particle Cryo-EM at Crystallographic Resolution. *Cell* **161**, 450-457 (2015).
8. S. Polier *et al.*, ATP-competitive inhibitors block protein kinase recruitment to the Hsp90-Cdc37 system. *Nat Chem Biol* **9**, 307-312 (2013).
9. W. Xu *et al.*, Sensitivity of mature Erbb2 to geldanamycin is conferred by its kinase domain and is mediated by the chaperone protein Hsp90. *J Biol Chem* **276**, 3702-3708 (2001).

10. C. S. Gerbin, R. Landgraf, Geldanamycin selectively targets the nascent form of ERBB3 for degradation. *Cell Stress Chaperones* **15**, 529-544 (2010).

11. M. G. Marcu *et al.*, Heat shock protein 90 modulates the unfolded protein response by stabilizing IRE1alpha. *Mol Cell Biol* **22**, 8506-8513 (2002).

12. M. J. Bijlmakers, M. Marsh, Hsp90 is essential for the synthesis and subsequent membrane association, but not the maintenance, of the Src-kinase p56(lck). *Mol Biol Cell* **11**, 1585-1595 (2000).

13. S. J. Arlander *et al.*, Chaperoning checkpoint kinase 1 (Chk1), an Hsp90 client, with purified chaperones. *J Biol Chem* **281**, 2989-2998 (2006).

14. W. Xu *et al.*, Surface charge and hydrophobicity determine ErbB2 binding to the Hsp90 chaperone complex. *Nat Struct Mol Biol* **12**, 120-126 (2005).

15. Y. Xu, S. Lindquist, Heat-shock protein hsp90 governs the activity of pp60v-src kinase. *Proc Natl Acad Sci U S A* **90**, 7074-7078 (1993).

16. L. Lamphere *et al.*, Interaction between Cdc37 and Cdk4 in human cells. *Oncogene* **14**, 1999-2004 (1997).

17. N. Grammatikakis, J. H. Lin, A. Grammatikakis, P. N. Tsichlis, B. H. Cochran, p50(cdc37) acting in concert with Hsp90 is required for Raf-1 function. *Mol Cell Biol* **19**, 1661-1672 (1999).

18. M. Taipale *et al.*, Quantitative analysis of HSP90-client interactions reveals principles of substrate recognition. *Cell* **150**, 987-1001 (2012).

19. E. E. Boczek *et al.*, Conformational processing of oncogenic v-Src kinase by the molecular chaperone Hsp90. *Proc Natl Acad Sci U S A* **112**, E3189-3198 (2015).

20. M. Taipale *et al.*, Chaperones as thermodynamic sensors of drug-target

interactions reveal kinase inhibitor specificities in living cells. *Nat Biotechnol* **31**, 630-637 (2013).

21. D. Keramisanou *et al.*, Molecular Mechanism of Protein Kinase Recognition and Sorting by the Hsp90 Kinome-Specific Cochaperone Cdc37. *Mol Cell* **62**, 260-271 (2016).

22. K. A. Verba *et al.*, Atomic structure of Hsp90-Cdc37-Cdk4 reveals that Hsp90 traps and stabilizes an unfolded kinase. *Science* **352**, 1542-1547 (2016).

23. Y. Shan, A. Arkhipov, E. T. Kim, A. C. Pan, D. E. Shaw, Transitions to catalytically inactive conformations in EGFR kinase. *Proc Natl Acad Sci U S A* **110**, 7270-7275 (2013).

24. J. Shao, A. Irwin, S. D. Hartson, R. L. Matts, Functional dissection of cdc37: characterization of domain structure and amino acid residues critical for protein kinase binding. *Biochemistry* **42**, 12577-12588 (2003).

25. E. Kirschke, D. Goswami, D. Southworth, P. R. Griffin, D. A. Agard, Glucocorticoid receptor function regulated by coordinated action of the Hsp90 and Hsp70 chaperone cycles. *Cell* **157**, 1685-1697 (2014).

26. E. L. Turnbull, I. V. Martin, P. A. Fantes, Cdc37 maintains cellular viability in Schizosaccharomyces pombe independently of interactions with heat-shock protein 90. *FEBS J* **272**, 4129-4140 (2005).

27. M. Carroni *et al.*, Head-to-tail interactions of the coiled-coil domains regulate ClpB activity and cooperation with Hsp70 in protein disaggregation. *Elife* **3**, e02481 (2014).

28. T. O. Street *et al.*, Cross-monomer substrate contacts reposition the Hsp90 N-

terminal domain and prime the chaperone activity. *J Mol Biol* **415**, 3-15 (2012).

29. O. Genest *et al.*, Uncovering a region of heat shock protein 90 important for client binding in E. coli and chaperone function in yeast. *Mol Cell* **49**, 464-473 (2013).

30. L. A. Lavery *et al.*, Structural asymmetry in the closed state of mitochondrial Hsp90 (TRAP1) supports a two-step ATP hydrolysis mechanism. *Mol Cell* **53**, 330-343 (2014).

31. Daniel Elnatan, Miguel Betegon, Yanxin Liu, Theresa Ramelot, Michael A Kennedy, David Agard. Symmetry broken and rebroken during the ATP hydrolysis cycle of the mitochondrial Hsp90 TRAP1. bioRxiv doi:10.1101/107094

32. S. M. Roe *et al.*, The Mechanism of Hsp90 regulation by the protein kinase-specific cochaperone p50(cdc37). *Cell* **116**, 87-98 (2004).

33. S. Sreeramulu *et al.*, The human Cdc37.Hsp90 complex studied by heteronuclear NMR spectroscopy. *J Biol Chem* **284**, 3885-3896 (2009).

34. J. M. Eckl *et al.*, Cdc37 (cell division cycle 37) restricts Hsp90 (heat shock protein 90) motility by interaction with N-terminal and middle domain binding sites. *J Biol Chem* **288**, 16032-16042 (2013).

35. W. Xu *et al.*, Dynamic tyrosine phosphorylation modulates cycling of the HSP90-P50(CDC37)-AHA1 chaperone machine. *Mol Cell* **47**, 434-443 (2012).

36. Y. Miyata, Protein kinase CK2 in health and disease: CK2: the kinase controlling the Hsp90 chaperone machinery. *Cell Mol Life Sci* **66**, 1840-1849 (2009).

37. C. K. Vaughan *et al.*, Hsp90-dependent activation of protein kinases is regulated by chaperone-targeted dephosphorylation of Cdc37. *Mol Cell* **31**, 886-895 (2008).

38. J. Oberoi *et al.*, Structural and functional basis of protein phosphatase 5 substrate specificity. *Proc Natl Acad Sci U S A* **113**, 9009-9014 (2016).

39. W. Xu, X. Yuan, K. Beebe, Z. Xiang, L. Neckers, Loss of Hsp90 association up-regulates Src-dependent ErbB2 activity. *Mol Cell Biol* **27**, 220-228 (2007).

40. A. Citri *et al.*, Hsp90 restrains ErbB-2/HER2 signalling by limiting heterodimer formation. *EMBO Rep* **5**, 1165-1170 (2004).

41. A. Ota, Y. Wang, Cdc37/Hsp90 protein-mediated regulation of IRE1alpha protein activity in endoplasmic reticulum stress response and insulin synthesis in INS-1 cells. *J Biol Chem* **287**, 6266-6274 (2012).

42. J. Lachowiec, T. Lemus, E. Borenstein, C. Queitsch, Hsp90 promotes kinase evolution. *Mol Biol Evol* **32**, 91-99 (2015).

43. C. Queitsch, T. A. Sangster, S. Lindquist, Hsp90 as a capacitor of phenotypic variation. *Nature* **417**, 618-624 (2002).

44. O. Miyashita, J. N. Onuchic, P. G. Wolynes, Nonlinear elasticity, proteinquakes, and the energy landscapes of functional transitions in proteins. *Proc Natl Acad Sci U S A* **100**, 12570-12575 (2003).

45. A. P. Kornev, S. S. Taylor, Dynamics-Driven Allostery in Protein Kinases. *Trends Biochem Sci* **40**, 628-647 (2015).

Chapter 4.

Future directions.

Although we finally saw how Hsp90 interacts with at least one of its clients, Cdk4 kinase, there are still major questions that are left un answered. There are two general levels of inquiry, which I think should be undertaken. First, the mechanism of Hsp90/Cdc37/kinase cycle, as a machine is not understood. How does the actual remodeling happen? What are the mechanistic steps of going through the cycle with the client? These are fairly basic, but important questions about Hsp90 working as a machine, utilizing Cdc37 or other co-chaperones when it needs. The second level of inquiry is about Hsp90 being a social member of the cell, ie, how does whatever Hsp90 does to the kinase fit into what cells want to do. How/what proteins guide kinases to Hsp90? How do interactions with Hsp90 play into kinase interactions with the rest of their binding partners? How do kinase-Hsp90 interactions go sour and there is a decision made that a kinase should be degraded? At this level the main question is how Hsp90/kinase cycle fits in with the rest of the cell machinery. I think both of these areas of study are tremendously important, and will describe more specific experiments addressing each of them in turn.

Mechanistic understanding of Hsp90-kinase cycle.

There is a myriad of questions about how these proteins interact and what modifications happen as the cycle progresses forward. I think that structural biology will be instrumental in answering many of these, by being able to capture structures of different states. However, dealing with unfolded proteins and weak binding affinities, there will be high degree of heterogeneity, making it difficult for study with standard structural techniques. Therefore, one will have to use a combination of many techniques,

with cryoEM likely playing a unifying, central role to answer these questions. There are at least two more structural states we know must exist, the kinase loading state and kinase release state. First, how does the initial interaction between Cdc37 and the client kinase happen? Utilizing bRaf system for in vitro reconstitution, I think readily attainable bRaf-Cdc37 complex is at the current limit of what one can do by cryoEM, utilizing latest advances in camera and phase plate (being about 80 kDa complex)(*1*). There certainly will be a need for optimization, but based on reported affinities the complex should stay together at concentrations needed for EM. Potentially, due to extreme dynamics of the complex, it will be difficult to get a coherent reconstruction due to high flexibility. Importantly, this complex is also workable by NMR if proteins are ILVA labeled. Therefore, one can envision utilizing restraints from NMR data to generate a number of well informed structural models which are energy minimized by molecular dynamics, and then score such models against the cryoEM images, sort of multi-reference 3D classification. Although such methodology does not exist yet, it certainly seems to be quite within reach, and should allow for solving exciting dynamic/flexible structures such as Cdc37/bRaf complex. Although binary complex is attainable, this interaction is likely to happen on Hsp90, as Hsp90 concentration is so much higher than Cdc37's in cells. This mode of interaction is likely captured by the *in vitro* Hsp90/Cdc37/bRaf complex. In my experience, due to poor affinities, this complex is not very stable, dissociating under concentrations needed for negative stain. However, combination of Cys mutations at the interface of the Cdc37-Hsp90 structure to stabilize it crystal structure like mode, or different ways of crosslinking the complex should potentially yield a stable enough interaction for cryoEM studies.

Attaining the dissociating state of the kinase may be difficult. One approach would be to try to engineer disulfides at the kinase-Hsp90 interface to lock the kinase in the lumen upon opening of Hsp90. A more exciting avenue would be to investigate the effects of asymmetry at the binding site interface and in the ATP hydrolysis in relation to the kinase progression through the cycle(*2*). Utilizing the yeast expression system, one can imagine utilizing SpyTag-SpyCatcher(*3*) pair to generate asymmetric Hsp90/Cdc37/kinase complexes, with either Cdk4 or Her2 or some other kinase. Then one can introduce asymmetric mutations in hydrolysis (ie one arm not being able to bind ATP or to hydrolyze ATP) or binding site for either kinase or Cdc37 and see the effects of these on the complex formation. If the sequential hydrolysis model is correct, being able to stall Hsp90 in the asymmetric state with one arm hydrolyzed and one not can unveil an intermediary conformation of the kinase between what I visualized in my structure and full release. Therefore I can envision a whole series of experiments assessing the effects of asymmetry on Hsp90-kinase interactions utilizing the yeast expression system, with the possibility of visualizing novel, intermediate processing states.

How do Hsp90/kinase interactions fit into the rest of the cell?

This area can be experimentally broken down further into two areas: *in vitro* investigation of effects of co-chaperones and post translational modifications and *in vivo* inquiry into Hsp90/kinase interactions.

It is known that Hsp90's interactions with kinases, although being through Cdc37 still are associated with Hsp70 and therefore Hsp40 machinery(*4*). It has been shown that early folding intermediates, ie when kinases are undergoing their first folding event,

Hsp70/Hsp40 system is required. However, at this moment it is completely unclear what affect this system has and where in the cycle it plays in. With evidence that Cdc37 may partially unfold kinases by itself, presenting the substrate in the correct state for the Hsp90 to interact with, it potentially may supplant the role Hsp70/Hsp40 plays with the glucocorticoid receptor(*5*). It is possible that Hsp40/Hsp70 interact with the kinases while it is in an even more unfolded state than as seen in the Hsp90/Cdc37/Cdk4 structure, therefore organizing the kinase to reach a state with enough folded bits to interact with the Cdc37. Another place in the cycle where Hsp70 has been observed with kinases are complexes formed after inhibition of Hsp90, in cells. A number of reports observe that upon Hsp90 inhibition the kinase population shifts from predominantly being in Hsp90 complexes to being in Hsp70 complexes with CHIP E3 ligase(*6*). To investigate Hsp70Hsp90/kinase complexes there are three approaches I can envision.

First, in the Chk1 reconstitution paper the complexes with Hsp70/Hsp90 and Chk1 kinase were all observed via immunopreciation *in vitro*. It is unclear how stable these complexes are, what are affinities, etc, but it would be worthwhile to re-visit this experimental system with more modern analytical techniques and characterize these interactions.

Second, taking the Hsp90/Cdc37/Cdk4 complex as purified from yeast, I was able to dissociate it by including a 37C heat step with ATP. In this case dissociation of complex is observed with the kinase mostly migrating to the void peak. It is still unclear how much this *in vitro* system can replicate the effects of addition of Hsp90 inhibitor in cells, but it is worth investigating. Therefore, one can do the same experiment as above but with Hsp70/Hsp40 present to see if kinase coming off Hsp90/Cdc37 can now form

quaternary complexes with Hsp70 system. One would also want to monitor the kinase activity during this hand off to see if there is activation. Moreover, it could be beneficial to add PP5 phosphatase to the same reactions, as it is known to dephosphorylate Cdc37 which is important for kinase release from the complex(*7*). To understand these processes more quantitatively it may be useful to establish a fluorescent based system of measuring interactions between the kinase and Cdc37/Hsp90, by for example incorporating Ruby/Clover fluorescent protein pair and expressing such complex in the yeast system. Then one would be able to measure kinetics of dissociation and monitor how co-chaperones like PP5, Aha1 and chaperones like Hsp70/Hsp40 affect this process.

Third, one can modify the yeast expression system to co-express Hsp70 together with CHIP E3 ligase and a kinase of choice. One may or may not need to co-express Hsp90 and Cdc37 also. Utilizing such system, and adding Hsp90 inhibitor during yeast protein expression, one may be able to capture the kinase degradatory complex for further characterization.

The experiments above are seeking to mechanistically connect Hsp90/kinase system to the nearest reasonable neighbor either directly upstream or downstream from the Hsp90/kinase complex, and elucidate how further regulation of this cycle via phosphorylation or co-chaperone expression/interactions happens. If during these experiments a change in kinase activity is observed, (ie activation as the kinase is completely inactive in the complex), then these experiment may also shine light on how chaperone system as a whole may affect kinase activity. However, I would argue these sort of experiments will tell us what the system can do, but not necessarily what it actually does. To figure out what chaperones actually do for kinase signaling, one would

need to look at these interactions *in vivo*.

Kinases are known to exist in dynamic complexes, either when they are inhibited or when they are activated(*8*). Depending on the exact kinase, these complexes vary. For EGFR family of kinase for example all members of the family intermix being able to make and exchange between homo-hetero dimers(*9*). There are at least two ways the kinase domains can dimerize in this family alone(*10*), and it is completely unknown what sort of interactions they make with kinase families outside its own. There is also evidence for the fact that these kinase form larger oligomers than dimers at the membrane upon activation, but details of this are unclear(*11, 12*). Raf family kinase also can form hetero- or homo-dimers(*13*). Furthermore, Raf is usually inhibited by interacting with extra domain of its own chain, and gets activated via interactions with Ras at the plasma membrane. Finally both, EGFR and Raf family undergo translocation to and from the plasma membrane in a very regulated manner.

The bottom line of all of this is that kinase families, which are also Hsp90 clients, live an intricate and sophisticated life, and we have a very faint idea what part interactions with Hsp90 or the other chaperones play in it. There have been studies trying to investigate some aspects of these interactions, but they usually only look at a handful of interaction partners and are done with IPs/western blots, therefore possessing obvious limitations. To investigate this area of interactions, one would have to set up system for monitoring Hsp90/kinase or Cdc37/kinase interactions in cells. The most obvious way of doing this would be a FRET pair between tethered fluorescent proteins, as discussed above. Utilizing yeast expression system one can screen a large number of constructs, to get the optimal positioning of the proteins for highest FRET signal. Utilizing this system,

one could look at various aspects of Hsp90/kinase interactions in cells. What is the interactions equilibrium in cell lines at rest? What if growth factor is added? What if Hsp90 inhibitor is added? Kinase inhibitor, which locks the kinase in the active or inactive state? For both EGFR and Raf kinase families there are a number of oncogenic mutants, being oncogenic via different aspects of kinase regulation (for example, some are dimerization dependent, some are not). What effects do these mutants have on the Hsp90/kinase equilibrium? I think looking into these questions at the cellular level is of crucial importance. If the live FRET system would prove un-workable, one can imagine raising an antibody for the Hsp90/Cdc37/kinase complex as purified from yeast, utilizing previously described methods(*14*), fixing cells and monitoring for Hsp90/Cdc37/kinase complexes under different conditions utilizing such antibody. This will not give kinetics of the interactions, but would at least provide high-resolution snapshots of the interactions at different stages of kinase activity cycle. Of course, this sort of work would need to be supplemented with the standard assortment of IPs and western blots assaying pathway activation, kinase heterodimer formation, etc.

The allosteric complexity of kinase signaling pathways is just starting to be fully appreciated. These are not simply stable proteins being able to populate just two states, on or off, but are very malleable, complicated machines which can utilize a domain with a relatively constrained structure, due to the fact that in needs to catalyze the phosphor-transfer reaction, for binding and regulation via a myriad of different partners. It seems like due to some aspects of such regulation and malleability, many kinases became obligate partners of Hsp90 chaperone machinery. Through studying these interactions both mechanistically and on a cellular level, not only we will learn about the primary

object of the study, ie chaperone/kinase interactions which by itself is extremely exciting and important, but learn invaluable aspects of kinase regulation. Finally, as kinases seem to populate structural space somewhere between fully folded proteins and intrinsically disordered proteins (See Chapter 3), studying such states via studying kinase/chaperone interactions will introduce new paradigms of structure-function dogma, where evolution may not only optimize the lowest energy state trying to reach it in the fastest possible way, but there may be evolutionary optimization of the whole folding funnel/landscape, with energy differences between multiple states, or changes in rates of transitions between multiple folding states being as important for function as the final crystallizable active state.

References.

1. Maryam Khoshouei, Mazdak Radjainia, Wolfgang Baumeister, Radostin Danev. Cryo-EM structure of haemoglobin at 3.2 A determined with the Volta phase plate. bioRxiv 087841; doi: https://doi.org/10.1101/087841
2. Daniel Elnatan, Miguel Betegon, Yanxin Liu, Theresa Ramelot, Michael A Kennedy, David Agard. Symmetry broken and rebroken during the ATP hydrolysis cycle of the mitochondrial Hsp90 TRAP1. bioRxiv 107094; doi: https://doi.org/10.1101/107094
3. B. Zakeri *et al.*, Peptide tag forming a rapid covalent bond to a protein, through engineering a bacterial adhesin. *Proc Natl Acad Sci U S A* **109**, E690-697 (2012).
4. S. J. Arlander *et al.*, Chaperoning checkpoint kinase 1 (Chk1), an Hsp90 client, with purified chaperones. *J Biol Chem* **281**, 2989-2998 (2006).
5. D. Keramisanou *et al.*, Molecular Mechanism of Protein Kinase Recognition and Sorting by the Hsp90 Kinome-Specific Cochaperone Cdc37. *Mol Cell* **62**, 260-271 (2016).
6. P. Zhou *et al.*, ErbB2 degradation mediated by the co-chaperone protein CHIP. *J Biol Chem* **278**, 13829-13837 (2003).
7. J. Oberoi *et al.*, Structural and functional basis of protein phosphatase 5 substrate specificity. *Proc Natl Acad Sci U S A* **113**, 9009-9014 (2016).
8. N. Jura *et al.*, Mechanism for activation of the EGF receptor catalytic domain by the juxtamembrane segment. *Cell* **137**, 1293-1307 (2009).
9. A. Citri *et al.*, Hsp90 restrains ErbB-2/HER2 signalling by limiting heterodimer formation. *EMBO Rep* **5**, 1165-1170 (2004).

10. N. Jura, Y. Shan, X. Cao, D. E. Shaw, J. Kuriyan, Structural analysis of the catalytically inactive kinase domain of the human EGF receptor 3. *Proc Natl Acad Sci U S A* **106**, 21608-21613 (2009).

11. Y. Sako, S. Minoghchi, T. Yanagida, Single-molecule imaging of EGFR signalling on the surface of living cells. *Nat Cell Biol* **2**, 168-172 (2000).

12. A. H. Clayton, S. G. Orchard, E. C. Nice, R. G. Posner, A. W. Burgess, Predominance of activated EGFR higher-order oligomers on the cell surface. *Growth Factors* **26**, 316-324 (2008).

13. T. Rajakulendran, M. Sahmi, M. Lefrancois, F. Sicheri, M. Therrien, A dimerization-dependent mechanism drives RAF catalytic activation. *Nature* **461**, 542-545 (2009).

14. J. Kim, R. M. Stroud, C. S. Craik, Rapid identification of recombinant Fabs that bind to membrane proteins. *Methods* **55**, 303-309 (2011).

Appendix.

Cloning, expression and purification of Hsp90/kinase complexes from yeast, a detailed protocol.

A. Generating the co-expression construct

1. 100 x 15 mm Petri dishes (Thermo Fisher Scientific)
2. 15 ml culture tubes (Thermo Fisher Scientific)
3. 1.5 ml microcentrifuge tubes
4. 83nu vector (obtained from Arkin lab)
5. GeneArt DNA Strings (Thermo Fisher Scientific)
6. NEB Gibson Kit (New England BioLabs, catalog number: E5510S)
7. Carbenicilin (Gold Biotechnology, catalog number: C-103-100)
8. PCR Clean up Kit (Promega, catalog number: A9281)
9. Miniprep Kit (Promega, catalog number: D6942)
10. NEB Quickchange Kit (New England BioLabs, catalog number: E0554S)
11. Bacto-tryptone (BD, Bacto)
12. Yeast extract (BD, Bacto)
13. NaCl (Sigma-Aldrich)
14. Agar (BD, Difco)
15. LB (see Recipes)
16. LB agar (see Recipes)

B. Expression Hsp90/Cdc37/Cdk4

1. JEL1 strain of Saccharomyces cerevisiae

2. Zymo Research EZ Transformation Kit (Zymo, catalog number: T2001)
3. Galactose (Sigma-Aldrich)
4. Yeast nitrogen base (YNB) (BD, Difco)
5. Glucose (Sigma-Aldrich)
6. CSM-His amino acid mixture (MP, catalog number: 4510-312)
7. Peptone (BD, catalog number: 211820)
8. Yeast extract (BD, catalog number: 212750)
9. Lactose (Sigma-Aldrich, catalog number: L1375)
10. Glycerol (Sigma-Aldrich)
11. SD-His (see Recipes)
12. YPGL media (see Recipes)

C. Purification of the Hsp90/Cdc37/Cdk4 complex.

1. 30 ml syringe with 16 gauge needle
2. 50 ml conical tubes
3. Concentrators, 15 ml, 30 kDa cutoff (Milipore Amicon Ultra, catalog number: UFC903096)
4. Dialysis tubing, 10 kDa cutoff (Thermo Fisher Scientific, catalog number: 68100)
5. MonoQ 10/100GL column (GE Healthcare)
6. Superdex 200 16/60 column (GE Healthcare)
7. Glass gravity columns (Biorad)
8. High-speed centrifuge tubes (capable of 30,000 G)
9. Spatulas

10. Liquid nitrogen Dewar
11. 12 x 75 mm tubes for fraction collection (Thermo Fisher Scientific)
12. Protease inhibitors, EDTA free (Roche Diagnostics, catalog number: 11873580001)
13. Ni-NTA Superflow beads (QIAGEN)
14. M2 Magnetic FLAG beads (Sigma-Aldrich, catalog number: M8823)
15. FLAG peptide (Genscript, catalog number: RP10586)
16. TEV protease, prepped in lab, 10 mg/ml
17. Liquid nitrogen
18. Trizma Base (Sigma-Aldrich)
19. NaCl (Sigma-Aldrich)
20. Imidazole (Sigma-Aldrich)
21. $MgCl_2$, 1M stock (Sigma-Aldrich)
22. KCl (Sigma-Aldrich)
23. $NaMoO_4$ (Sigma-Aldrich)
24. DTT (Sigma-Aldrich)
25. Lysis buffer (see Recipes)
26. Dialysis buffer (see Recipes)
27. Gel filtration buffer (see Recipes)

Equipment

A. Generating the co-expression construct

1. PCR Machine
2. 37 °C culture shaker
3. 4 °C and -20 °C fridge
4. 42 °C heat block

B. Expression Hsp90/Cdc37/Cdk4

1. 2.5 L flasks(Ultra Yield) (Thomson Instrument Company, catalog number: 931136)
2. Autoclave
3. Centrifuge capable of 3,000 G utilizing 1 L bottles
4. 30 °C incubator for plates
5. 30 °C culture shaker capable of shaking at 200 rpm 250 ml and 1 L flasks

C. Purification of the Hsp90/Cdc37/Cdk4 complex.

1. Emulsiflex C3 (Avestin)
2. Centrifuge (Beckman Coulter)
3. Rocker
4. Akta Purifier (GE Healthcare)
5. -80 °C fridge
6. Assortment of beaker sizes
7. Magnetic Stand (like EMD Millipore LSKMAGS15)

<u>Procedure</u>

A. Generating the co-expression construct

1. To co-express human Hsp90β, human Cdc37 and human Cdk4 we utilized viral 2A peptides. This way we were able to construct a single plasmid, which had all three proteins in it. The exact 2A sequence we used (P2A) was sourced from Porcine Teschovirus-1 and was GSGATNFSLLKQAGDVEENPGP. The resulting construct was of this arrangement: hCdc37-TEVsite-P2A-hHsp90β-TEVsite-FLAG-P2A-hCdk4-TEVsite-HisTag. The nucleotide sequence which was inserted between hCdc37 and hHsp90 was: CAGAACCTGTACTTTCAGGGCGGATCCGGTGCCACCAACTTTAGCTTGTTGAAGCAGGCTGGAGACGTGGAGGAAAATCCTGGACCC, between hHsp90 and hCdk4 was: CAAAACTTATACTTCCAGGGTGACTATAAGGACGATGACGACAAAGGCTCCGGTGCCACCAACTTCTCATTATTGAAACAGGCCGGTGATGTAGAGGAAAATCCAGGACCT, and after hCdk4 was: CAGAATCTGTATTTTCAGGGACATCATCACCATCACCATTAATGA. The complete sequence above was codon optimized (the regions between proteins were manually checked to be dissimilar to ease cloning).
2. The sequence was then split into two pieces (at nucleotide number 2,212) and both parts were ordered as GeneArt DNA Strings from Thermo Fisher Scientific. Using NEBuilder, primers were designed to amplify the 83nu vector (obtained from a colleague) and each of the GeneArt DNA Strings as to clone them using Gibson assembly.

3. 83nu vector and each of the GeneArt DNA Strings were amplified using a PCR machine, then digested with DpnI at 37C O/N, PCR cleaned up, assembled using NEB Gibson Kit and transformed into E. coli TOP10 cells supplied with the kit, which were plated and grown O/N at 37 °C on LB-carbenicilin plates.
4. Next day 10 colonies were picked and each was used to inoculate 5 ml of LB together with 100 mg/L of carbenicilin.
5. After 24 h growth at 37 °C with shaking, the DNA was extracted utilizing miniprep kit and DNA was sent for sequencing (tiling every 500 bp through the whole gene). The best clone had one mutation due to synthesis errors, which was corrected utilizing NEB Quickchange Kit and the protocol therein.
6. The final construct was sequenced and stored in water at -20 °C for future use.

B. Expression Hsp90/Cdc37/Cdk4

1. The plasmid was transformed into JEL1 (MAT-alpha, leu2 trp1 ura3-52 prb1-1122 pep4-3 deltahis3::PGAL10-GAL4) yeast strain using Zymo Research EZ Transformation protocol and plated on SD-His plates.
2. After 3 days at 30 °C a colony was picked and 100 ml O/N culture in 250mL flask (SD–His) was inoculated and grown at 30 °C O/N shaking at 200 rpm.
3. Next day 6 x 1 L flasks of YPGL media (autoclaved) were inoculated with 10 ml of the O/N culture each.
4. After about 24 h at 30 °C and 200 rpm (OD of 1), powder galactose was added to a final concentration of 2% w/v to induce protein expression.
5. The culture was pelleted after 6 h of growth at 3,000 x g for 20 min.

6. Pellets were scooped up and frozen at -80 °C.

C. Purification of the Hsp90/Cdc37/Cdk4 complex

1. The cell pellets were resuspended in lysis buffer with Roche protease inhibitors first with spatula, then by passing through a 16 G syringe needle (about 160 ml total for 6 L yeast growth).
2. The lysate was then passed through Emulsiflex machine at 25,000 psi, 5 complete passes for lysis.
3. Lysate was cleared by centrifuging at 30,000 x g for 30 min.
4. 5 ml bed volume of Ni-NTA beads were equilibrated in 20 bed volumes of lysis buffer at room temp utilizing a gravity column. The supernatant from the centrifuge spin was added to the beads, and then rocked for 1 h at 4 °C.
5. The loaded beads were washed with 20 bed volumes of lysis buffer, and then were eluted into 10 bed volumes of lysis buffer + 500 mM imidazole.
6. The resulting eluate was then incubated with pre-equilibrated (10 bed volumes) 1 ml bed volume of M2 Anti FLAG magnetic beads in 50 ml tube for 1 h at 4 °C, rocking.
7. Beads were washed with 10 bed volumes of lysis buffer utilizing the magnetic stand and a 15 ml tube, and the sample was eluted with 3 bed volumes of lysis buffer with 75 µg/ml of FLAG peptide, twice, 25 min each time
8. TEV was added to the eluent (2.5 mg) and it was dialyzed against 4 L of dialysis buffer O/N utilizing dialysis tubing.

9. The sample was then diluted 1:1 with the dialysis buffer without NaCl and was loaded onto pre-equilibrated 10/100GL MonoQ column on an AKTA Purifier system.
10. After washing out the unbound sample (about 3 CV), a gradient was run up to 1 M NaCl (over 20 CV) with fractionation to elute the bound complex (came off at about 25% conductivity).
11. The fractions were pooled, concentrated and then loaded on 16/60 S200 Superdex column pre-equilibrated in gel filtration buffer.
12. The peak fractions (at about 0.5 CV) were pooled, concentrated, flash frozen in liquid nitrogen and stored at -80 °C. At various points during the purification aliquots were taken to be run on SDS-PAGE gel (Fig1).

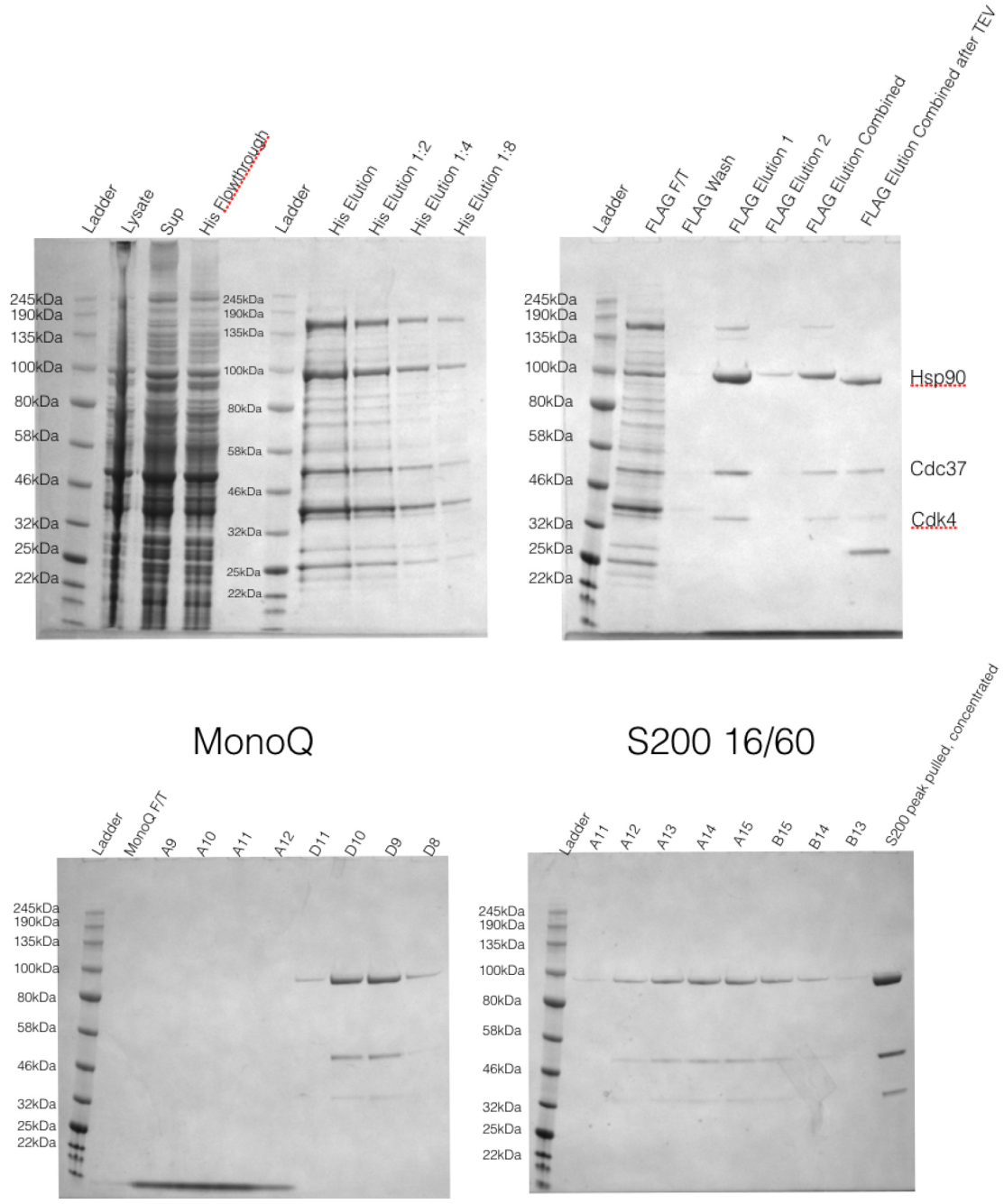

Figure 1. SDS-PAGE gels of Hsp90-Cdc37-Cdk4 purification from yeast

Note:

1. Scaling up the purification Genscript Anti-DYKDDDDK G1 affinity resin (L00432) was also used successfully with BioRad gravity column instead of

magnetic anti-FLAG beads. Use the same amount of beads/proportion of wash/elution buffers.

2. This protocol has also been sucesfully used for expression and purification of Hsp90/Cdc37/Her2 complex.
3. Expression of kinase alone, without Hsp90/Cdc37 yields soluble, active kinase.

Recipes

1. LB

   10 g Bacto-tryptone

   5 g yeast extract

   10 g NaCl

   in 1 L of water
2. LB agar

   As above with 15 g agar
3. SD-His

   6.7 g of yeast nitrogen base

   5 g glucose

   0.77 g CSM-His amino acid mix

   in 1 L of water (or 100 ml for 10x)
4. YPGL media

   2% peptone

   1% yeast extract

3% glycerol

2% lactate

in 1 L of water

Autoclave

5. Lysis buffer

   20 mM Tris pH 7.5

   150 mM NaCl

   20 mM imidazole

   10 mM $MgCl_2$

   10 mM KCl

   20 mM $NaMoO_4$

6. Dialysis buffer

   20 mM Tris pH 7.5

   100 mM NaCl

   10 mM $MgCl_2$

   10 mM KCl

   20 mM $NaMoO_4$

7. Gel filtration buffer

   20 mM Tris pH 7.5

   150 mM NaCl

   10 mM KCl

   20 mM $NaMoO_4$

   1 mM DTT

Publishing Agreement

It is the policy of the University to encourage the distribution of all theses, dissertations, and manuscripts. Copies of all UCSF theses, dissertations, and manuscripts will be routed to the library via the Graduate Division. The library will make all theses, dissertations, and manuscripts accessible to the public and will preserve these to the best of their abilities, in perpetuity.

Please sign the following statement:

I hereby grant permission to the Graduate Division of the University of California, San Francisco to release copies of my thesis, dissertation, or manuscript to the Campus Library to provide access and preservation, in whole or in part, in perpetuity.

Author Signature

03/28/2017

Date